Sorption Experiments with Sedimentary Rocks for Sn, Zr, Cs, Th and Pd under Saline Conditions

NWMO-TR-2018-16 December 2018

Peter Vilks and Neil H. Miller

Canadian Nuclear Laboratories

nwmo
NUCLEAR WASTE MANAGEMENT ORGANIZATION
SOCIÉTÉ DE GESTION DES DÉCHETS NUCLÉAIRES

Nuclear Waste Management Organization
22 St. Clair Avenue East, 6th Floor
Toronto, Ontario
M4T 2S3
Canada

Tel: 416-934-9814
Web: www.nwmo.ca

Sorption Experiments with Sedimentary Rocks for Sn, Zr, Cs, Th and Pd under Saline Conditions

NWMO-TR-2018-16

December 2018

Peter Vilks and Neil H. Miller
Canadian Nuclear Laboratories

This report has been prepared under contract to NWMO. The report has been reviewed by NWMO, but the views and conclusions are those of the authors and do not necessarily represent those of the NWMO.

All copyright and intellectual property rights belong to NWMO.

Document History

Title:	Sorption Experiments with Sedimentary Rocks for Sn, Zr, Cs, Th and Pd under Saline Conditions		
Report Number:	NWMO-TR-2018-16		
Revision:	R000	Date:	December 2018
Canadian Nuclear Laboratories, Whiteshell Laboratory			
Authored by:	Peter Vilks and Neil H. Miller		
Verified by:	Charles Kitson		
Approved by:	Jim Betteridge		
Department of Engineering Physics, McMaster University			
Reviewed by:	Shinya Nagasaki		
Nuclear Waste Management Organization			
Reviewed by:	Tammy Yang, Frank Garisto, Monique Hobbs		
Accepted by:	Paul Gierszewski		

ABSTRACT

Title: **Sorption Experiments with Sedimentary Rocks for Sn, Zr, Cs, Th and Pd under Saline Conditions**
Report No.: **NWMO-TR-2018-16**
Author(s): Peter Vilks and Neil H. Miller
Company: Canadian Nuclear Laboratories, Whiteshell Laboratory
Date: December 2018

Abstract
The purpose of this work is to measure sorption distribution coefficient (K_d) values for Cs, Pd, Zr, Sn and Th on Canadian sedimentary rocks (shale and limestone) and bentonite in a synthetic brine (reference brine SR-270-PW, Na-Ca-Cl type with a TDS of 275 g/L). The experimental measurements were conducted by (1) batch sorption tests using single and multiple elements tests lasting up to 6 months; and (2) long term (one year) diffusion tests for shale and limestone using multiple elements Li, Ni, Cs, Pd, Zr, Sn and Th. Batch sorption tests were also performed in a reference dilute solution (Na-Ca-Cl type with a TDS of 0.49 g/L) to provide a reference case to investigate the effect of salinity on sorption.

Results of batch tests indicated that sorption in the brine was lower for Cs, Pd, Zr, Sn and Th than in the dilute solution. The K_d values for Pd were reduced by factors of about 100 to 900, Th by factors of 3 to 30, Zr by factors of 10 to 20, Sn by factors of 4 to 7, and Cs by factors of 3 to 7. Cs showed strong sorption to bentonite and moderate sorption to shale and limestone in brine. The variation in K_d values with pH did not display any clear trends for most elements, and none of the elements displayed a distinct sorption edge over the investigated pH range. A desorption test indicated that the sorption of Pd, Zr, Sn and Th was reversible for most substrates. Cs sorption was not reversible, possibly due to fixation within clay mineral structures.

Surface complexation modelling was performed for bentonite (approximated by montmorillonite) and shale (approximated by 60% illite) in the reference brine and dilute solutions using a 2-site protolysis non-electrostatic surface complexation (2SPNE SC) model. The surface complexation constants for Pd, Zr and Sn (sorption on liilite) were derived by linear free energy relationships (LFER) whereas complexation constants for other elements were obtained from the literature. In the brine at pH of 6 to 7, the simulated K_d values for Zr were lower than measured values by factors of 3 to 13; the simulated K_d values for Sn and Th were greater than measured values by factors of 3 to 220 and 7 to 26, respectively. In the dilute solution at pH of 7 to 8, the simulated K_d values for Zr were lower than measured values by factors of 6 to 41; and simulations provided approximations for Sn (within a factor of 9 for bentonite and 4 for shale) and Th (within a factor of 2 for bentonite and 7 for shale). The 2SPNE SC model did not work for Pd, indicating that other sorption mechanisms (e.g., sorption of chloride complexes of Pd) must be also considered.

During the 368 days of diffusion, Li diffused through the limestone and shale rock samples, but no breakthrough was observed for Ni, Zr, Pd, Sn and Cs. Zr and Pd diffused less than 0.1 mm into limestone and shale, which demonstrated that Zr and Pd were strongly sorbed, consistent with the results of the batch tests. Sn diffused ~0.3 mm in limestone and 2 mm in shale. Cs diffused ~1.5 mm in limestone and ~4 mm in shale. Ni diffused ~2 mm in limestone and 9 mm in shale. Diffusion profiles for Th could not be obtained due to the high background concentration of natural Th in the limestone and shale test rock samples.

The sorption data obtained from this study will be used to update the NWMO's database of sorption values for Canadian sedimentary rocks and bentonite in highly saline solutions.

TABLE OF CONTENTS

Page

ABSTRACT ..... **iii**

1. INTRODUCTION **1**

2. BATCH SORPTION TESTS **4**

2.1 METHODS **4**
2.1.1 Long Term Sorption Tests 9
2.1.2 Effect of pH 10
2.1.3 Desorption Tests 11
2.2 RESULTS **12**
2.2.1 Effect of Sorption Time 18
2.2.2 Effect of pH 25
2.2.3 Desorption Test 31

3. SURFACE COMPLEXATION MODELLING **37**

3.1 Approach **37**
3.2 Palladium **42**
3.3 Zirconium **45**
3.4 Tin **48**
3.5 Thorium **50**

4. DIFFUSION TESTS **53**

4.1 DEFINITIONS **53**
4.2 METHODS **56**
4.2.1 Experimental 56
4.2.2 Calculation of Diffusion Profiles 63
4.3 RESULTS **63**
4.4 MODELLING **72**
4.4.1 Method 72
4.4.2 Diffusive Transport Modelling Results 76

5. SUMMARY AND DISCUSSION **78**

ACKNOWLEDGEMENTS **83**

REFERENCES **83**

APPENDIX A: COMPARISON OF SIMULATED AND MEASURED K_D VALUES **87**

LIST OF TABLES

Page

Table 1: Experimental Solutions Used for Sorption Tests 3
Table 2: Solids Used in Sorption Experiments 7
Table 3: Element Concentrations Used to Initiate Sorption Tests 8
Table 4: Buffers Used For Sorption Tests 10
Table 5: Cesium Sorption Coefficients from Batch Tests 13
Table 6: Palladium Sorption Coefficients from Batch Tests 14
Table 7: Zirconium Sorption Coefficients from Batch Tests 15
Table 8: Tin Sorption Coefficients from Batch Tests 16
Table 9: Thorium Sorption Coefficients from Batch Tests 17
Table 10: Batch Test K_d Values (cm^3/g) in Brine 35
Table 11: Batch Test K_d Values (cm^3/g) in Dilute Solution 36
Table 12: Surface Protolysis Reactions and Protolysis Constants for Na-illite and Montmorillonite 38
Table 13: Nickel Surface Complexation Reactions and Surface Complexation Constants for Na-Montmorillonite 39
Table 14: Simulated Ni K_d Values on Montmorillonite for Selected Solution Compositions 42
Table 15: Palladium Surface Complexation Reactions and Surface Complexation Constants for Montmorillonite and Illite 43
Table 16: Zirconium Surface Complexation Reactions and Surface Complexation Constants for Montmorillonite and Illite and Hydrolysis Constants 45
Table 17: Tin Surface Complexation Reactions and Surface Complexation Constants for Montmorillonite and Illite and Hydrolysis Constants 48
Table 18: Thorium Surface Complexation Reactions and Surface Complexation Constants for Montmorillonite and Illite 50
Table 19: Tracer Properties Used in Diffusion Test 57
Table 20: Parameters Used for Diffusive Mass Transport Modelling with AMBER 74
Table 21: Element Free Water Diffusion Coefficients 75
Table 22: Sorption Coefficients (cm^3/g) in Brine Solutions Derived from Batch Tests and Sorption Modelling 80
Table 23: Summary of Sorption Properties for Each Element 81

LIST OF FIGURES

Page

Figure 1: Glove Box Used for Batch Sorption and Diffusion Tests....6
Figure 2: Cesium Sorption as a Function of Time on Bentonite, Shale and Limestone in Brine (*I* = 6.0 M) and Dilute solution (*I* = 0.01 M).... 20
Figure 3: Palladium Sorption as a Function of Time on Bentonite, Shale and Limestone in Brine (*I* = 6.0 M) and Dilute solution (*I* = 0.01 M) 21
Figure 4: Zirconium Sorption as a Function of Time on Bentonite, Shale and Limestone in Brine (*I* = 6.0 M) and Dilute Solution (*I* = 0.01 M).... 22
Figure 5: Tin Sorption as a Function of Time on Bentonite, Shale and Limestone in Brine (*I* = 6.0 M) and Dilute Solution (*I* = 0.01 M).... 23
Figure 6: Thorium Sorption as a Function of Time on Bentonite, Shale and Limestone in Brine (*I* = 6.0 M) and Dilute Solution (*I* = 0.01 M).... 24
Figure 7: Cesium Sorption as a Function of pH on Bentonite, Shale and Limestone in Brine (*I* = 6.0 M) and Dilute Solution (*I* = 0.01 M).... 26
Figure 8: Palladium Sorption as a Function of pH on Bentonite, Shale and Limestone in Brine (*I* = 6.0 M) and Dilute Solution (*I* = 0.01 M).... 27
Figure 9: Zirconium Sorption as a Function of pH on Bentonite, Shale and Limestone in Brine (*I* = 6.0 M) and Dilute Solution (*I* = 0.01 M).... 28
Figure 10: Tin Sorption as a Function of pH on Bentonite, Shale and Limestone in Brine (*I* = 6.0 M) and Dilute Solution (*I* = 0.01 M).... 29
Figure 11: Thorium Sorption as a Function of pH on Bentonite, Shale and Limestone in Brine (*I* = 6.0 M) and Dilute Solution (*I* = 0.01 M) 30
Figure 12: Cesium Desorption with Time on Bentonite, Shale and Limestone in Brine... 31
Figure 13: Palladium Desorption with Time on Bentonite, Shale and Limestone in Brine.... 32
Figure 14: Zirconium Desorption with Time on Bentonite, Shale and Limestone in Brine.... 33
Figure 15: Tin Desorption with Time on Bentonite, Shale and Limestone in Brine 34
Figure 16: Thorium Desorption with Timeon Bentonite, Shale and Limestone in Brine .. 34
Figure 17: Simulated Palladium Sorption on Montmorillonite and Shale in SR-270-PW Brine and Dilute Solution under Different pH Values (Triangle and Square Points are the Range of Experimental Measurements at pH of 6 and 8).... 44
Figure 18: Simulated Zirconium Sorption on Montmorillonite and Shale in SR-270-PW Brine and Dilute Solution under Different pH Values 47
Figure 19: Simulated Tin Sorption on Montmorillonite and Shale in SR-270-PW Brine and Dilute Water Under Different pH Values.... 49
Figure 20: Simulated Thorium Sorption in SR-270-PW Brine and Dilute Water Under Different pH Values 52
Figure 21: Limestone (DIF1 & DIF2) and Shale (DIF3 & DIF4) Test Rock Samples.... 58
Figure 22: Schematic Diagram of Diffusion Cell.... 58
Figure 23: Test Rock Sample and Diffusion Cell Parts 59
Figure 24: Assembled Diffusion Cell with Test Sample.... 59
Figure 25: Cutting Test Rock Sample into Smaller Sections for Profile Sampling 61
Figure 26: Examples of Potential Diffusion Profile Samples 61
Figure 27: Removing Material from Test Rock Samples to be Used for Determining Tracer Concentrations.... 62
Figure 28: Leaching of a Diffusion Profile Sample with Nitric Acid to Extract Tracers 62
Figure 29: Lithium Diffusion Profiles in Limestone and Shale 65
Figure 30: Nickel Diffusion Profiles in Limestone and Shale.... 66

Figure 31: Cesium Diffusion Profiles in Limestone and Shale 67
Figure 32: Palladium Diffusion Profiles in Limestone and Shale 68
Figure 33: Zirconium Diffusion Profiles in Limestone and Shale..... 69
Figure 34: Tin Diffusion Profiles in Limestone and Shale 70
Figure 35: Thorium Diffusion Profiles in Limestone and Shale..... 71
Figure 36: Simulated and Measured Lithium Diffusion Profiles in Limestone and Shale 77

1. INTRODUCTION

In Canada, Adaptive Phased Management (APM) is the federally approved approach for the long term management of Canada's used nuclear fuel. From a technical perspective, APM involves the emplacement of used nuclear fuel within a Deep Geologic Repository (DGR) within a suitable crystalline or sedimentary rock formation (NWMO 2005). At typical repository depths (~500 mBGS), sedimentary rocks in Ontario, Canada may contain Na-Ca-Cl brines with a total dissolved solid (TDS) concentration ranging between 200 and 375 g/L (NWMO 2011). Sorption is a potential mechanism for retarding radionuclide transport from a DGR for used nuclear fuel to the environment. Sorption of radionuclides in the geosphere and in the engineered barrier systems depends on factors such as the properties of radionuclides, radionuclide concentration, the properties of sorbing minerals and groundwater chemistry (especially pH, Eh, salinity and available complexing agents).

NWMO initiated the development of a Canadian sorption database for highly saline groundwaters by conducting a review of the open literature and international sorption databases to find the available data relevant to Canadian sedimentary rocks and bentonite for the elements of interest for safety assessment (Vilks 2011). This database has been augmented with sorption data measured experimentally for Canadian sedimentary rocks (shale and limestone) and bentonite in saline solutions (Vilks et al. 2011; Vilks and Miller 2014; Bertetti 2016; Nagasaki et al. 2016, 2017; Nagasaki 2018). The sorption database supports the preparation of safety assessments and safety cases for a deep geological repository in a Canadian sedimentary environment.

The purpose of this study is to further the development of the NWMO sorption database by (1) measuring sorption values for elements/radionuclides of interest using both batch and diffusion tests in brine solutions; and (2) performing thermodynamic sorption modeling to improve the understanding of the sorption mechanisms of these elements/radionucldies in brine solutions. Measured sorption coefficient (K_d) values are compared with simulated values with the goals of (i) improving the understanding of sorption processes in highly saline solutions in response to components of solution chemistry, such as pH, salinity, chloride and carbonate complexation; and (ii) evaluating the ability of surface complexation based sorption models to predict sorption properties under saline conditions. Batch sorption tests are also conducted in a dilute solution to investigate the effect of salinity on sorption.

The elements of interest for the development of a sorption database for Canadian sedimentary rocks in contact with highly saline solutions include Ag, Am, As, Bi, C, Ca, Cd, Cl, Cs, Cu, Eu, Hg, I, Mo, Nb, Ni, Np, Pa, Pb, Pd, Pu, Ra, Se, Sn, Tc, Th, U and Zr. Of these, the following 5 elements have been selected for sorption tests in brine solutions as part of this study: Sn, Zr, Cs, Th and Pd. In brine solutions the most likely mechanism of Cs(I) sorption is by the displacement of Na and K from the interlayers of clay minerals. This needs to be confirmed by experimental measurements, particularly longer term kinetic studies which may determine whether Cs is entering clay minerals by slow diffusive processes. Sorption data for Pd(II) are of interest because Pd sorption values for sedimentary rocks in brine conditions are scarce and are based on using Pb(II) as a chemical analog. Data for the tetravalent elements, Zr(IV), Sn(IV) and Th(IV) are of interest to determine to what extent these elements can be used as chemical analogs for each other and other tetravalent elements. Surface complexation constants on montmorillonite and illite are available in the literature for Sn and Th, and can be estimated for Pd and Zr by linear free energy relationship (LFER). Experimental measurements

in brine solutions for these 4 elements would make a valuable contribution to testing current tools for surface complexation modelling in brine solutions.

The strategy of the experimental program was to use a combination of static batch sorption tests and long term diffusion tests to characterize sorption reactions and to evaluate their role in mass transport. The following sorption tests were conducted:

(1) Batch tests studied sorption as a function of time to identify reaction times required to achieve sorption equilibrium or steady state in brine and dilute solutions;

(2) Desorption tests were performed to evaluate the reversibility of sorption to the dilution of tracer concentrations in solution (keeping in mind that reactions that are too slow under lab conditions may be reversible over geologic time scales);

(3) Batch tests compared sorption in a reference brine to a reference dilute solution in order to illustrate the effect of salinity on sorption and to help in the testing of sorption models by providing an extreme range in solution compositions;

(4) Sorption experiments were performed using multiple elements for comparison to single-element tests to determine whether trace elements compete for sorption sites;

(5) Sorption tests in brine solutions were performed with different pH values to characterize the variation in sorption with pH. This information is valuable in formulating sorption models. Since minerals buffer the pH of brine and dilute solution, pH buffers were used to control pH.

(6) Diffusion tests were performed to study the migration of Li (as a conservative tracer), Ni, Cs, Zr, Sn and Th in shale and limestone. The purpose of the diffusion tests is to compare the sorption coefficients obtained from the diffusion tests to those obtained from the batch sorption tests to determine whether the sorption coefficients derived from batch tests can be applied to account for sorption effects (i.e., retardation) during mass transport of the element through the rock matrix.

Batch sorption measurements were performed with Ordovician shale and limestone rock samples supplied by NWMO, and with bentonite samples supplied by AECL. Sorption tests were performed in an experimental reference brine solution SR-270-PW (with a TDS of 275 g/L or an ionic strength (*I*) of 6.0 M (mol/kgw)) slightly modified based on the SR-270-PW reference porewater, and a reference dilute solution (with a TDS of 0.5 g/L or an ionic strength of 0.01 M) (Table 1).

Table 1: Experimental Solutions Used for Sorption Tests

Water Chemistry	**Reference Porewater SR-270-PW**	**Experimental Reference Brine SR-270-PW**	**Experimental Reference Dilute Solution**
Nominal pH **Redox state** **Nominal Eh (mV)**	6.0 Reducing -200	6.3 to 6.5 N_2 atmosphere not determined	8.0 to 8.2 N_2 atmosphere not determined
Solutes	(mol/L)	(mol/L)	(mol/L)
Na	2.179	2.179	0.0042
K	0.320	0.320	-
Ca	0.798	0.798	0.0018
Mg	0.337	0.337	-
HCO_3	0.0018	0.0018	0.0018
SO_4	0.00458	0.00458	-
Cl	4.753	4.753	0.0060
Br	0.0213	0.0213	-
Sr	0.0137	0.0137	-
Li	0.00072	0.00072	-
F	0.000105	0.000105	-
I	0.000024	0.000024	-
B	0.0074	-	-
Si	0.00014	0.00014	-
Fe	0.00054	-	-
NO_3	<0.0002	-	-
PO_4	-	-	-
TDS (g/L)	275	275	0.49
Water type	Na-Ca-Cl	Na-Ca-Cl	Na-Ca-Cl-HCO_3
***Ionic Strength (*I*) (mol/kgw)**	6.0	6.0	0.01

* Ionic strength was calculated using PHREEQC, version 2.18.5570 and the SIT database (released on August 15, 2011) (Parkhurst and Appelo 1999). The ionic strength of SR-270-PW is 6.7 M (mol/kgw) calculated with the Pitzer.dat thermodynamic database incorporated in PHREEQC.

2. BATCH SORPTION TESTS

Batch tests were performed using the 200 mL solution volume sorption tests, as described by Vilks et al. (2011), to measure the sorption of Cs, Pd, Sn, Zr and Th on bentonite, shale and limestone. Sorption measurements were performed with a synthetic brine composition (I = 6.0 M) equivalent to the reference porewater, SR-270-PW, to further the understanding of sorption processes for these elements in brine solution and to determine sorption coefficient (K_d) values that can be used in the sorption database for sedimentary rocks. A more limited number of sorption tests were also performed in a reference dilute solution with a Na-Ca-Cl-HCO_3 type composition and a TDS of approximately 0.49 g/L (I = 0.01 M). The purpose of these tests at low ionic strength was to provide a reference to which sorption at high ionic strength can be compared.

The initial concentrations of the test elements Cs, Pd, Sn, Zr and Th were determined by considering the element detection limits that can be achieved by high resolution ICP-MS, and taking into account their likely solubility limits in SR-270-PW brine and in the reference dilute solution as predicted by thermodynamic simulations using PHREEQC (Parkhurst and Appelo 1990).

The majority of sorption tests were performed as mulit-element tests, containing Cs, Pd, Sn, Zr and Th. In addition, a select number of single element tests, i.e., with a single element per test, were performed to evaluate the assumption that in a multiple elements test these elements do not interfere with each other during the sorption process.

The batch sorption studies included: 1) long term sorption tests to measure sorption as a function of time for up to 6 months in brine and dilute solutions; 2) desorption tests to evaluate sorption reversibility; and 3) sorption measurements over a broad range of solution pH (approximately 3 to 8) to evaluate the effect of pH on sorption and to provide sorption data for comparison to the results of sorption modelling.

Although Cs, Pd, Sn, Zr and Th are not affected by redox conditions, all of the batch sorption tests were performed in a glove box containing N_2, H_2 and CO_2 to maintain low O_2 conditions (< 100 ppm) and a constant partial pressure of CO_2 (Figure 1). The advantage of using low O_2 conditions is that it mimimizes any changes to mineral surfaces that could be caused by oxidation reactions.

2.1 METHODS

Ordovician shale and limestone rock samples were supplied by NWMO. The limestone rock sample (ID: DGR5-733.62, core run #178, drilled on October 25, 2009) was taken from borehole DGR5 drilled at the Bruce nuclear site in southern Ontario (e.g. INTERA, 2011). The shale rock sample (ID: DGR4-460.78, core run #145, drilled on September 24, 2008) was also from the Bruce nuclear site taken from borehole DGR4. Both core samples were shipped from site nitrogen gas purged and vacuum sealed in 2 polyethylene bags and 1 foil film for sample preservation. The bentonite used in sorption tests was a Na Wyoming bentonite supplied by

National Bentonite (MX-80). It was taken from bentonite stocks originally purchased for use at AECL's Underground Research Laboratory (URL), near Pinawa, Manitoba.

The shale and limestone rock samples were first crushed and powdered in the laboratory. The shale, limestone and bentonite samples were dry sieved to collect a size fraction between 100 and 200 μm for use in batch sorption experiments. Between 4 and 23 g of shale, limestone and bentonite powders were sent to Activation Laboratories Ltd. in Ancaster, Ontario, for mineral compositional analyses by X-ray diffraction. The shale and limestone samples were analysed using the protocol CODE 9 – mineral identification (quantitative), while the bentonite sample was analyzed with the protocol CODE 9 – mineral identification + clay speciation (quantitative). The results of the mineral analyses can be found in Table 2.

SR-270-PW brine solution was prepared using reagent grade NaCl, KCl, $CaCl_2 \bullet 2H_2O$, $MgCl_2 \bullet 6H_2O$, $NaHCO_3$, $SrCl_2 \bullet 6H_2O$, LiBr, NaI, NaF, $CaSO_4 \bullet 0.5H_2O$, $CaBr_2 \bullet 2H_2O$ and $NaSiO_3 \bullet 9H_2O$ compounds and deionized water. Reference Na-Ca-Cl-HCO_3 dilute solution was prepared from $CaCl_2 \bullet 2H_2O$, $NaHCO_3$ and NaCl compounds and deionized water.

The sorbate tracers were prepared from the following compounds. Cesium was obtained as CsCl (J.T. Baker, Ultrapure Bioreagent). Palladium was obtained as $PdCl_2$ (Sigma-Aldrich), which was dissolved in 1 mol/L HCl solution to make a Pd stock solution. Tin was obtained as a $SnCl_4$ liquid (Sigma-Aldrich), which was dissolved in 1 mol/L HCl under a N_2 atmosphere to avoid a violent reaction with the atmosphere. Zirconium tracer was prepared by dissolving zirconyl chloride octahydrate ($Cl_2OZr \bullet 8H_2O$) (Sigma-Aldrich, lot#09696APV) into 0.1 mol/L HCl solution. Thorium was obtained as a 100 mg quantity ThO_2 oxide (reference no. INMOS 50866) from AECL's Analaytical Sciences group. The ThO_2 oxide was dissolved in a mixture of 0.05 mol/L HF and 13 mol/L HNO_3 solution, which was heated and evaporated to dryness. The dried Th was then dissolved in concentrated HCl solution. Since a white precipitate remained, the solution was evaporated to dryness and the dissolution procedure was repeated numerous times until no precipitate was visible.

All of the batch sorption tests were performed in a glove box containing N_2 (94.5%), H_2 (5%) and CO_2 (0.5%) to maintain low O_2 conditions (< 100 ppm) and a constant partial pressure of CO_2. A constant CO_2 partial pressure is required because all of the three solid substrates contain a carbonate component which would release CO_3^{2-} to the experimental solutions. Unless the experimental solutions are covered with an atmosphere containing a controlled CO_2 partial pressure, they would constantly lose CO_3^{2-} to the atmosphere, leading to pH drifts and possibly enhancing carbonate dissolution. The oxygen content of the glove box was reduced with a slow $N_2/H_2/CO_2$ purge of the glove box, and by allowing the excess H_2 to react with O_2 while passing the gas in the glove box over a Pd catalyst. The oxygen content of the glove box was checked daily with anaerobic indicator test strips (Oxoid indicator strip, BR0055), which turns pink when the oxygen in the atmosphere exceeds 100 ppm.



Figure 1: Glove Box Used for Batch Sorption and Diffusion Tests

The general method for batch sorption tests consisted of multiple sorption measurements at different time intervals from a single large volume reaction vessel. The advantage of using larger quantities of solid and solution is that the effect of sample variability (heterogeneity of powdered material) is reduced and sorption can be monitored as a function of time using the same solid sample. With this protocol a solution containing a known concentration of sorbate was contacted with a sorbing solid. At designated time intervals, the reaction vessel was sampled in such a way as to not change the solid/liquid ratio for the experiment. This was accomplished by shaking the reaction vessel to suspend the solids immediately before withdrawing a volume of sample solution with suspended solids. The solution was separated from the solid in each sample by centrifugation for 20 minutes at 15,000 rpm and analyzed to determine the decrease in sorbate concentration. This decrease in sorbate concentration was used to calculate the amount of sorbate that had sorbed to the solid and to determine a K_d value.

Table 2: Solids Used in Sorption Experiments

Geologic Material	Reference	Major Minerals
Queenston shale from the Bruce nuclear site. (Used in this study for batch and diffusion mass transport tests.)	This study	illite (44.3 wt%) chlorite (12.2 wt%) quartz (12.1 wt%) calcite (18.1 wt%) ankarite (12.8 wt%) hematite (0.5 wt%)
Queenston shale from the Bruce nuclear site.	Wigston and Jackson (2010)	sheet silicate (44 wt%) quartz (23 wt%) ankarite (12%) calcite (10 wt%) microcline (5%) halite (3%) hematite (0.9%) rutile (0.7%)
Argillaceous limestone (Used in this study for batch and diffusion mass transport tests.)	This study	calcite (75.4 wt%) ankerite (16.1 wt%) quartz (4.9 wt%) feldspar (2.0 wt%) illite (1.6 wt%)
Cobourg argillaceous limestone	Jackson and Murphy (2011)	calcite (87.7 wt%) orthoclase (4.1 wt%) sheet silicate (3.5t%) quartz (2.9 wt%) ankerite (1.8%)
Wyoming sodium bentonite	Lajudie et al. (1995); Liu and Neretnieks (2006)	montmorillonite (75 wt%) quartz (15.2 wt%) feldspar (5 to 8 wt%) calcite (1.4 wt%) kaolinite < 1 wt%) illite (< 1 wt%)
Wyoming sodium bentonite	This study	montmorillonite (84.8 wt%) quartz (4.0 wt%) feldspar (11.2 wt%)

The reaction vessels used in batch tests were 250 mL Nalgene (polypropylene) wide mouth bottles. The mass of solid sorbent that was quantitatively added to the reaction vessel was 0.01 g, 0.02 g, and 0.05 g for bentonite, shale, and limestone, respectively, for single element

and multiple elements tests in brine and dilute solutions, except for the single element tests for Cs and Pd in brine solution, where the respective masses of bentonite, shale and limestone were 1 g, 2 g and 4 g. The volume of ionic medium added to the reaction vessel was 200 ± 2 mL. In order to precondition the solids, the first addition of the ionic medium did not contain sorbate. Sorption data obtained from tests with conditioned solids are considered to be more useful since artefacts from the rock crushing have been reduced (Vilks et al. 2011). After allowing the solids to be conditioned in the ionic medium for a week or longer, 100 mL of the ionic medium was removed by decanting into a graduated cylinder. The sorption tests were initiated by replacing the removed volume with 100 mL of ionic medium containing known concentrations of sorbate elements. The target initial concentrations are given in Table 3. Note that for Th, 2.9×10^{-9} mol/L initial concentration was used for multiple elements tests and 2.9×10^{-8} mol/L initial concentration was used for all the other sorption tests to improve Th detection. Blank tests to monitor sorbate losses to reaction vessel walls were initiated at the same time. The blank tests were identical to the sorption tests, except that no sorbate solids were present. During the sorption period the reaction vessels were shaken on a routine basis (1 to 5 times a week), with a higher frequency at the start of the sorption test. At each designated sampling time interval, the reaction vessels were shaken to ensure that the solids are evenly dispersed in suspension and immediately 5 mL of solution with entrained solids was removed. After centrifuging each solution sample (for 20 minutes at 15,000 rpm) and decanting the centrifuged supernatant, a portion of the supernatant was diluted in 20 mL of 1 mol/L nitric acid. The volume of diluted surpernatant was 0.2 mL for brine solutions (requiring more dilution) and 2.5 mL for dilute solutions. The pH of the remaining supernatant was measured to establish the pH at the time of sampling. A measured portion of the remaining sample was also diluted in 20 mL of nitric acid and archived till the end of the project. The acidified samples were sent for concentration analysis to Activation Laboratories Ltd. in Ancaster, Ontario. The Code 6MB protocol was used to analyse solutions for Cs, Pd, Sn, Zr and Th by ICP-MS.

Table 3: Element Concentrations Used to Initiate Sorption Tests

Cs(I) (mol/L)	Pd(II) (mol/L)	Zr(II) (mol/L)	Sn(IV) (mol/L)	Th(IV)* (mol/L)
$1x10^{-5}$	$5.7x10^{-6}$	$1x10^{-7}$	$3.6x10^{-7}$	$2.9\ x10^{-9}$ and $2.9\ x10^{-8}$

*Th initial concentration of 2.9×10^{-9} mol/L was used only for one sorption test in brine, and Th initial concentration of 2.9×10^{-8} mol/L was used for all the other sorption tests in brine and dilute solutions.

The pH of sample solutions was determined with a Radiometer Analytical SAS combined pH electrode (pH C2401-8). The pH electrode was calibrated with NBS reference buffer solution with an ionic strength of 0.1 mol/L (Wu et al. 1988). It is recognized that pH measurements in brine solutions (in neutral pH ranges) may be affected by changes in liquid junction potentials as a result of higher salt concentrations (Hinds et al. 2009; Baumann 1973) which was not specifically considered in this work. A standard procedure of measuring pH was adopted that consisted of determining pH in unstirred samples after the majority of solids had settled out of suspension. The measured pH values were electrode indicated values.

2.1.1 **Long Term Sorption Tests**

Long term sorption tests were intended to study sorption as a function of time, to further the understanding of sorption kinetics and to establish whether sorption reactions have reached equilibrium or a steady state. If measured sorption values are not significantly different in two consecutive sampling periods, one considered that equilibrium has been achieved. Two sorption values were considered to be significantly different when the difference in their average values exceeds the combined standard deviations of the two values. The long term sorption tests are performed for a time period of up to 6 months. Each reaction vessel was sampled approximately 6 times (1 day, 1 week, 2 weeks, 1 month, 3 months, and 6 months) to establish a K_d versus time relationship.

The long term sorption tests were performed with the experimental SR-270-PW reference brine solution, as well as with the reference dilute solution. The multiple elements tests were performed in triplicate (3 separate reaction vessels) for bentonite, shale, limestone and blanks (solid-free tests). The single element sorption tests with Cs, Pd, Sn, Zr and Th were performed to determine whether the K_d values of these elements are different when sorption tests are performed without the other elements. These single element sorption tests were performed in duplicate, using the same procedures and reaction time periods as used with the multiple elements tests to facilitate comparisons, and to provide a backup in case an unforeseen problem arose with the multiple elements tests.

Sorption results were expressed as sorption coefficients (K_d), which were calculated as follows:

$$K_d = \frac{S}{C} = \frac{(C_0 - C) \times Vol}{C \times m} \times 1000 \qquad (cm^3/g) \qquad (1)$$

Where: C_0 = initial concentration of sorbate (mol/L)
C = equilibrium concentration of sorbate measured in solution (mol/L)
S = concentration of sorbate on the solid (mol/g)
Vol = total volume of solution that was in the reaction vessel (L)
m = mass of sorbing solid (*sorbent*) in the system (g)
Conversion factor: 1000 cm^3/L

The percent sorbed is defined as:

$$percent\ sorbed = \frac{mass\ \ sorbate\ \ removed\ \ from\ \ solution\ \ \times 100\%}{total\ \ sorbate\ \ available\ \ for\ \ sorption} \qquad (cm^3/g) \qquad (2)$$

2.1.2 **Effect of pH**

When bentonite, shale and limestone rock samples are suspended in SR-270-PW brine solution, the solids buffer the pH of brine solution to around 6.2 to 6.5. In the reference dilute solution, the solids buffer the pH of solution to around 8. The K_d values from the pH range of 6.0 to 7.0 in brine solutions are mainly of interest for the sorption database for Canadian sedimentary rocks. However, since sorption may be pH sensitive, it is important to evaluate how sorption varies with pH experimentally and to compare experimental sorption coefficient data with simulated sorption coefficient values determined using sorption modelling. This is important for assessing the performance of the sorption models for SR-270-PW brine and the reference dilute solution.

Vilks and Miller (2014) noted that the pH buffering by suspensions of sedimentary rocks and bentonite is very strong, and that if pH was adjusted with additions of strong acid or base, the pH would return to equilibrium values within hours. In this study pH manipulation was accomplished by reducing the concentrations of suspended solids by a factor of 100 from concentrations used by Vilks and Miller (2014), and by the use of pH buffers. The pH buffers used in brine and dilute solutions are summarized in Table 4, showing the pH ranges achieved in these solutions. The range of experimental pH values achieved for brine solutions was from 3.1 to 7.1, while pH values in dilute solution ranged from 3.9 to 8 (including the non-buffered tests). The acetic acid buffer was purchased from Fisher Scientific (ACS Reagent), while the MES, MOPS, and TRIS buffers were obtained from Sigma-Aldrich.

Prior to addition of pH buffers in sorption tests, the performance of the buffers was tested in brine and dilute solutions with and without the presence of mineral solids. These tests were used to identify the optimum buffer concentrations required, as well as the pH values that can be achieved. The pK_a values and pH ranges listed in Table 4 are for an ionic strength of 0.1 mol/L and will likely be different in brine solutions. The experimental time frame was days to weeks, depending upon the stability of the solution pH. Experiments were performed in triplicate for bentonite, shale and limestone, using multiple tracers. The results of the sorption tests without pH buffering were integrated with the results of the pH buffered tests since both tests followed the same protocol.

Table 4: Buffers Used For Sorption Tests

Buffer	*pK_a	pH Range Used in Sorption Tests	
		Brine	Dilute Solution
AA (acetic acid)	4.76	3.1 – 3.5	3.9 – 4.5
MES (2-(N-Morpholino)ethane-sulphonic acid)	6.15	-	7.2 – 7.7
MOPS (3-(N-Morpholino)propanesulphonic acid)	7.2	6.4 – 6.5	6.2 – 6.4
TRIS (Tris(hydroxymethyl)aminomethane)	8.06	6.5 – 7.1	-

*From Baeyens and Bradbury (1997)
Buffer concentration used to achieve these pH ranges was 1×10^{-3} mol/L.

2.1.3 **Desorption Tests**

The purpose of performing desorption experiments is to test the reversibility of a sorbate's sorption by decreasing the dissolved sorbate concentration in the sorption equilibrium system and observing the response of sorption coefficient values. If the sorption process is completely reversible, over a relatively short time period, enough sorbate will be desorbed to return the system to equilibrium and the observed sorption coefficients will be very similar to the values before the desorption test. If the process is not reversible within the experimental time span, the observed sorption coefficient values will be higher because insufficient sorbate would have desorbed to return the system to equilibrium. The strategy is to separate the solids from the solution with dissolved sorbates and replace it with a smaller volume of sorbate-free ionic medium. The solid to liquid ratio will be higher than in the original sorption experiments.

Desorption tests were initiated immediately after completion of the long term, multiple elements sorption tests in brine solution containing the MOPS pH buffer. Desorption was performed after a sorption time of 104 days. Desorption was initiated by first decanting the solution from the reaction vessels, leaving 3 to 10 mL behind. The remaining solution and solids were then transferred to a 30 mL volume, Oak Ridge style centrifuge tube. After centrifuging the solids (15,000 rpm for 20 minutes), a significant portion of the supernatant was removed and sampled (0.2 mL) for concentration analyses. The measured dissolved sorbate concentrations from this sample provided values for the concentration of sorbate in solution (C_{rem}) that was removed from the reaction vessel. The C_{rem} values were used to determine the K_d value before desorption and to help determine how much sorbate was removed from the system. After combining the supernatant removed from the centrifuge tube with the solution that was decanted before centrifuging, the total volume of solution removed from each sorption test was determined. This becomes the removed volume (vol_{rem}), which could be up to 98% of total solution volume before desorption.

A 30 mL volume of sorbate-free ionic medium was added to each Oak Ridge centrifuge tube (which became the new reaction vessel) to initiate the desorption process by diluting the sorbate concentration. The reaction vessel (centrifuge tube) was shaken to disperse the solids. Immediately afterward the reaction vessel was sampled (4 mL) to determine how much sorbate was in solution at the start of the desorption test. This is an important value because it overcomes any uncertainty associated with not knowing exactly how much of the original reaction solution may have been left behind with the solid. The reaction vessel was sampled at a number of different time intervals to monitor sorbate desorption with time.

The sorption coefficients (K_d) determined before desorption are calculated with equation 1. This calculation of sorption coefficients is not strictly valid for the desorption phase because the total sorbate concentration in the system has been reduced by removing a volume of the reacting solution. The basic approach to calculating K_d values during desorption was to determine the mass of sorbate that has desorbed, based on the increase in dissolved sorbate concentration in solution. The K_d value at the time of desorption was calculated by dividing the concentration of sorbate remaining on the solid by the dissolved sorbate concentration. For a given sampling event n (where n is a number 1, 2, etc.), the concentration of sorbate that was sorbed was S_n, given by:

$$S_n = S_{n-1} - desS_n \text{ (mol/g)} \qquad (3)$$

Where: S_{n-1} = total concentration of sorbate on solid in previous sampling period (mol/g)
$desS_n$ = desorbed sorbate concentration at sampling interval n
$= vol_n \times (C_n - C_{n-1})/m$ (mol/g)
vol_n = total volume in reaction vessel at interval n before sample removed (L)
$= vol_{n-1} - vol_{samp}$
vol_{n-1} = volume in reaction vessel at previous sampling event (L)
vol_{samp} = volume of sample removed from the reaction vessel (L)
C_n = dissolved sorbate concentration at interval n (mol/L)
C_{n-1} = dissolved sorbate concentration in previous interval (mol/L)
m = mass of sorbing solid (*sorbent*) in the system (g)

The sorption coefficient for desorption interval n becomes:

$$^{n}K_d = \frac{S_n}{C_n} \times 1000 \qquad (cm^3/g) \qquad (4)$$

2.2 **RESULTS**

The results of the batch sorption tests are presented in Table 5 through to Table 9 for SR-270-PW brine solution and the reference dilute solution. The K_d values are average values based on 2 to 3 replicate measurements. The errors are based on standard deviations. In those cases where an error value is not given, the K_d value is based on a single measurement because the other replicates failed to produce a usable value. These tables include results from different test types that include multiple elements tests (MX), single element tests (S), multiple elements tests with acetate pH buffer (MXA), multiple elements tests with MOPS pH buffer (MXMOPS), multiple elements tests with TRIS pH buffer (MXTRIS), and multiple elements tests with MES pH buffer (MXMES). The pH values represent the pH conditions at sampling time.

Section 2.2.1 discusses the results in these tables in terms of the variation of K_d values with sorption time. Emphasis was placed on tests performed with multiple and single element tracers. Results using pH buffers were not considered in the discussion.

Section 2.2.2 addresses the variation of K_d values with pH. Data values from all reaction times (MX, S, MXA, MXMOPS, MXTRIS, MXMES) were considered for evaluating the effects of pH variation.

Section 2.2.3 discusses the results of the desorption tests based on diluting the sorbate concentration in the multiple elements tests that included the MOPS pH buffer.

The results of batch sorption tests are summarized in Section 2.2.4 with the aim of producing a set of K_d values that can be used for representing sorption on bentonite, shale and limestone in brine solutions and dilute solutions. The K_d values are presented as averages with standard deviations, as well as geometric means with corresponding geometric standard deviations.

Table 5: Cesium Sorption Coefficients from Batch Tests

SR-270-PW Brine

Test Type	Time (day)	Bentonite		Shale		Limestone	
		pH	K_d (cm^3/g)	pH	K_d (cm^3/g)	pH	K_d (cm^3/g)
MX	1	6.3	$(1.3 \pm 0.7) \times 10^3$	6.3	$(6.1 \pm 6.4) \times 10^2$	6.4	$(2.1 \pm 2.1) \times 10^2$
MX	8	6.2	$(1.8 \pm 3.2) \times 10^2$	6.3	$(1.4 \pm 2.5) \times 10^2$	6.2	$(7.0 \pm 9.9) \times 10^1$
MX	14	6.3	$(8.5 \pm 7.6) \times 10^2$	6.3	$(3.9 \pm 3.5) \times 10^2$	6.3	$(6.9 \pm 8.8) \times 10^2$
MX	28	6.3	$(2.0 \pm 1.9) \times 10^2$	6.3	$(9.5 \pm 9.3) \times 10^1$	6.3	$(5.7 \pm 5.0) \times 10^1$
MX	195	5.9	$(1.4 \pm 0.2) \times 10^3$	5.6	$(5.5 \pm 1.1) \times 10^2$	5.7	$(5.8 \pm 3.7) \times 10^2$
S	7	6.2	$(1.4 \pm 0.2) \times 10^2$	6.1	$(6.9 \pm 0.6) \times 10^1$	6.0	$(3.2 \pm 0.6) \times 10^1$
S	89	6.2	$(1.6 \pm 0.1) \times 10^2$	6.1	$(7.9 \pm 0.1) \times 10^1$	6.1	$(3.5 \pm 0.0) \times 10^1$
S	180	5.6	$(3.2 \pm 1.2) \times 10^2$	5.5	$(1.3 \pm 0.1) \times 10^2$	5.6	$(6.0 \pm 0.6) \times 10^1$
MXA	1	3.2	$(6.7 \pm 7.4) \times 10^2$	3.2	$(1.1 \pm 0.3) \times 10^3$	3.4	$(2.2 \pm 2.4) \times 10^2$
MXA	14	3.3	$(1.1 \pm 0.4) \times 10^3$	3.3	$(7.3 \pm 5.0) \times 10^2$	3.5	$(4.0 \pm 0.6) \times 10^2$
MXMOPS	1	6.5	$(1.0 \pm 0.9) \times 10^3$	6.5	$(3.1 \pm 3.2) \times 10^2$	6.5	$(7.3 \pm 13) \times 10^1$
MXMOPS	17	6.4	$(2.6 \pm 0.8) \times 10^3$	6.4	$(8.5 \pm 7.5) \times 10^2$	6.4	$(5.4 \pm 1.5) \times 10^2$
MXTRIS	1	7.1	$(1.9 \pm 1.5) \times 10^3$	7.1	$(2.4 \pm 0.4) \times 10^3$	7.1	$(7.2 \pm 2.2) \times 10^1$
MXTRIS	14	6.9	$(3.8 \pm 3.7) \times 10^2$	6.8	$(7.8 \pm 11) \times 10^2$		

Dilute Solution

Test Type	Time (day)	Bentonite		Shale		Limestone	
		pH	K_d (cm^3/g)	pH	K_d (cm^3/g)	pH	K_d (cm^3/g)
MX	1	8.3	$(2.1 \pm 0.2) \times 10^3$	8.4	$(1.3 \pm 0.2) \times 10^3$	8.3	$(4.8 \pm 2.0) \times 10^2$
MX	7	8.1	$(3.7 \pm 0.8) \times 10^3$	8.1	$(2.7 \pm 0.9) \times 10^3$	8.1	$(8.0 \pm 6.0) \times 10^2$
MX	14	8.2	$(2.8 \pm 0.2) \times 10^3$	8.3	$(1.1 \pm 0.1) \times 10^3$	8.4	$(6.5 \pm 6.6) \times 10^2$
MX	93	7.8	$(1.8 \pm 3.0) \times 10^3$	7.8	$(2.5 \pm 0.4) \times 10^3$	7.9	$(1.1 \pm 0.0) \times 10^3$
MX	187	6.9	$(1.4 \pm 2.4) \times 10^3$	7.1	$(2.2 \pm 0.3) \times 10^3$	7.4	$(9.2 \pm 1.8) \times 10^2$
S	27	7.9	$(5.7 \pm 2.4) \times 10^2$	7.8	$(6.5 \pm 3.0) \times 10^2$	7.9	$(9.4 \pm 13) \times 10^1$
S	183	7.3	$(1.6 \pm 0.7) \times 10^3$	7.4	$(7.3 \pm 0.5) \times 10^2$	7.6	$(2.4 \pm 0.3) \times 10^2$
MXA	1	3.9	$(5.9 \pm 3.6) \times 10^2$	4.0	$(4.7 \pm 0.7) \times 10^2$	4.3	$(4.6 \pm 5.2) \times 10^1$
MXA	14	3.8	$(1.3 \pm 1.2) \times 10^3$	3.9	$(2.9 \pm 5.0) \times 10^2$	4.2	$(2.0 \pm 1.8) \times 10^2$
MXMOPS	1	6.5	$(6.4 \pm 5.6) \times 10^2$	6.5	$(9.4 \pm 16) \times 10^1$	6.5	$(2.6 \pm 4.5) \times 10^1$
MXMOPS	17	6.4	$(1.9 \pm 0.2) \times 10^3$	6.4	$(6.3 \pm 5.5) \times 10^2$	6.4	$(3.9 \pm 1.4) \times 10^2$
MXMES	1	7.2	$(1.1 \pm 0.3) \times 10^3$	7.3	$(6.3 \pm 1.4) \times 10^2$	7.3	$(2.9 \pm 2.4) \times 10^2$

MX: multiple elements test
S: single element test
MXA: multiple elements with acetate pH buffer
MXMOPS: multiple elements with MOPS pH buffer
MXTRIS: multiple elements with TRIS pH buffer
MXMES: multiple elements with MES pH buffer

Table 6: Palladium Sorption Coefficients from Batch Tests

SR-270-PW Brine

Test Type	Time (day)	Bentonite		Shale		Limestone	
		pH	K_d (cm^3/g)	pH	K_d (cm^3/g)	pH	K_d (cm^3/g)
MX	1	6.3	$(1.5 \pm 0.6) \times 10^4$	6.3	$(9.1 \pm 3.0) \times 10^3$	6.4	$(2.2 \pm 0.0) \times 10^3$
MX	8	6.2	$(4.4 \pm 6.4) \times 10^3$	6.3	$(4.0 \pm 1.7) \times 10^3$	6.2	$(4.3 \pm 0.0) \times 10^3$
MX	14	6.3	$(2.4 \pm 4.2) \times 10^2$	6.3	$(1.4 \pm 0.6) \times 10^4$	6.3	$(2.2 \pm 0.2) \times 10^4$
S	7	6.2	$(1.4 \pm 0.3) \times 10^2$	6.1	$(4.2 \pm 0.1) \times 10^1$	6.0	$(1.2) \times 10^2$
S	28	6.2	$(5.7 \pm 0.7) \times 10^3$			6.1	$(2.4 \pm 0.1) \times 10^3$
S	180	5.7	$(1.4 \pm 0.0) \times 10^4$	5.6	$(1.3 \pm 0.0) \times 10^4$	5.7	$(1.7 \pm 0.8) \times 10^3$
MXA	1	3.2	$(6.1 \pm 0.1) \times 10^2$				
MXA	14	3.3	$(5.7 \pm 3.5) \times 10^2$	3.3	$(9.0 \pm 4.4) \times 10^2$	3.5	$(3.8 \pm 5.9) \times 10^1$
MXMOPS	1	6.5	$(6.0 \pm 1.5) \times 10^2$	6.5	$(5.2 \pm 9.1) \times 10^1$	6.5	$(5.5 \pm 5.0) \times 10^1$
MXMOPS	17	6.4	$(2.4 \pm 2.2) \times 10^2$	6.4	$(3.5 \pm 5.5) \times 10^2$	6.4	$(4.9 \pm 5.5) \times 10^1$
MXMOPS	104	6.0	$(1.4 \pm 0.6) \times 10^5$	6.1	$(1.1 \pm 0.2) \times 10^4$	6.0	$(4.6 \pm 1.8) \times 10^4$
MXTRIS	1			7.1	$(8.8 \pm 11) \times 10^1$		
MXTRIS	14	6.9	$(3.8 \pm 4.6) \times 10^2$	6.8	$(5.2 \pm 6.0) \times 10^2$		

Dilute Solution

Test Type	Time (day)	Bentonite		Shale		Limestone	
		pH	Kd (cm3/g)	pH	Kd (cm3/g)	pH	K_d (cm^3/g)
MX	93	7.8	$(7.3 \pm 2.1) \times 10^4$	7.8	$(8.5 \pm 7.6) \times 10^4$	7.9	$(2.6 \pm 2.3) \times 10^4$
MX	187	6.9	$(4.1 \pm 5.1) \times 10^4$	7.1	$(5.4 \pm 2.7) \times 10^4$	7.4	$(1.4 \pm 1.8) \times 10^5$
S	7	7.8	$(7.5 \pm 2.8) \times 10^6$	7.7	$(4.3 \pm 0.3) \times 10^6$	7.8	$(3.4 \pm 1.3) \times 10^5$
S	29	7.9	$(1.6 \pm 0.3) \times 10^5$	8.0	$(5.3 \pm 1.6) \times 10^4$	8.1	$(2.0 \pm 2.20) \times 10^5$
S	183	7.6	$(3.5 \pm 0.5) \times 10^6$	7.7	$(1.1 \pm 1.4) \times 10^6$	7.8	$(2.1 \pm 1.2) \times 10^5$
MXA	1	3.9	$(1.3 \pm 0.5) \times 10^4$	4.0	$(5.6 \pm 0.6) \times 10^3$	4.3	$(2.5 \pm 0.2) \times 10^2$
MXA	14	3.8	$(3.5 \pm 1.2) \times 10^4$	3.9	$(1.6 \pm 0.2) \times 10^4$	4.2	$(4.0 \pm 1.5) \times 10^4$
MXMOPS	17	6.4	$(2.4 \pm 2.2) \times 10^2$	6.4	$(3.5 \pm 5.5) \times 10^2$	6.4	$(4.9 \pm 5.5) \times 10^1$
MXMES	1	7.2	$(2.3 \pm 0.6) \times 10^3$	7.3	$(1.0 \pm 0.2) \times 10^3$	7.3	$(8.3 \pm 2.6) \times 10^2$

MX: multiple elements test
S: single element test
MXA: multiple elements with acetate pH buffer
MXMOPS: multiple elements with MOPS pH buffer
MXTRIS: multiple elements with TRIS pH buffer
MXMES: multiple elements with MES pH buffer

Table 7: Zirconium Sorption Coefficients from Batch Tests

SR-270-PW Brine

Test Type	Time (day)	Bentonite		Shale		Limestone	
		pH	K_d (cm^3/g)	pH	K_d (cm^3/g)	pH	K_d (cm^3/g)
MX	1	6.3	$(3.5 \pm 3.0) \times 10^3$	6.3	$(3.0 \pm 1.0) \times 10^3$	6.4	$(1.8 \pm 3.2) \times 10^2$
MX	8	6.2	$(4.2 \pm 0.8) \times 10^3$			6.2	$(3.3 \pm 4.6) \times 10^2$
MX	14	6.3	$(1.8 \pm 1.9) \times 10^3$	6.3	$(9.7 \pm 2.5) \times 10^2$	6.3	$(2.1 \pm 2.3) \times 10^2$
MX	28	6.3	$(4.9 \pm 4.0) \times 10^2$	6.3	$(3.2 \pm 1.1) \times 10^2$	6.3	$(1.3 \pm 0.5) \times 10^2$
MX	195	5.9	$(1.3 \pm 1.3) \times 10^3$	5.6	$(3.3 \pm 2.3) \times 10^2$	5.7	$(3.1 \pm 3.9) \times 10^2$
S	1	6.3	$(3.6 \pm 0.8) \times 10^3$	6.3	$(9.1 \pm 2.5) \times 10^2$	6.3	$(1.5 \pm 2.1) \times 10^2$
S	14	6.5	$(8.7 \pm 0.2) \times 10^3$	6.5	$(2.2 \pm 3.1) \times 10^3$	6.5	$(4.7 \pm 4.1) \times 10^3$
S	89	6.2	$(3.2 \pm 4.5) \times 10^3$	6.2	$(1.6 \pm 2.2) \times 10^3$	6.3	$(1.3 \pm 0.0) \times 10^3$
S	180	6.0	$(1.5 \pm 0.2) \times 10^4$	6.1	$(7.8 \pm 0.3) \times 10^3$	6.1	$(3.4 \pm 0.4) \times 10^3$
MXA	1	3.2	$(6.3 \pm 3.7) \times 10^2$	3.2	$(2.0 \pm 1.7) \times 10^2$	3.4	$(1.4 \pm 2.4) \times 10^1$
MXA	14			3.3	$(3.2 \pm 4.5) \times 10^2$	3.5	$(9.1 \pm 16) \times 10^1$
MXMOPS	17	6.4	$(1.0 \pm 1.8) \times 10^4$	6.4	$(1.7 \pm 0.3) \times 10^4$	6.4	$(6.9 \pm 0.6) \times 10^3$
MXMOPS	104	6.0	$(3.4 \pm 2.0) \times 10^4$	6.1	$(2.0 \pm 0.2) \times 10^4$	6.0	3.3×10^1
MXTRIS	1	7.1	$(7.3 \pm 13) \times 10^2$	7.1	$(3.0 \pm 5.2) \times 10^1$		
MXTRIS	14	6.9	$(1.1 \pm 1.6) \times 10^4$	6.8	$(1.0 \pm 1.4) \times 10^4$		

Dilute Solution

Test Type	Time (day)	Bentonite		Shale		Limestone	
		pH	K_d (cm^3/g)	pH	K_d (cm^3/g)	pH	K_d (cm^3/g)
MX	14	8.2	$(9.1 \pm 2.4) \times 10^3$	8.3	$(3.7 \pm 0.6) \times 10^3$	8.4	$(1.2 \pm 0.0) \times 10^3$
MX	93	7.8	$(1.0 \pm 0.7) \times 10^5$	7.8	$(8.5 \pm 0.4) \times 10^4$	7.9	$(3.4 \pm 0.0) \times 10^4$
MX	187	6.9	$(5.9 \pm 4.6) \times 10^4$	7.1	$(5.5 \pm 1.1) \times 10^3$	7.4	$(1.3 \pm 0.3) \times 10^3$
S	1	7.6	$(7.1 \pm 4.7) \times 10^4$	7.7	$(4.4 \pm 0.1) \times 10^4$	7.9	$(1.9 \pm 0.1) \times 10^4$
S	27	7.9	$(1.1 \pm 0.1) \times 10^5$	8.0	$(5.0 \pm 0.2) \times 10^4$	8.0	$(2.2 \pm 0.1) \times 10^4$
S	183	7.6	$(2.7 \pm 0.4) \times 10^4$	7.7	$(2.0 \pm 0.0) \times 10^4$	8.0	$(9.1 \pm 5.5) \times 10^3$
MXA	1					4.3	$(9.9 \pm 0.2) \times 10^3$
MXA	14	3.8	$(2.8 \pm 0.2) \times 10^4$	3.9	3.7×10^4	4.2	$(1.2 \pm 0.3) \times 10^4$
MXMOPS	17			6.4	$(5.8 \pm 1.0) \times 10^2$	6.4	$(1.7 \pm 1.5) \times 10^2$
MXMES	1	7.2	$(1.5 \pm 0.2) \times 10^3$	7.3	$(8.4 \pm 0.7) \times 10^2$	7.3	$(1.2 \pm 2.1) \times 10^2$

MX: multiple elements test
S: single element test
MXA: multiple elements with acetate pH buffer
MXMOPS: multiple elements with MOPS pH buffer
MXTRIS: multiple elements with TRIS pH buffer
MXMES: multiple elements with MES pH buffer

Table 8: Tin Sorption Coefficients from Batch Tests

SR-270-PW Brine

Test Type	Time (day)	Bentonite		Shale		Limestone	
		pH	K_d (cm^3/g)	pH	K_d (cm^3/g)	pH	K_d (cm^3/g)
MX	8	6.2	$(1.4 \pm 2.4) \times 10^1$	6.3	$(6.8 \pm 12) \times 10^0$	6.2	
MX	14	6.3	$(4.5 \pm 3.9) \times 10^3$	6.3	$(3.4 \pm 0.1) \times 10^3$	6.3	$(1.3 \pm 0.0) \times 10^3$
MX	28	6.3	$(1.7 \pm 1.3) \times 10^4$	6.3	$(2.3 \pm 1.4) \times 10^4$	6.3	$(6.0 \pm 0.0) \times 10^3$
MX	195	5.9	$(1.4 \pm 0.0) \times 10^4$	5.6	$(6.7 \pm 0.2) \times 10^3$	5.7	$(2.7 \pm 0.0) \times 10^3$
S	1	6.3	$(3.7 \pm 0.1) \times 10^4$	6.3	$(3.0 \pm 1.8) \times 10^4$	6.3	$(6.9 \pm 0.1) \times 10^3$
S	14	6.2	$(9.5 \pm 0.2) \times 10^4$	6.2	$(4.4 \pm 0.1) \times 10^4$	6.2	$(1.8 \pm 0.0) \times 10^4$
S	89	6.3	$(9.5 \pm 0.2) \times 10^4$	6.3	$(4.4 \pm 0.1) \times 10^4$	6.3	$(1.8 \pm 0.0) \times 10^4$
S	180	5.4	$(7.9 \pm 0.2) \times 10^3$	5.5	$(3.6 \pm 0.1) \times 10^3$	5.4	$(1.5 \pm 0.0) \times 10^3$
MXA	1			3.2	$(6.4 \pm 0.1) \times 10^2$	3.4	$(5.6 \pm 4.8) \times 10^2$
MXA	14	3.3	$(9.0 \pm 7.8) \times 10^2$	3.3	$(6.6 \pm 0.2) \times 10^2$	3.5	$(1.4 \pm 0.0) \times 10^3$
MXMOPS	1	6.5	$(2.6 \pm 2.3) \times 10^3$			6.5	-
MXMOPS	17	6.4	$(4.2 \pm 0.8) \times 10^3$	6.4	$(1.5 \pm 1.4) \times 10^3$	6.4	$(9.9 \pm 0.4) \times 10^2$
MXMOPS	104	6.0	$(2.2 \pm 1.4) \times 10^4$	6.1	$(1.1 \pm 0.3) \times 10^4$	6.0	$(4.6 \pm 1.9) \times 10^3$
MXTRIS	1	7.1	$(2.7 \pm 2.4) \times 10^3$	7.1	$(6.8 \pm 12) \times 10^2$		
MXTRIS	14	6.9	$(2.7 \pm 2.4) \times 10^3$	6.8	$(3.0 \pm 3.3) \times 10^3$	6.8	$(6.5 \pm 5.6) \times 10^2$

Dilute Solution

Test Type	Time (day)	Bentonite		Shale		Limestone	
		pH	K_d (cm^3/g)	pH	K_d (cm^3/g)	pH	K_d (cm^3/g)
MX	7	8.1	$(1.4 \pm 0.4) \times 10^5$	8.1	$(9.0 \pm 3.1) \times 10^4$	8.1	$(2.5 \pm 0.7) \times 10^4$
MX	14	8.2	$(7.5 \pm 1.5) \times 10^4$	8.3	$(5.8 \pm 1.8) \times 10^4$	8.4	$(2.2 \pm 1.2) \times 10^4$
MX	93	7.8	$(7.2 \pm 2.3) \times 10^4$	7.8	$(1.2 \pm 1.3) \times 10^5$	7.9	$(4.4 \pm 5.3) \times 10^4$
MX	187	6.9	$(6.1 \pm 1.1) \times 10^4$	7.1	$(2.9 \pm 1.5) \times 10^4$	7.4	$(9.0 \pm 4.8) \times 10^3$
S	1	7.8	$(1.2 \pm 0.4) \times 10^5$	7.7	$(1.2 \pm 0.0) \times 10^5$	7.8	$(3.8 \pm 1.3) \times 10^4$
S	27	8.0	$(7.9 \pm 2.3) \times 10^4$	8.0	$(4.7 \pm 0.9) \times 10^4$	8.1	$(3.4 \pm 1.7) \times 10^4$
S	183	7.6	$(5.9 \pm 2.8) \times 10^4$	7.6	$(6.4 \pm 1.5) \times 10^4$	7.9	$(3.0 \pm 0.1) \times 10^4$
MXA	1	3.9	$(1.3 \pm 1.2) \times 10^3$	4.0	$(8.9 \pm 7.7) \times 10^2$	4.3	$(3.1 \pm 2.7) \times 10^2$
MXA	14	3.8	$(7.2 \pm 0.9) \times 10^4$	3.9	$(8.5 \pm 2.2) \times 10^4$	4.2	$(2.6 \pm 0.7) \times 10^4$
MXMOPS	1	6.5	$(2.6 \pm 2.3) \times 10^3$				
MXMOPS	17	6.4	$(1.4 \pm 4.5) \times 10^3$	6.4	$(5.1 \pm 4.5) \times 10^2$	6.4	$(3.3 \pm 0.2) \times 10^2$
MXMES	1	7.2	$(8.5 \pm 2.0) \times 10^4$	7.3	$(6.0 \pm 1.7) \times 10^4$	7.3	$(2.8 \pm 0.5) \times 10^4$

MX: multiple elements test
S: single element test
MXA: multiple elements with acetate pH buffer
MXMOPS: multiple elements with MOPS pH buffer
MXTRIS: multiple elements with TRIS pH buffer
MXMES: multiple elements with MES pH buffer

Table 9: Thorium Sorption Coefficients from Batch Tests

SR-270-PW Brine

Test Type	Time (day)	Bentonite		Shale		Limestone	
		pH	K_d (cm^3/g)	pH	K_d (cm^3/g)	pH	K_d (cm^3/g)
MX	1	6.3	$(1.1 \pm 0.0) \times 10^4$	6.3	$(3.5 \pm 3.0) \times 10^3$	6.4	
MX	8	6.2	$(1.1 \pm 0.0) \times 10^4$	6.3	$(5.3 \pm 0.1) \times 10^3$	6.2	$(2.1 \pm 0.0) \times 10^3$
MX	14	6.3	$(3.4 \pm 0.0) \times 10^3$	6.3	$(2.7 \pm 1.7) \times 10^3$	6.3	$(2.1 \pm 0.5) \times 10^3$
MX	28	6.3	$(7.1 \pm 6.8) \times 10^3$				
MX	195	5.9	$(5.1 \pm 0.0) \times 10^3$	5.6	$(3.4 \pm 1.4) \times 10^3$	5.7	$(2.0 \pm 0.0) \times 10^3$
S	1	6.2	$(3.3 \pm 0.9) \times 10^3$	6.3	$(1.1 \pm 0.0) \times 10^3$	6.2	$(1.7 \pm 2.5) \times 10^2$
S	14	6.2	$(8.6 \pm 3.6) \times 10^3$	6.1	$(1.7 \pm 0.5) \times 10^3$	6.2	$(6.0 \pm 2.5) \times 10^2$
S	89	6.2	$(6.4 \pm 2.7) \times 10^3$	6.2	$(4.3 \pm 1.4) \times 10^3$	6.2	$(2.1 \pm 0.1) \times 10^3$
S	180	6.2	$(1.6 \pm 0.1) \times 10^4$	6.2	$(6.8 \pm 1.1) \times 10^3$	6.5	$(2.7 \pm 0.0) \times 10^3$
MXA	1	3.2	$(8.0 \pm 0.9) \times 10^3$	3.2	$(3.7 \pm 6.5) \times 10^1$	3.4	$(1.6 \pm 2.8) \times 10^1$
MXA	14	3.3	$(4.4 \pm 3.8) \times 10^2$	3.3	$(2.2 \pm 3.9) \times 10^2$	3.5	$(2.6 \pm 0.5) \times 10^3$
MXMOPS	1	6.5	$(9.9 \pm 1.9) \times 10^3$	6.5	$(5.3 \pm 0.5) \times 10^3$	6.5	$(2.2 \pm 0.4) \times 10^3$
MXMOPS	17	6.4	$(1.7 \pm 0.1) \times 10^4$	6.4	$(1.1 \pm 0.0) \times 10^4$	6.4	$(5.1 \pm 0.5) \times 10^3$
MXMOPS	104	6.0	$(1.8 \pm 0.6) \times 10^4$	6.1	$(7.9 \pm 0.9) \times 10^3$	6.0	5.6×10^2
MXTRIS	1	7.1	$(1.1 \pm 0.3) \times 10^4$	7.1	$(5.7 \pm 1.8) \times 10^3$	7.1	$(1.2 \pm 0.4) \times 10^3$
MXTRIS	14	6.9	$(2.4 \pm 1.5) \times 10^4$	6.8	$(2.1 \pm 1.3) \times 10^4$	6.8	$(4.5 \pm 1.2) \times 10^3$

Dilute Solution

Test Type	Time (day)	Bentonite		Shale		Limestone	
		pH	K_d (cm^3/g)	pH	K_d (cm^3/g)	pH	K_d (cm^3/g)
MX	1	8.3	$(8.1 \pm 8.7) \times 10^4$	8.4	$(2.1 \pm 0.8) \times 10^5$	8.3	$(7.5 \pm 2.0) \times 10^4$
MX	7	8.1	$(2.5 \pm 3.4) \times 10^4$	8.1	$(3.1 \pm 0.3) \times 10^4$	8.1	$(1.9 \pm 0.5) \times 10^4$
MX	14			8.3	$(5.2 \pm 1.1) \times 10^4$	8.4	$(2.1 \pm 1.4) \times 10^4$
MX	93	7.8	$(1.8 \pm 4.9) \times 10^3$	7.8	$(5.7 \pm 3.7) \times 10^4$	7.9	$(2.8 \pm 3.0) \times 10^4$
MX	187			7.1	3.3×10^4	7.4	$(9.3 \pm 6.3) \times 10^3$
S	1	7.8	$(1.0 \pm 0.9) \times 10^5$	7.8	$(3.6 \pm 1.7) \times 10^4$	7.7	$(4.6 \pm 1.3) \times 10^4$
S	27	8.3	$(3.0 \pm 0.7) \times 10^4$	8.3	$(1.4 \pm 0.1) \times 10^5$	8.4	$(2.6 \pm 1.3) \times 10^5$
S	183	7.7	$(4.4 \pm 2.1) \times 10^4$	7.9	$(2.4 \pm 2.2) \times 10^5$	8.1	$(1.4 \pm 0.4) \times 10^5$
MXA	1	3.9	$(2.2 \pm 0.7) \times 10^4$	4.0	$(1.2 \pm 0.3) \times 10^4$	4.3	$(4.0 \pm 1.0) \times 10^3$
MXA	14	3.8	$(5.0 \pm 1.7) \times 10^4$	3.9	$(4.9 \pm 0.9) \times 10^4$	4.2	$(1.6 \pm 1.0) \times 10^4$
MXMOPS	1	6.5	$(1.2 \pm 0.6) \times 10^3$	6.5	$(4.7 \pm 0.8) \times 10^2$	6.5	$(2.4 \pm 2.1) \times 10^2$
MXMOPS	17	6.4	$(6.0 \pm 0.6) \times 10^3$	6.4	$(4.0 \pm 0.8) \times 10^3$	6.4	$(2.2 \pm 0.3) \times 10^3$
MXMES	1	7.2	$(1.0 \pm 0.5) \times 10^5$	7.3	$(3.2 \pm 3.4) \times 10^5$	7.3	$(8.1 \pm 1.0) \times 10^4$

MX: multiple elements test
S: single element test
MXA: multiple elements with acetate pH buffer
MXMOPS: multiple elements with MOPS pH buffer
MXTRIS: multiple elements with TRIS pH buffer
MXMES: multiple elements with MES pH buffer

2.2.1 **Effect of Sorption Time**

The long term sorption tests were performed to further the understanding of sorption kinetics and to establish whether sorption reactions have reached equilibrium or steady state.

The K_d values from multiple elements and single element sorption tests were not significantly different, suggesting that the elements Cs, Pd, Zr, Sn and Th did not compete for the same sorption sites or else their concentrations on the surface sites were too low to cause interferences. The data from both multiple elements and single element tests were used to evaluate the effect of sorption time. The variation of K_d values as a function of time from brine and dilute solutions are compared in Figures 2 to 6.

Figure 2 shows the variation of Cs K_d values in brine and dilute solution as a function of time. In brine the Cs K_d values appear to have reached maximum values on bentonite and shale within 1 day, while the maximum K_d value for limestone was reached after 14 days. Following this initial sorption values, K_d values decreased and then increased, with K_d values at 195 days similar to the K_d values measured after one day. In dilute solution maximum K_d values are reached after 7 days, which was followed by a steady state. The Cs K_d values were lower in brine compared to dilute solution, which was expected due to the competitive sorption of cations (e.g. Na, Ca, K) in the brine solution. If one uses the geometric means given in Table 10 and Table 11 as a comparison, the K_d values in brine were lower than in dilute solution for bentonite, shale and limestone by factors of 4, 7 and 3, respectively.

The variation in Pd sorption with time in brine and dilute solution is illustrated in Figure 3. Palladium steady state K_d values in dilute solution were about an order of magnitude higher than in brine based on the geometric means given in Table 10 and Table 11. In brine the highest K_d values were observed after 1 day for bentonite and 14 days for shale and limestone, with K_d values at 180 days similar to the highest K_d values for bentonite and shale. At about 180 days the data point for shale overlaps the bentonite data point. In dilute solution the highest K_d values for all solids were observed after 7 days, indicating that the steady state took no longer than 7 days to achieve. Using geometric means for comparison, Pd sorption in brine was lower than in dilute solution on bentonite, shale and limestone by factors of 920, 120 and 130, respectively. The lower K_d values and longer time to reach steady state in brine indicate that the competitive sorption of cations in brine and the complexation of Pd by Cl had significantly suppressed Pd sorption in brine.

Figure 4 summarizes the effect of time on Zr sorption in brine and dilute solution. The Zr K_d values in brine were lower than in dilute solution on bentonite, shale and limestone by factors of 20, 11 and 12, respectively. The Zr K_d values do not indicate a consistent increase in brine solution after 14 days for bentonite, shale and limestone. In dilute solution Zr sorption appears to have reached a steady state by about 27 days.

The sorption of Sn in brine and dilute solution as a function of time is summarized in Figure 5. Tin sorption in brine was lower than in dilute solution on bentonite, shale and limestone by factors of 4, 7 and 7, respectively. The Sn K_d values in brine did not show any significant increases after 28 days, while in dilute solution a steady state was achieved after 1 to 7 days.

Figure 6 summarizes the variation in Th K_d values in brine and dilute solution as a function of time. Thorium sorption on bentonite, shale and limestone was lower in brine compared to dilute

solution by factors of 3, 21 and 27, respectively. The brine solution contains F^- which complexes with Th (e.g., about 30% of Th is ThF_2^{+2} and 9% is ThF^{+3} in SR-270-PW brine based on speciation calculation by PHEEQC with SIT database, see table 25) and may be responsible for the significantly reduced Th sorption on shale and limestone. Thorium sorption appears to reach steady state very quickly in both brine (8 days) and dilute solution (1 day).

In summary, the times for sorption reactions to reach an apparent maximum in brine and dilute solution ranged from 1 day to 28 days. In all cases the K_d values measured in brine were lower than in dilute solution. However, the reduction in K_d values was element dependent. The greatest reduction in K_d values (between brine and dilute solution) was for Pd, followed in order of decreasing effect by Th, Zr, Sn and Cs. The reduction in Pd K_d values is most likely because all of the Pd in brine is present as negatively charged Cl^- complexes, while in dilute solution Pd is present only as OH complexes (as surface species attached to exposed oxygens of the rock samples). In brine close to 40% of Th is associated with F^- complexes, which could account for reduced Th sorption in brine. The reduction of Cs sorption in brine (factors 3 to 7) is rather small, considering that over half of the Cs in brine is a neutral Cl^- complex and the brine contains a high salt concentration that is expected to reduce the sorption of all alkalis. The most likely explanation for Cs sorption in brine is for the ability of Cs to displace other alkali elements from the interlayers of clay minerals. The solution chemistries of both Zr and Sn are dominated by OH complexes in both brine and dilute solution, yet both elements displayed reduced sorption in brine. This suggests that the competitive sorption of cations (e.g., Ca, Na, K) in the brine solution was able to reduce the sorption sites available to Zr and Sn in some way.

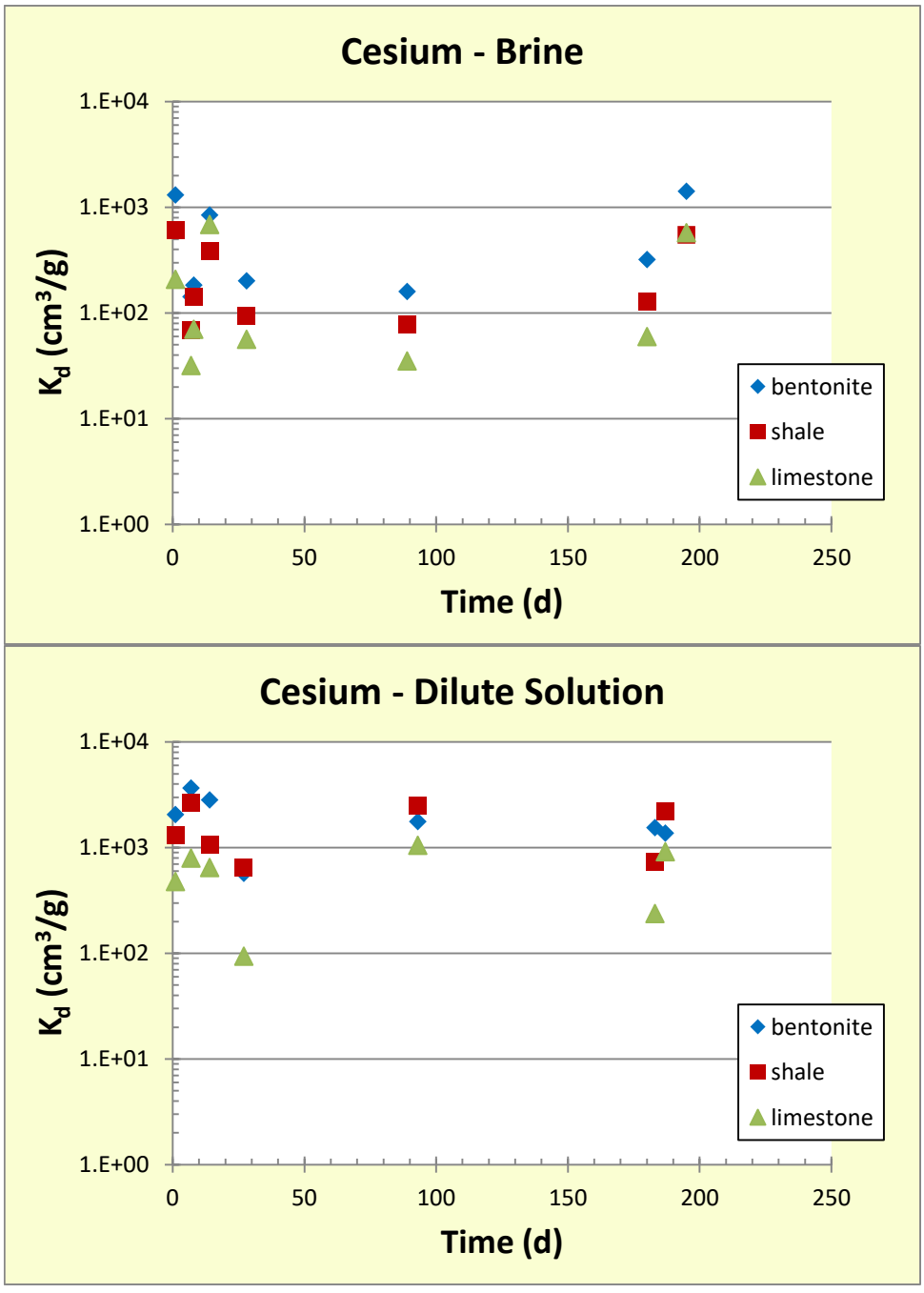


Figure 2: Cesium Sorption as a Function of Time on Bentonite, Shale and Limestone in Brine (*I* = 6.0 M) and Dilute solution (*I* = 0.01 M)

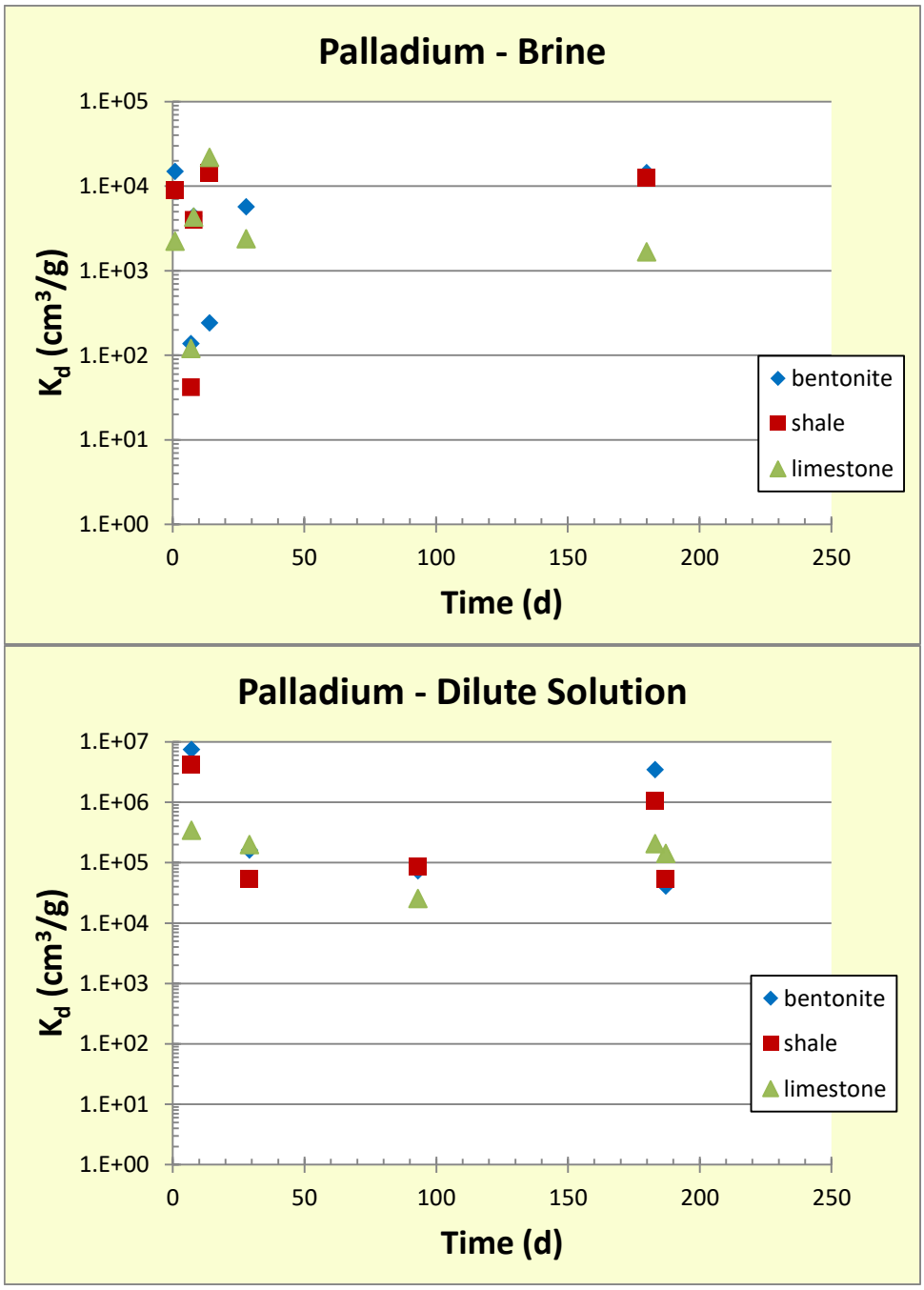


Figure 3: Palladium Sorption as a Function of Time on Bentonite, Shale and Limestone in Brine (*I* = 6.0 M) and Dilute solution (*I* = 0.01 M)

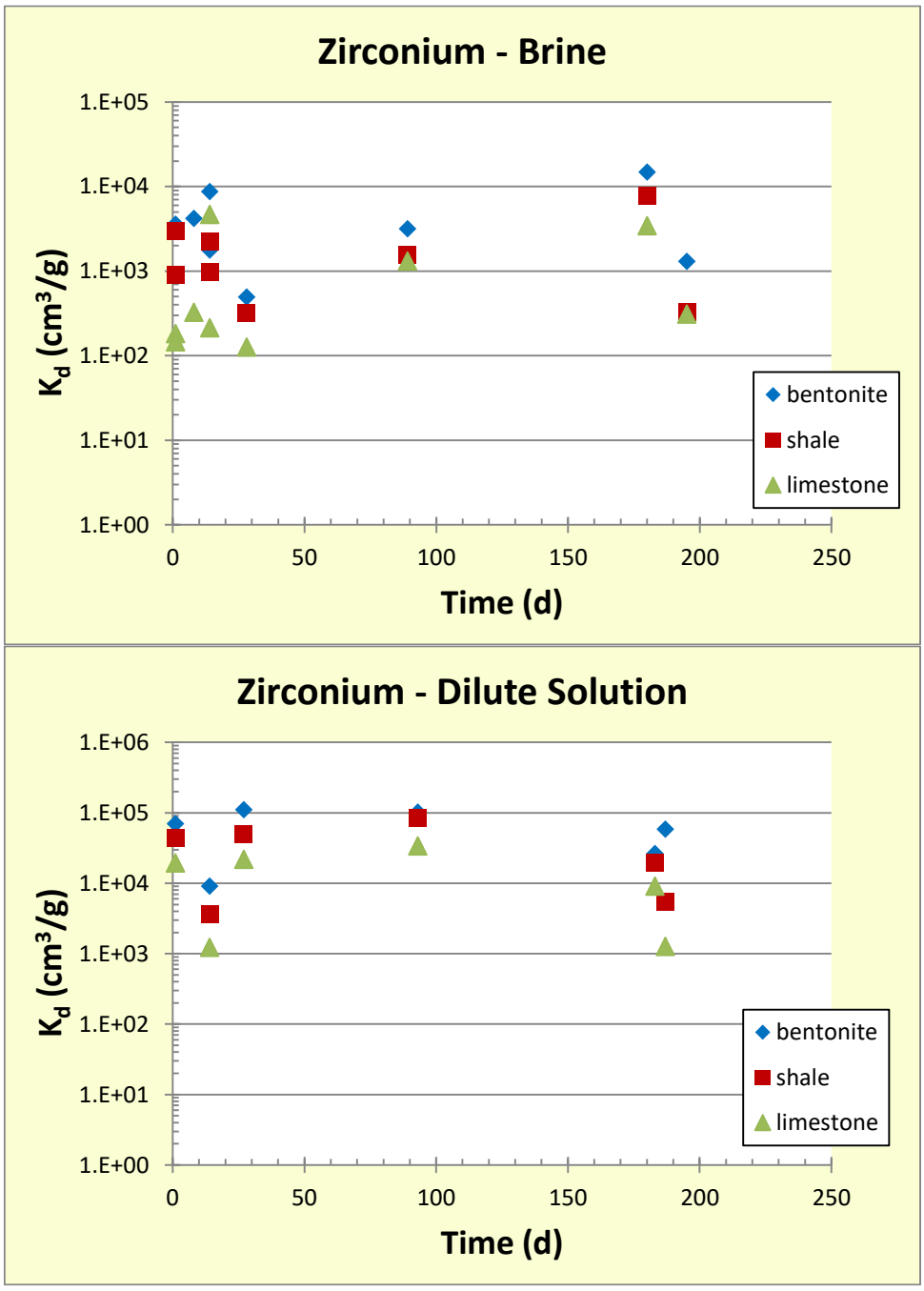


Figure 4: Zirconium Sorption as a Function of Time on Bentonite, Shale and Limestone in Brine (*I* = 6.0 M) and Dilute Solution (*I* = 0.01 M)

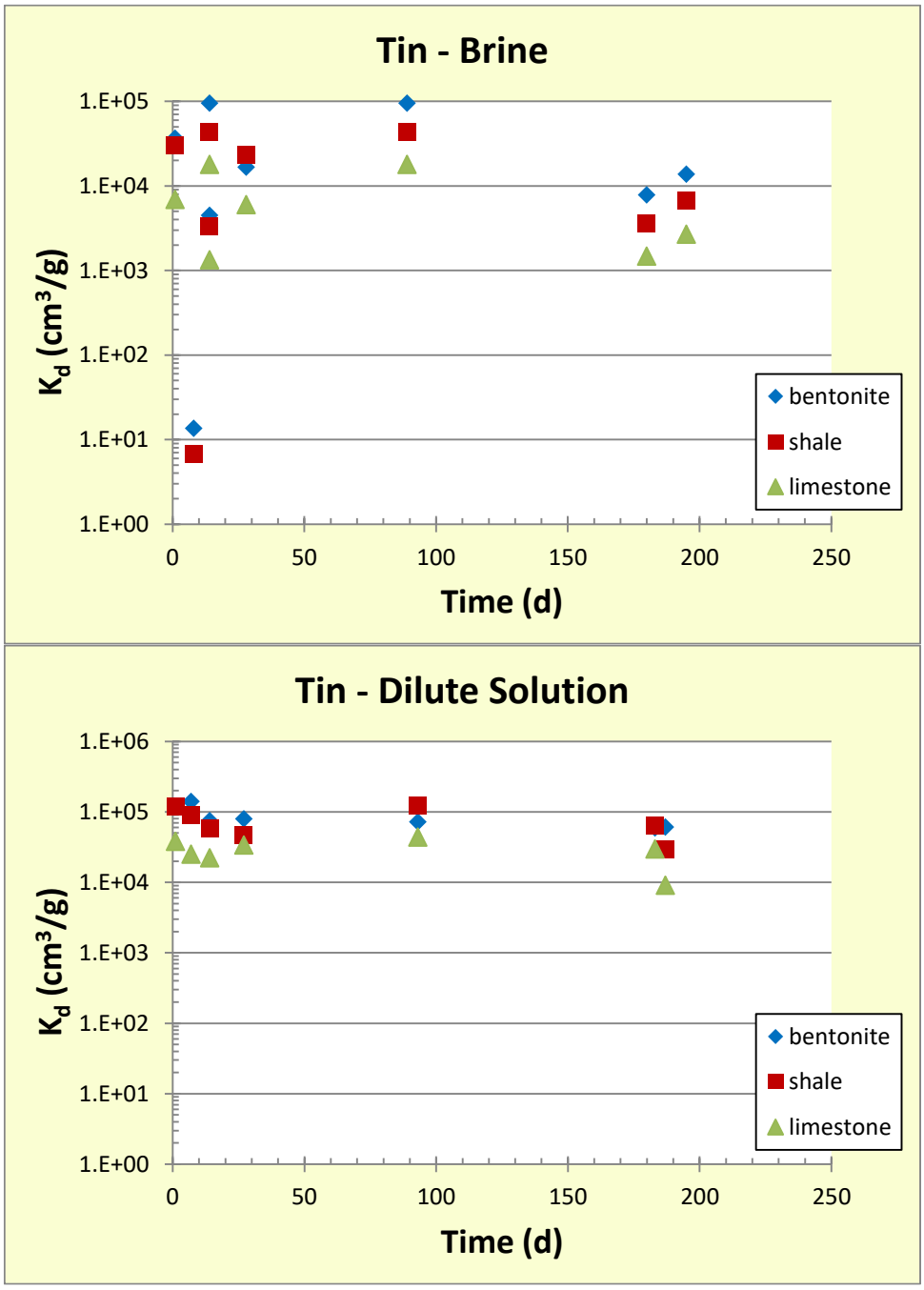


Figure 5: Tin Sorption as a Function of Time on Bentonite, Shale and Limestone in Brine (*I* = 6.0 M) and Dilute Solution (*I* = 0.01 M)

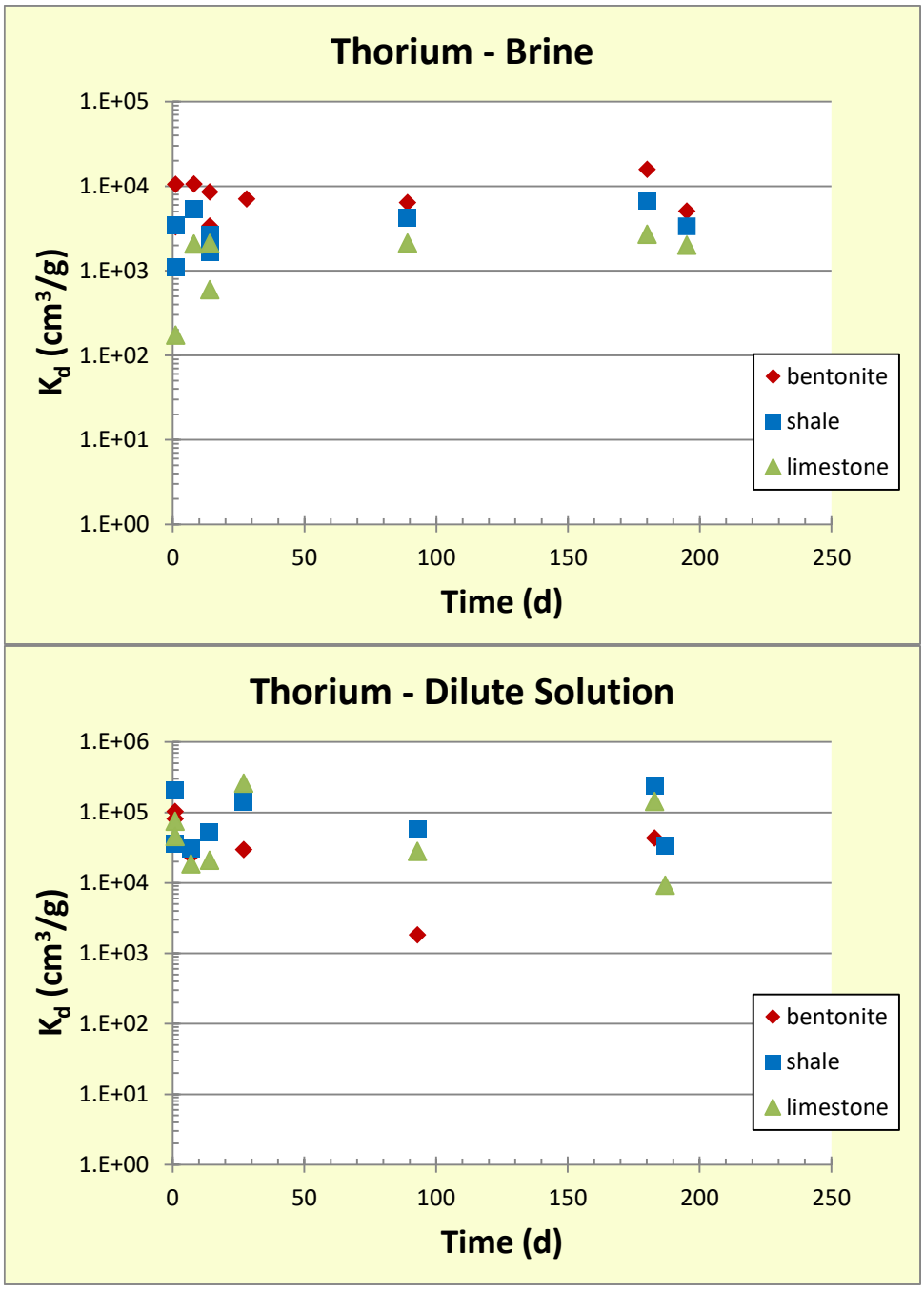


Figure 6: Thorium Sorption as a Function of Time on Bentonite, Shale and Limestone in Brine (*I* = 6.0 M) and Dilute Solution (*I* = 0.01 M)

2.2.2 **Effect of pH**

Sorption measurements were performed over a broad range of solution pH values (approximately pH 3 to 8) to evaluate the effect of pH on sorption and to provide sorption data for comparison to the results of sorption modelling. The K_d values measured as a function of pH for Cs, Pd, Zr, Sn and Th on bentonite, shale and limestone are summarized in Figure 7 through to Figure 11. The figures include results from the reference brine and dilute solutions, plotted together for ease of comparison.

Figure 7 shows Cs sorption as a function of pH (indicated value by pH meter) using separate plots for bentonite, shale and limestone. For any given pH there was significant variability in K_d values in both brine and dilute solutions that was independent of pH. Due to this variability Cs sorption on all solids in brine appeared to be independent of pH. In dilute solution Cs sorption on bentonite appeared to be independent of pH, which is consistent with the findings by Wang et al. (2005). Given the data variability and the experimental uncertainty, Cs sorption on shale and limestone did not display a clear trend with pH. In no instance did Cs display a sorption edge, which is defined as a significant jump in sorption with increasing pH that occurs over a narrow pH range. K_d values on shale measured in brine (pH 6 to 6.4) are lower than K_d values measured in dilute solution (pH 7.8 to 8.4).

The Pd K_d values measured in brine and dilute solutions as a function of pH are illustrated in Figure 8. There is variability in the Pd K_d values that tends to mask variations with pH. There is too much variability in sorption around pH 6 in brine to define a clear trend for Pd sorption with pH on bentonite, shale and limestone. In dilute solution, Pd K_d values increase from pH 6 to pH 8. At the lower pH values, there is no significant trend in sorption variability with pH for any of the solids. The higher Pd K_d values around pH 8 in dilute solution would contribute to the higher average K_d values in dilute solution compared to brine.

Zirconium sorption in brine and dilute solution measured as a function of pH is summarized in Figure 9. The Zr sorption on bentonite and shale measured in brine displayed too much scatter to show any clear trends with pH. The Zr K_d values for sorption on limestone indicate higher sorption in the region around pH 6 compared to pH 3.8. However, the scatter in K_d values is still too large to display a clear trend. In dilute solution the scatter in Zr K_d values is also too large to define any clear trends with pH. Therefore, pH effects cannot be used to explain why the average Zr sorption in brine is lower than in dilute solution.

Figure 10 summarizes Sn sorption as a function of pH in brine and dilute solutions. In brine the scatter in Sn K_d values masks any clear trends with pH. The Sn K_d values determined in dilute solution did not display any trends with pH, mainly due to the variability in K_d values. The effect of pH on sorption does not explain the lower average Sn sorption measured in the reference brine (pH around 6) compared to the reference dilute solution (pH around 8).

The variation in Th K_d values as a function of pH for brine and dilute solutions is shown in Figure 11. In brine the measured Th sorption on shale increased from pH 3 to pH 7. Thorium sorption on bentonite and limestone did not display any clear trends with pH due to variability in K_d values. The Th K_d values measured in dilute solution did not display any clear trends with pH for any of the solids. Therefore, pH effects do not account for the difference in average Th K_d values measured in brine compared to dilute solution.

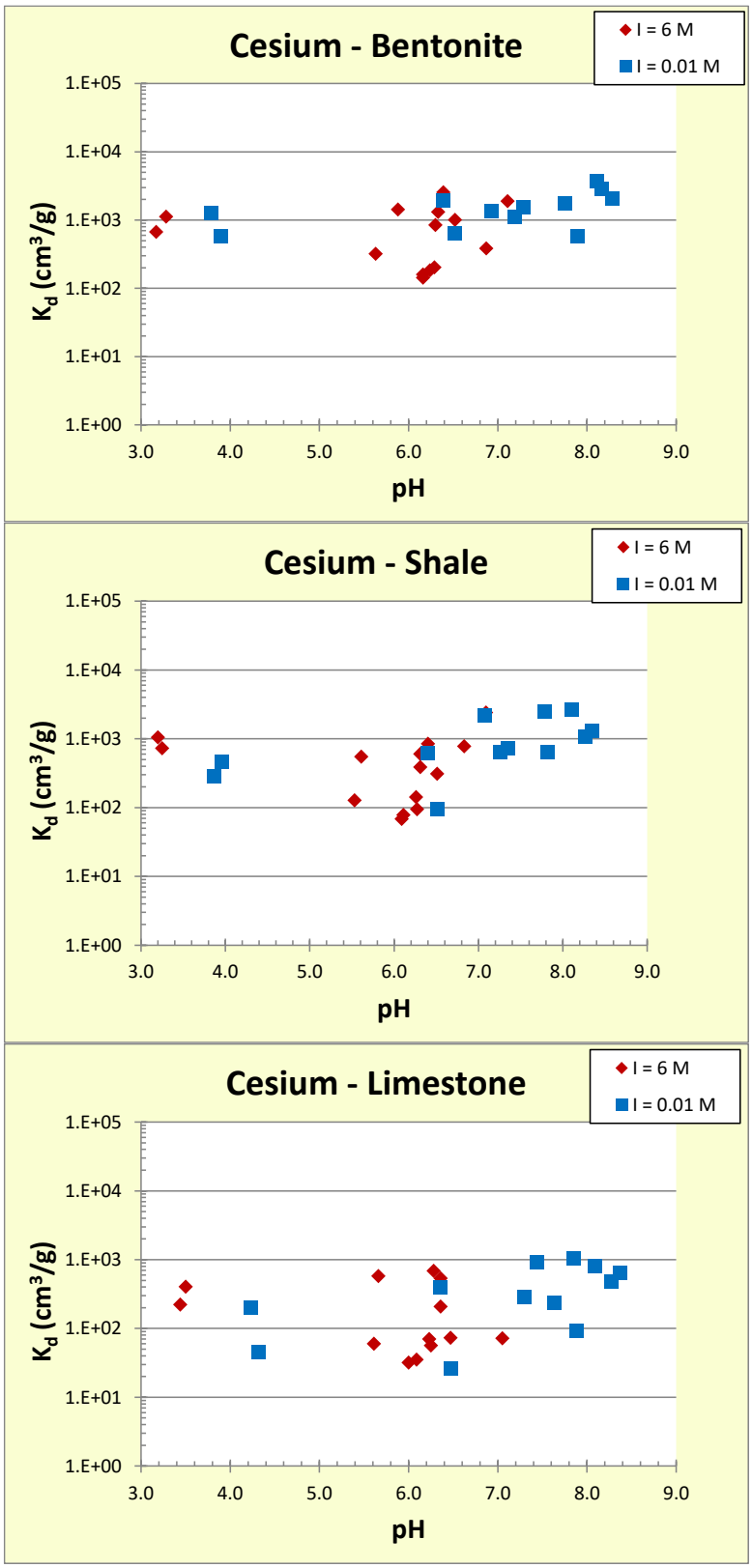


Figure 7: Cesium Sorption as a Function of pH on Bentonite, Shale and Limestone in Brine (*I* = 6.0 M) and Dilute Solution (*I* = 0.01 M)

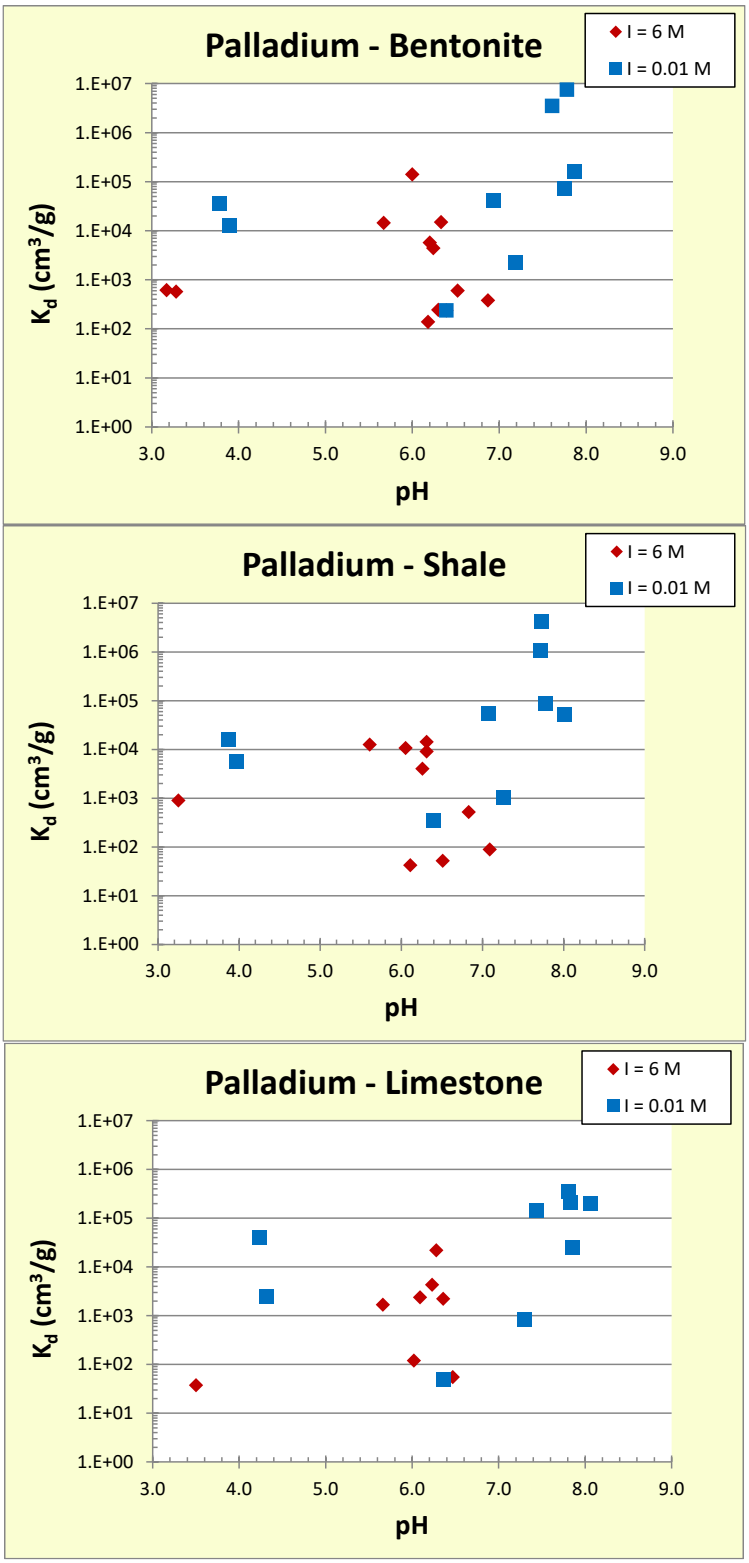


Figure 8: Palladium Sorption as a Function of pH on Bentonite, Shale and Limestone in Brine (*I* = 6.0 M) and Dilute Solution (*I* = 0.01 M)

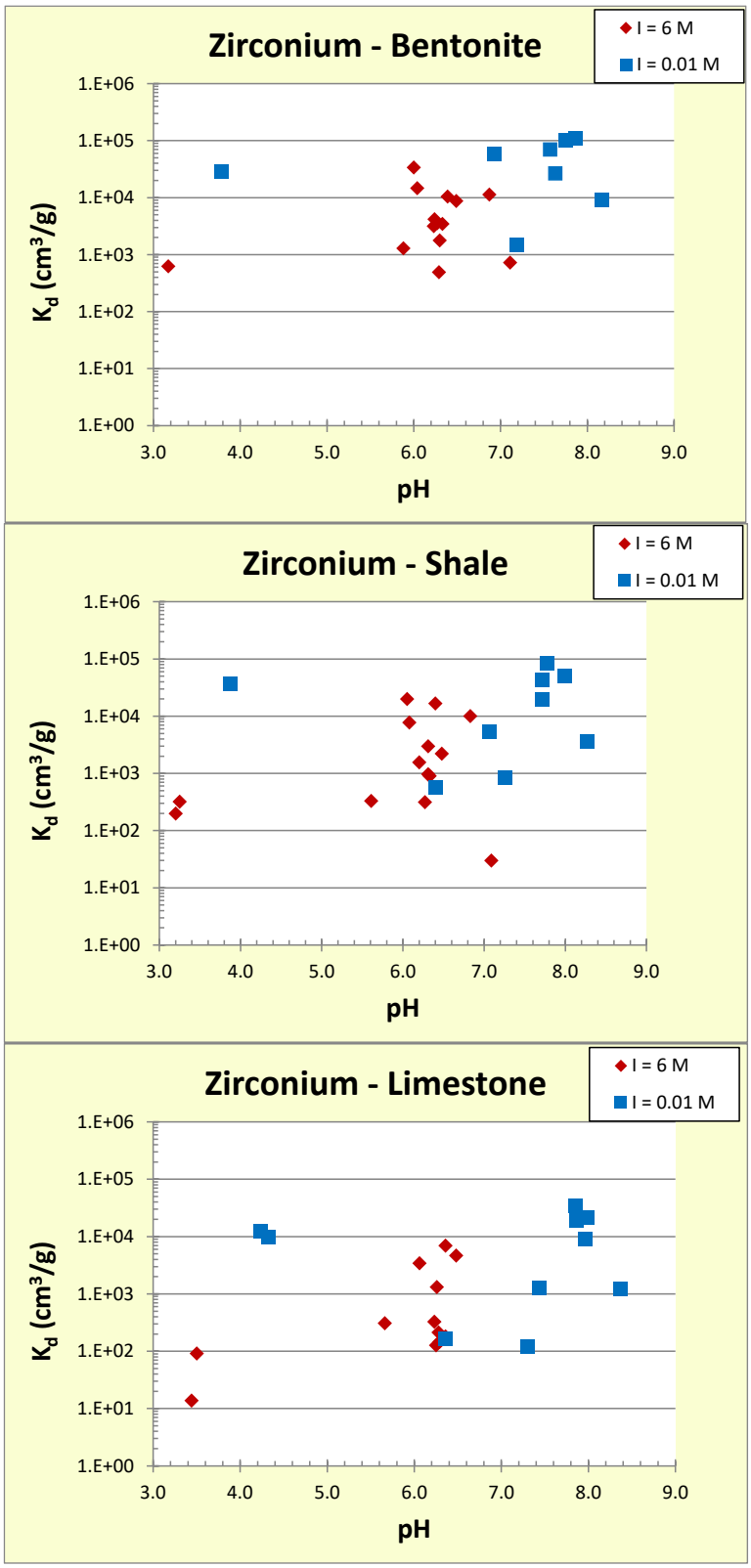


Figure 9: Zirconium Sorption as a Function of pH on Bentonite, Shale and Limestone in Brine (*I* = 6.0 M) and Dilute Solution (*I* = 0.01 M)

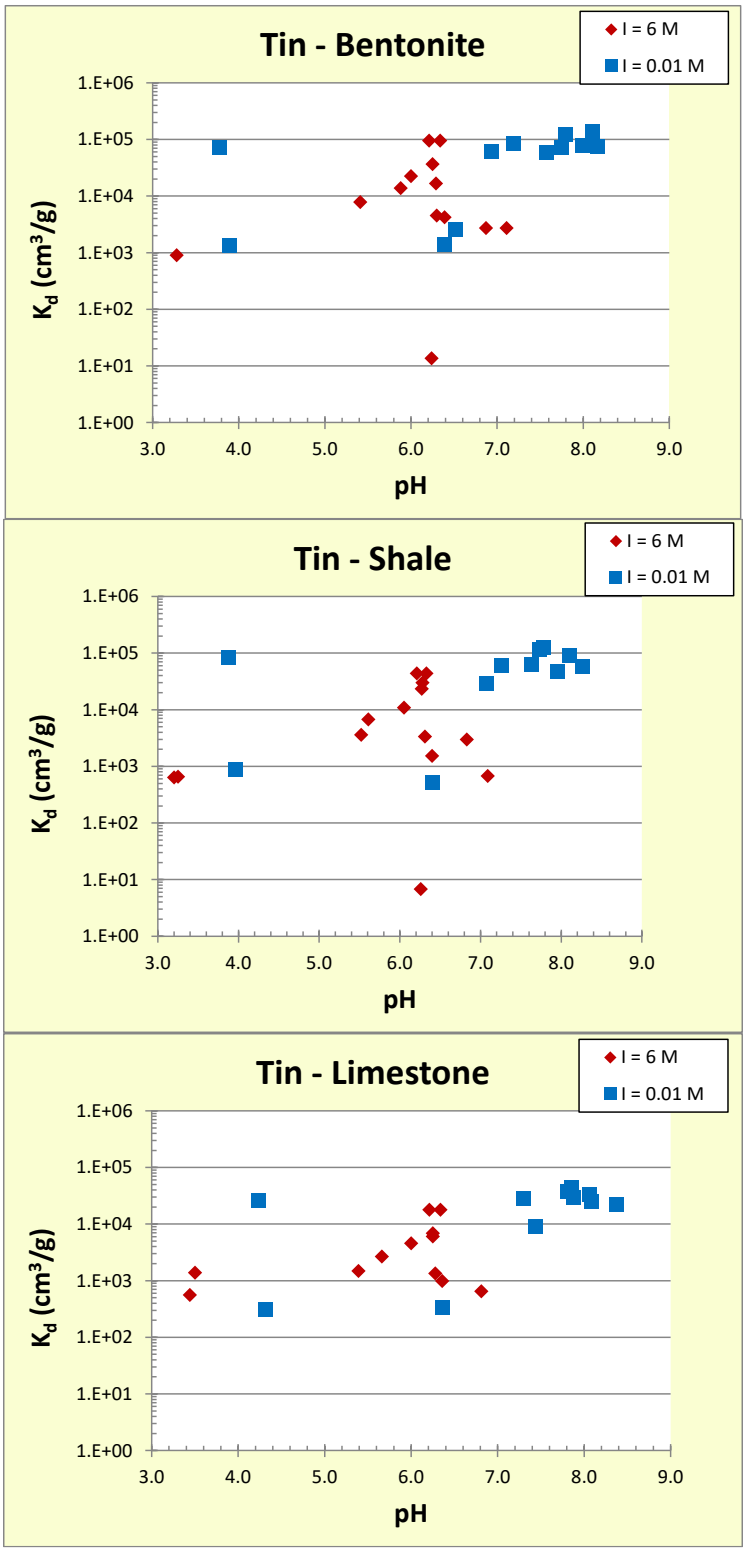


Figure 10: Tin Sorption as a Function of pH on Bentonite, Shale and Limestone in Brine (*I* = 6.0 M) and Dilute Solution (*I* = 0.01 M)

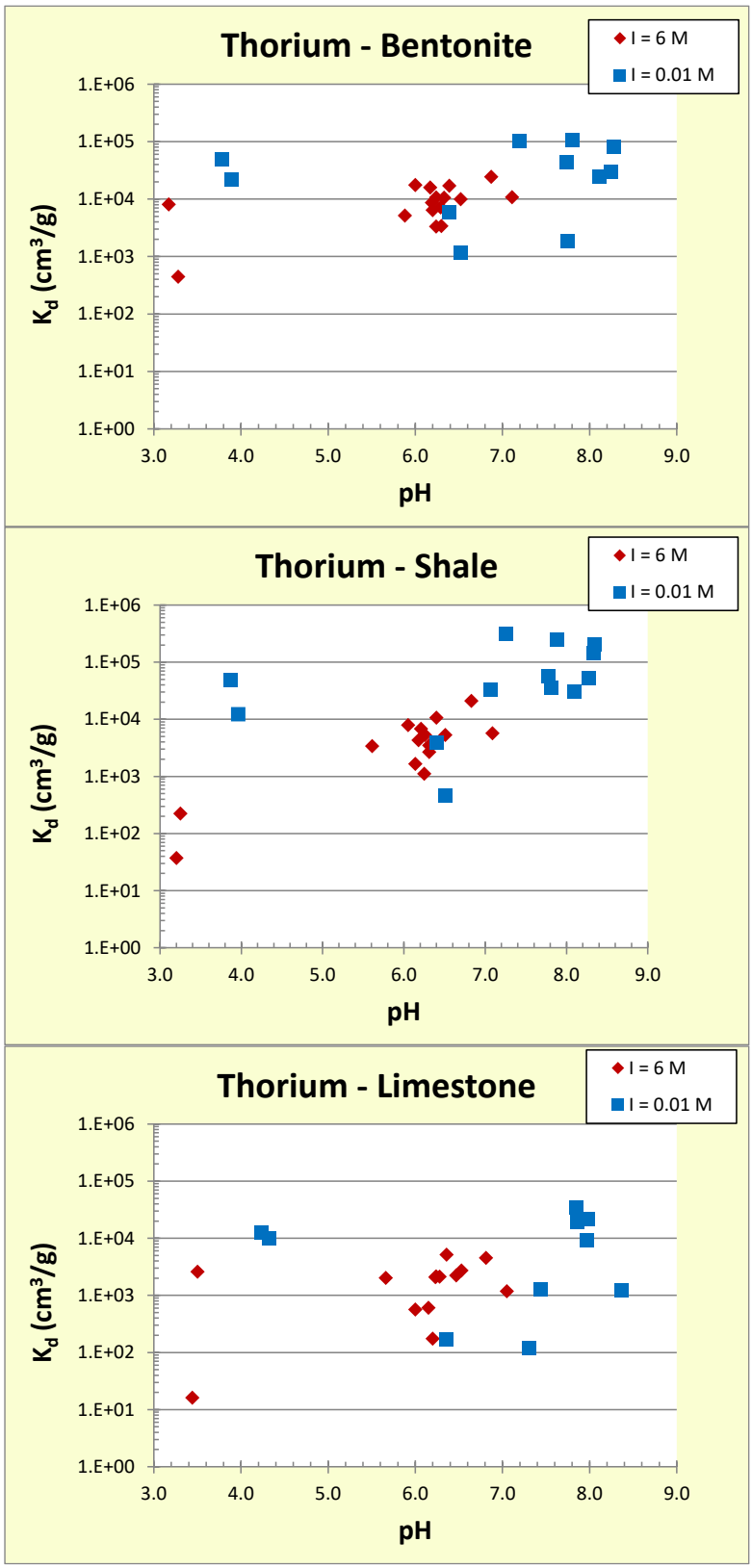


Figure 11: Thorium Sorption as a Function of pH on Bentonite, Shale and Limestone in Brine (*I* = 6.0 M) and Dilute Solution (*I* = 0.01 M)

2.2.3 **Desorption Test**

A desorption test was initiated immediately after completion of the long term, multiple elements sorption test in brine solution containing the MOPS pH buffer. Desorption was performed after a sorption time of 104 days by diluting the concentration of sorbate in solution. The concentration of remaining sorbate in solution was measured as a function of time for up to 8 days to determine whether the elements of interest were desorbing from the solid in response to having their solution concentrations diluted. The measured sorbate concentrations were used to calculate the desorption K_d values. These K_d values determined during the desorption phase are compared to a sorption coefficient (K_d^o) measured at the end of the 104 day sorption test that is assumed to represent the equilibrium state of sorption at the time desorption was inititiated. Expressing the desorption K_d value as the ratio K_d/K_d^o allows one to quantify how close to equilibrium the system may be. A K_d/K_d^o value of 1.0 indicates that the system is in equilibrium. If K_d/K_d^o values are greater than 1.0, the system is not in equilibrium because the sorbate has not desorbed in response to the decrease of sorbate concentration in solution. The observation of K_d/K_d^o values less than 1.0 suggests that the desorption process released excess sorbate from the surface, or else the estimated K_d^o value was too high. Given the observed standard deviation in K_d values observed at the end of sorption tests, the latter is a possibility. The results of desorption experiments for each element are summarized in Figure 12 through to Figure 16. Each figure includes a plot of the K_d values determined as a function of time for the sorption phase of the test, and a plot of K_d/K_d^o ratio as a function of desorption time.

The Cs desorption with time is summarized in Figure 12. The Cs concentrations observed in the Day 104 solution samples appeared to be high, resulting in an apparent desorption that dropped K_d values to 0. These high Cs concentrations were considered to be a measurement error. Strictly speaking, this made the evaluation of the Cs desorption data poorly defined. However, an attempt was made to evaluate the Cs desorption results using the measured sorption amounts from day 17.

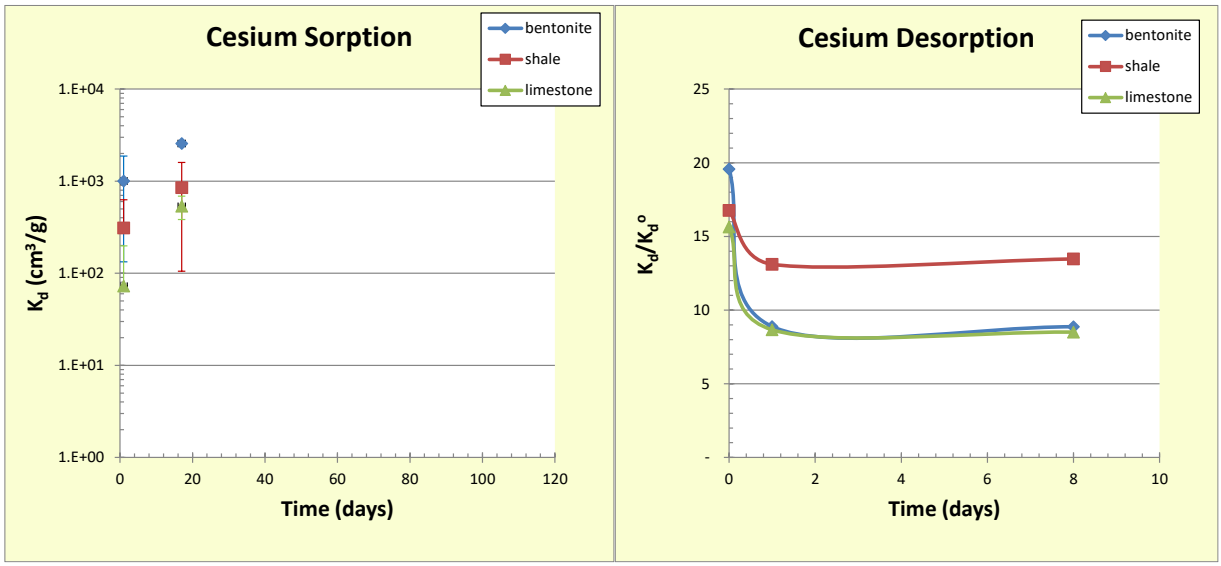


Figure 12: Cesium Desorption with Time on Bentonite, Shale and Limestone in Brine

At the time desorption was initiated the initial desorption K_d values, as shown by K_d/K_d^o values in Figure 12, were factors of 16 to 20 higher than the Day 17 K_d values. The increase in apparent K_d values when the Cs concentration in solution was reduced indicated that Cs was not able to desorb sufficiently rapidly to re-establish equilibrium. The desorption K_d values dropped after 1 day and then remained the same for the next 7 days. The stability in the desorption K_d values suggests no further Cs desorption. Since Cs is expected to be fixed in the interlayers of clay minerals (e.g., as observed by Sawhney (1972) and Eberl (1980)), this is not surprising.

The Pd desorption as a function of time is summarized in Figure 13. Palladium desorption was evaluated using the amounts of sorbed Pd determined at day 104 (i.e. highest Pd K_d values observed). When desorption was initiated, the desorption K_d/K_d^o values for bentonite and limestone were close to 1 if experimental errors are considered, while the desorption K_d/K_d^o value for shale was 5.7. This indicates that at the time of desorption, Pd sorption on bentonite and limestone had rapidly reached apparent equilibrium, while a fraction of the Pd on shale remained fixed on the solid. Desorption K_d/K_d^o values on bentonite and limestone increased after 1 day, and then stabilized over the next 7 days. Given the uncertainty in the K_d^o values determined from the sorption phase of the test, the K_d^o/K_d values for Pd sorption on bentonite and limestone indicate that the sorption process is reversible. Palladium sorption on shale continued to increase, and showed no evidence of desorption, which may represent an experimental error.

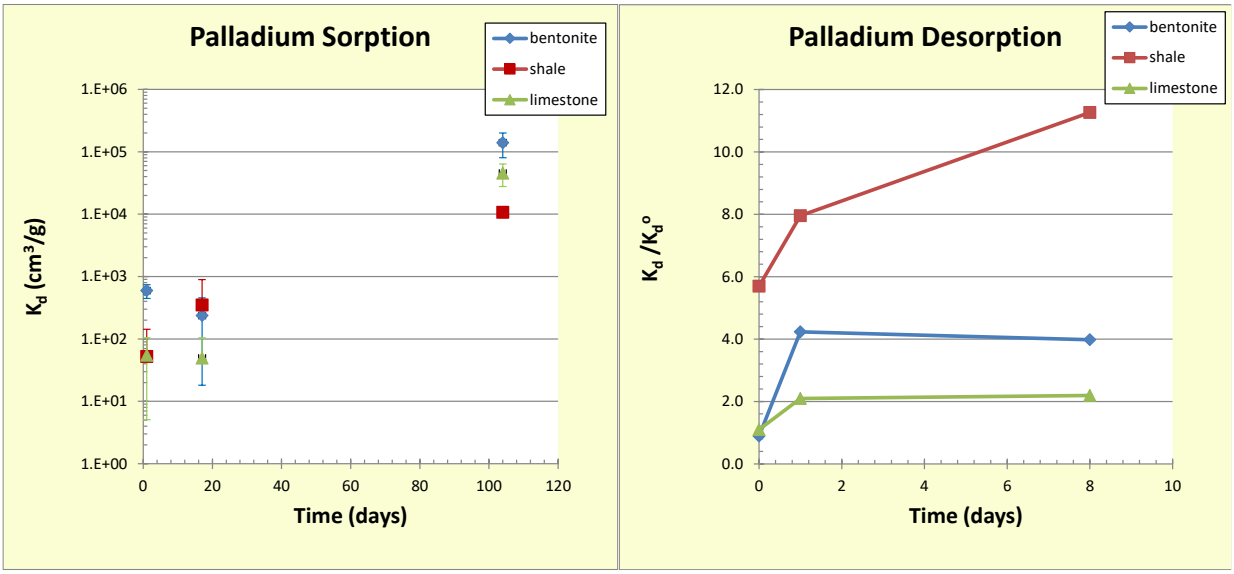


Figure 13: Palladium Desorption with Time on Bentonite, Shale and Limestone in Brine

Figure 14 presents the results of the Zr desorption with time. In the sorption phase Zr sorption displayed a progressive increase with time for bentonite and shale. Sorption on limestone peaked at 17 days and then decreased significantly by 104 days due to an apparent release of sorbed Zr to solution, which may represent an experimental error. Therefore, the desorption test data could not be used to follow Zr desorption on limestone.

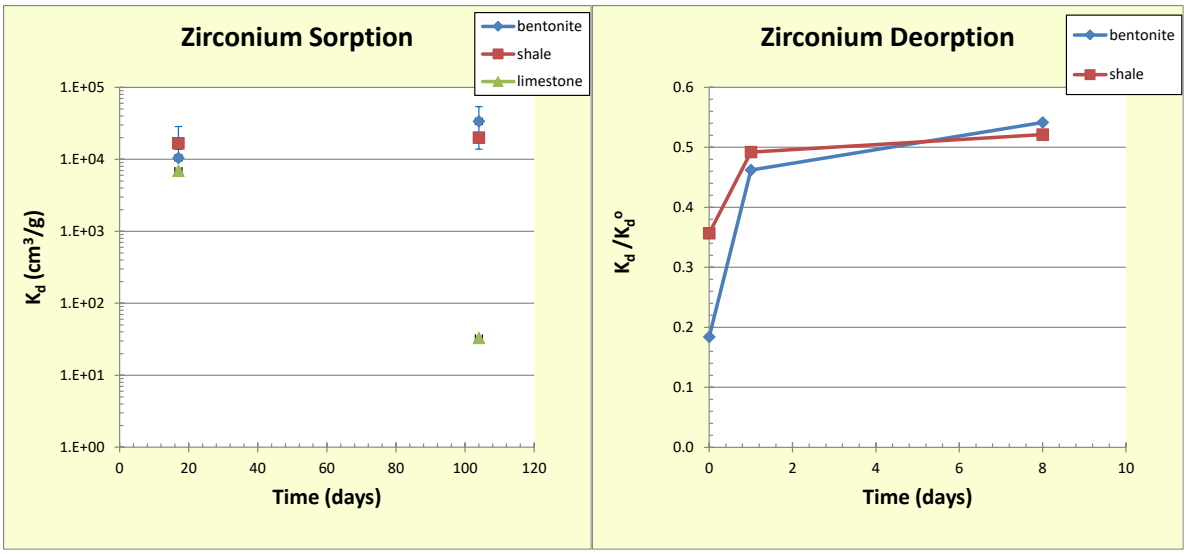


Figure 14: Zirconium Desorption with Time on Bentonite, Shale and Limestone in Brine

As indicated by the K_d^o/K_d values in Figure 14, the Zr desorption K_d values for betonite and shale were less than half of the K_d^o values values when the desorption tests were initiated. The K_d^o/K_d values increased with time, suggesting that Zr sorption on bentonite and shale may eventually reach the predesorption K_d values. These results, combined with the uncertainty in K_d^o values suggest that Zr sorption on bentonite and shale may be reversible.

The results of the Sn desorption with time are presented in Figure 15. In the sorption phase of these tests, Sn K_d values increased with time on all solids, reaching their highest values at 104 days. When desorption was initiated, the desorption K_d values for all solids dropped below K_d^o values before desorption, as shown by the K_d^o/K_d values in Figure 15. Desorption K_d values increased with time over the next 8 days, approaching predesorption values. Given the uncertainty in K_d^o values before desorption, the desorption K_d values after 8 days are not significantly different from K_d values before desorption. This suggests that Sn sorption is reversible.

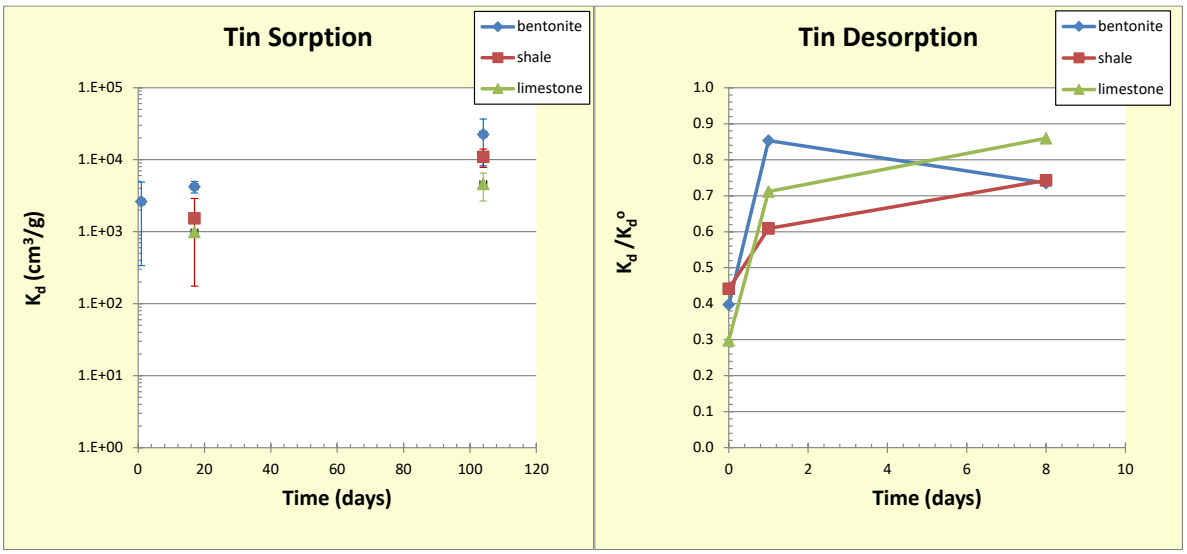


Figure 15: Tin Desorption with Time on Bentonite, Shale and Limestone in Brine

Figure 16 summarizes the results of Th desorption with time. In the sorption phase of these tests, Th sorption on bentonite and shale appears to have reached a steady state by 20 days. Sorption on limestone initially increased by 20 days but then decreased by 104 days. At the start of the desorption test, the Th desorption K_d values for all solids have dropped to one half of the K_d^o values before the desorption test. After 1 day, sorption on all solids has returned to apparent equilibrium values. However, as indicated by the K_d/K_d^0 values at day 8, sorption on limestone appeared to keep increasing, while sorption on the bentonite and shale remains at close to predesorption test values. These results indicate that Th sorption on bentonite and shale may be reversible. Considering the experimental errors, sorption on limestone may also be reversible, although it has not reached a steady state during the desorption experimental time of 8 days.

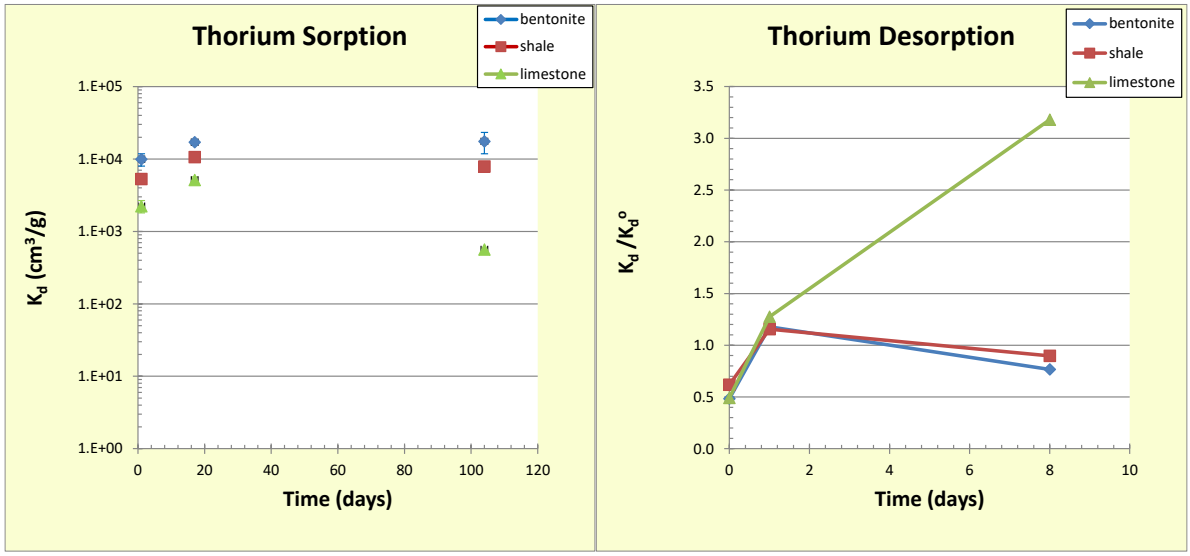


Figure 16: Thorium Desorption with Timeon Bentonite, Shale and Limestone in Brine

In summary, the sorption of Pd, Zr, Sn and Th appeared to be reversible for most solids. Cs sorption was not reversible, possibly due to fixation within clay mineral structures.

The K_d values that were selected to represent sorption in brine and dilute solutions were selected from tests with reaction times of 7 to 187 days at sorption apparent equilibrium. Single and multiple element tests (S and MX) were considered. Tests within the pH range of 5.6 to 6.5 were considered representative of brine solutions, while dilute solutions were represented by tests with pH values of 7.1 to 8.5. Table 10 summarizes K_d values for Cs, Pd, Zr, Sn and Th that are representative of brine solution. The table includes the range of K_d values observed for each solid. An average value was calculated along with a standard deviation that is given as an uncertainy. In many instances the magnitude of the standard deviation is greater than the average K_d values. Therefore, the geometric mean may be a better representation of K_d values that may facilitate comparisons between solids and elements. The geometric standard deviation given with each geometric mean, helps to characterize the full variation of observed K_d values. Sorption in dilute solution is summarized in Table 11.

Table 10: Batch Test K_d Values (cm^3/g) in Brine

Element	Solid	Range	Average	Geomean	n
Cs	bentonite	140 – 1,430	$(7.9 \pm 9.2) \times 10^2$	4.3×10^2 (3.3)	7
	shale	69 - 630	$(3.1 \pm 3.0) \times 10^2$	2.0×10^2 (2.8)	7
	limestone	32 - 690	$(2.9 \pm 3.0) \times 10^2$	1.4×10^2 (4.0)	7
Pd	bentonite	140 – 14,500	$(4.2 \pm 5.6) \times 10^3$	1.2×10^3 (7.5)	6
	shale	42 – 14,300	$(7.0 \pm 6.3) \times 10^3$	2.2×10^3 (11)	6
	limestone	49 – 22,000	$(5.1 \pm 8.4) \times 10^3$	1.1×10^3 (9.8)	6
Zr	bentonite	490 – 14,800	$(4.4 \pm 5.4) \times 10^3$	2.1×10^3 (3.8)	7
	shale	320 – 7,800	$(3.8 \pm 0.6) \times 10^3$	1.5×10^3 (4.3)	8
	limestone	130 – 4,700	$(2.1 \pm 2.6) \times 10^3$	8.0×10^2 (4.6)	8
Sn	bentonite	4,200 – 95,400	$(3.6 \pm 4.1) \times 10^4$	1.9×10^4 (3.6)	7
	shale	1,500 – 44,000	$(1.9 \pm 1.8) \times 10^4$	1.1×10^4 (3.6)	7
	limestone	990 – 18,000	$(7.4 \pm 7.5) \times 10^3$	4.4×10^3 (3.2)	7
Th	bentonite	3,380 – 15,900	$(1.0 \pm 0.5) \times 10^4$	8.9×10^3 (1.8)	9
	shale	1,700 – 6,800	$(5.3 \pm 3.0) \times 10^3$	4.6×10^3 (1.8)	8
	limestone	600 – 2,700	$(2.4 \pm 1.4) \times 10^3$	2.1×10^3 (1.9)	8

Geometric standard deviation given in brackets beside geometric mean value (Geomean)
n: number of data points included.

Table 11: Batch Test K_d Values (cm^3/g) in Dilute Solution

Element	Solid	Range	Average	Geomean	N
Cs	bentonite	570 – 2,820	$(2.1 \pm 1.2) \times 10^3$	1.8×10^3 (2.0)	5
	shale	650 – 2,650	$(1.5 \pm 1.0) \times 10^3$	1.3×10^3 (1.9)	5
	limestone	94 – 1,050	$(5.7 \pm 4.0) \times 10^2$	4.2×10^2 (2.7)	5
Pd	bentonite	41,300 – 7,500,000	$(2.2 \pm 3.3) \times 10^6$	1.1×10^6 (15)	5
	shale	53,600 – 4,300,000	$(1.1 \pm 1.8) \times 10^6$	2.6×10^5 (7.4)	5
	limestone	25,600 – 143,000	$(1.8 \pm 1.2) \times 10^5$	1.4×10^5 (3.6)	5
Zr	bentonite	9,110 – 112,000	$(6.3 \pm 5.2) \times 10^4$	4.1×10^4 (3.3)	4
	shale	3,670 – 85,000	$(3.2 \pm 3.5) \times 10^4$	1.6×10^4 (5.9)	4
	limestone	1,240 – 33,900	$(1.7 \pm 1.4) \times 10^4$	9.6×10^3 (4.3)	4
Sn	bentonite	59,000 – 140,700	$(8.5 \pm 2.9) \times 10^4$	8.2×10^4 (1.3)	6
	shale	47,100 – 123,600	$(7.4 \pm 2.8) \times 10^4$	7.0×10^4 (1.4)	6
	limestone	22,200 – 43,700	$(3.0 \pm 0.8) \times 10^4$	3.0×10^4 (1.3)	6
Th	bentonite	1,840 – 103,700	$(4.8 \pm 3.8) \times 10^4$	2.8×10^4 (4.3)	6
	shale	30,800 – 319,000	$(1.4 \pm 1.1) \times 10^5$	9.6×10^4 (2.5)	8
	limestone	18,600 – 263,000	$(8.5 \pm 8.3) \times 10^4$	5.7×10^4 (2.6)	8

Geometric standard deviation given in brackets beside the geometric mean value (Geomean)
n: number of data points included.

3. SURFACE COMPLEXATION MODELLING

Sorption modelling improves the understanding of sorption processes and has the potential for estimating sorption values that are applicable for in-situ groundwater compositions based on laboratory measured sorption values or sorption properties reported in the literature. For some elements, it may be possible to derive sorption values based on surface site binding constants that are estimated from Linear Free Energy Relationships (LFER) (Bradbury and Baeyens 2005b, 2009b). LFER assumes that for a given metal, there is a relationship between free energies of formation of aqueous complexes and thermodynamic properties of the metal ions or ligands. In surface chemistry, LFERs are presented as a linear correlation between the surface complexation constants on amphoteric surface hydroxyl sorption sites and the first hydrolysis constants for a list of metals. This relationship is established for a given solid using measured sorption values for a number of metals. Using this relationship one can estimate surface binding constants for other metals for which there are no measured data based on their aqueous hydrolysis constants.

It was assumed that montmorillonite and illite can be used to approximate the sorption properties of bentonite and shale. The major component of bentonite is montmorillonite (75 to 85 wt.%) and illite is representative of the clay component in shale (about 60 wt.%). The modelling objectives were: (1) to improve the understanding of sorption processes for previously studied elements (e.g., Ni) and elements that were tested in this study (Pd, Zr, Sn, Th); (2) to simulate the variation of sorption with solution chemistry, considering parameters such as pH, ionic strength, and concentrations of complexing anions (Cl, F, HCO_3); and (3) to develop tools and confidence to extrapolate sorption values to reference brine compositions for elements whose sorption data are not available under saline conditions.

3.1 **Approach**

Sorption modelling was performed with PRHEEQC, using the SIT thermodynamic database. PHREEQC (Parkhurst and Appelo 1999) incorporates a 2-site protolysis non-electrostatic surface complexation and cation exchange model (2SPNE SC/CE) as described by Baeyens and Bradbury (1997) and Bradbury and Baeyens (1997, 2005a, 2009a). This model assumes that sorption occurring on oxygen sites associated with broken bonds (located on edge sites in clay minerals) can be described by strong and weak amphoteric surface sites. It is also assumed that different minerals may contain the same basic type of sites, except with different site densities (to determine site capacities) and slightly different surface binding constants. Site densities and binding constants are determined from acid-base titrations of mineral surfaces (Baeyens and Bradbury 1997). Examples of acid-base surface reactions and associated protolysis constants determined in 0.1 mol/L $NaClO_4$ are given in Table 12. Sorption modelling with Ni is used as an example to illustrate the application of sorption modelling for predicting sorption processes. Site binding constants are determined by fitting metal sorption data covering a range of pH values and metal concentrations. Model fitting is time consuming because values of site density, protolysis constants and binding constants must be consistent with acid-base titration and sorption edge data (Bradbury and Baeyens 2005a). The constants for the surface complexes are considered to be independent of ionic strength and the activities of surface species are considered not to vary with ionic strength. Only the activities of dissolved species are calculated.

Table 12: Surface Protolysis Reactions and Protolysis Constants for Na-illite and Montmorillonite

Surface Protolysis Reaction	[a]log $K_{protolysis}$ Na-illite	[b]log $K_{protolysis}$ Montmorillonite
$\equiv S^sOH + H^+ \Leftrightarrow \equiv S^sOH_2^+$	4.0	4.5
$\equiv S^sOH \Leftrightarrow \equiv S^sO^- + H^+$	-6.2	-7.9
$\equiv S^{w1}OH + H^+ \Leftrightarrow \equiv S^{w1}OH_2^+$	4.0	4.5
$\equiv S^{w1}OH \Leftrightarrow \equiv S^{w1}O^- + H^+$	-6.2	-7.9
$\equiv S^{w2}OH + H^+ \Leftrightarrow \equiv S^{w2}OH_2^+$	8.5	6.0
$\equiv S^{w2}OH \Leftrightarrow \equiv S^{w2}O^- + H^+$	-10.5	-10.5

[a]Bradbury and Baeyens (2009a)
[b]Bradbury and Baeyens (2005b)

If sorption isotherms are not linear over the range of metal concentrations used to derive experimental data, a combination of strong and weak sites is required to explain the sorption data. Although strong surface sites, $\equiv S^sOH$, have a small surface density (site capacity), they sorb strongly and account for sorption at trace metal concentrations. The weaker sites have a much higher capacity, but weaker binding constants. The role of the weak sites, $\equiv S^{w1}OH$ and $\equiv S^{w2}OH$, is to account for non-linear sorption behaviour in the presence of high metal concentrations. If the sorption isotherm is linear, the sorption model could be limited to only one type of site. When elements have very low concentrations due to solubility restrictions, as for Th, the contribution of weak sites to the overall sorption process is not significant. Bradbury and Baeyens (2005b) did their original model development for montmorillonite and included both strong and weak sites. When work continued on illite, they chose to use only the strong sites. However, even if sorption can be described by one type of site, three sites are required to explain the acid-base titration data for clays.

Surface complexation reactions for metals are formulated by first considering the dominant aqueous species and which species are likely to sorb. The approach taken by Bradbury and Baeyens (1997) is to focus on the types of metal hydrolysis species that are present and then to formulate analogous surface species. For example, if the dominant hydroxyl Ni^{+2} species in solution is $NiOH^+$, the corresponding surface species is $\equiv S^sONi^+$. The surface species $\equiv S^sONi(OH)_2^-$ would be equivalent to $Ni(OH)_3^-$. The surface species has one less hydroxyl than the equivalent solution species. An example of surface complexation reactions and surface complexation constants for Ni sorbing on montmorillonite (determined in 0.01 to 0.1 mol/L $NaClO_4$ solutions) are provided in Table 13. The general equation used to formulate surface complexation reactions with a metal, Me, having a charge, z, is as follows:

$$\equiv S^sOH + Me^z + yH_2O \Leftrightarrow \equiv S^sOMe(OH)_y^{z-(y+1)} + (y+1)H^+ \qquad (5)$$

Table 13: Nickel Surface Complexation Reactions and Surface Complexation Constants for Na-Montmorillonite

Ni Surface Complexation Reaction	Strong Site log $^{s}K_{x-1}$ Montmorillonite	Weak Site log $^{w1}K_{x-1}$ Montmorillonite
$\equiv S^{s}OH + Ni^{+2} \Leftrightarrow \equiv S^{s}ONi^{+} + H^{+}$	-0.6	-
$\equiv S^{s}OH + Ni^{+2} + H_2O \Leftrightarrow \equiv S^{s}ONiOH^{0} + 2H^{+}$	-10	-
$\equiv S^{s}OH + Ni^{+2} + 2H_2O \Leftrightarrow \equiv S^{s}ONi(OH)_2^{-} + 2H^{+}$	-20	-
$\equiv S^{w1}OH + Ni^{+2} \Leftrightarrow \equiv S^{w1}ONi^{+} + H^{+}$	-	-3.3

From Bradbury and Baeyens (2005a)
-: no values

Sorption by coulombic cation exchange reactions can be described with the following exchange reaction describing the exchange of element B, having a charge of b, with element A on solid, having a charge a.

$$bA^{a}\text{-solid} + aB^{b} \Leftrightarrow aB^{b}\text{-solid} + bA^{a} \quad (6)$$

The thermodynamic exchange constant for the reaction can be defined as:

$$ {}^{B}_{A}K = \frac{(N_B)^a}{(N_A)^b} \times \frac{(f_B)^a}{(f_A)^b} \times \frac{[A]^b}{[B]^a} \times \frac{(\gamma_A)^b}{(\gamma_B)^a} = {}^{B}_{A}K_c \times \frac{(f_B)^a}{(f_A)^b} \quad (7)$$

The thermodynamic exchange constant is ${}^{B}_{A}K$, and ${}^{B}_{A}K_C$ is the selectivity coefficient that is valid when the fraction of B on the exchange sites is very small to avoid issues of nonideal mixing of A and B. The equivalent fractions of A and B located on the exchange sites are N_A and N_B, which are defined as equivalents of A or B sorbed per unit mass, divided by the Cation Exchange Capacity (CEC). The total amount of cations in the exchange sites is determined by the CEC which is given in terms of equivalents per mass of solid (equivalents/kg). The surface activity coefficients are f_A and f_B, while the aqueous activity coefficients are γ_A and γ_B. Aqueous concentrations are [A] and [B]. The distribution ratio between solid and solution ($^{B}R_d$) of element B that is attributed to cation exchange is defined as:

$$ {}^{B}R_d = \frac{Amount\ \ of\ sorbate\ \ B\ on\ solid\ per\ unit\ mass}{Sorbate\ \ aqueous\ \ concentration} \quad (8)$$

The value of $^{B}R_d$ can be related to the selectivity coefficient if the CEC and the solution activity coefficients are known (Bradbury and Baeyens 2005b).

$$ {}^{B}_{A}K_c = ({}^{B}R_d)^a \times \frac{(b)^a}{(CEC)^a} \times [A]^b \times \frac{(\gamma_A)^b}{(\gamma_B)^a} \quad (9)$$

In practice, it is assumed that the CEC of the sorbing solid is dominated by either Na or Ca. Selectivity coefficients with respect to Na or Ca are available for clay minerals for a number of

elements. When cation exchange is included in sorption modelling with a code such as PHREEQC, it is apparent that cation exchange of metals with Na or Ca is most important when the concentrations of Na and Ca in solution are low, and at lower pH values where the aqueous speciation of sorbing species is dominated by positively charged species. Cation exchange is not considered for elements dominated by neutral or anionic species.

Bradbury and Baeyens (2005a) used laboratory measured (in $NaClO_4$ solutions) and literature published sorption data to derive surface complexation constants for a number of elements (Mn(II), Co(II), Ni(II), Zn(II), Cd(II), Eu(III), Am(III), Sn(IV), Th(IV), Np(V) and U(VI)) sorbing on montmorillonite. They used the derived surface binding constants (surface complexation constants) to find a correlation between the logarithms of the surface binding constants and the logarithms of the formation constants of the corresponding hydrolysis species ($^{OH}K_x$). The purpose of the correlation was to estimate surface complexation constants for elements whose sorption properties had not been measured. The correlation obtained for strong surface sites was:

$$\log {}^{s}K_{x-1} = (8.1\pm0.3) + (0.90\pm0.02) \log {}^{OH}K_x \qquad (10)$$
$$R = 0.99$$

The correlation for weak surface sites was:

$$\log {}^{w1}K_{x-1} = (6.2\pm0.8) + (0.98\pm0.09) \log {}^{OH}K_x \qquad (11)$$
$$R = 0.98$$

The above correlations were used to estimate values of $\log {}^{s}K_{x-1}$ and $\log {}^{w1}K_{x-1}$ for a number of elements including Pd(II), Pb(II), Pu(III), Zr(IV), U(IV), Np(IV), Pu(IV) and Pa(V).

Bradbury and Baeyens (2009a) repeated the above exercise for Na-illite using experimental data for Ni(II), Co(II), Eu(III), Sn(IV), Am(III), Th(IV), Np(V), Pa(V) and U(VI) in $NaClO_4$ solutions. Sorption on illite was modelled using one strong site, and the resulting constants were correlated with hydrolysis constants. The correlation equation using this LFER approach for illite is given by equation 12. Any information on the sorption properties of illite provides insight into the sorption properties of shale.

$$\log {}^{s}K_{x-1} = (7.9\pm0.4) + (0.83\pm0.02) \log {}^{OH}K_x \qquad (12)$$
$$R = 0.99$$

Sorption modelling with Ni is used as an example to illustrate the application of sorption modelling for predicting sorption processes. Vilks and Miller (2014) used PHREEQC to simulate Ni sorption on Na-montmorillonite and Ca-montmorillonite using a 2SPNE SC model. Nickel selectivity coefficients for cation exchange reported for Na-montmorillonite and Ca-montmorillonite are 3.1 (determined in 0.01, 0.03, 0.1 mol/L $NaClO_4$ solutions) and 0.8 (determined in 0.0033 and 0.033 mol/L $Ca(NO_3)_2$ solutions), respectively (Bradbury and Baeyens 2005b). The surface complexation constants for Ni sorption on montmorillonite are given in Table 13. The CEC for both types of montmorillonite is 0.87 equivalents/kg. The site capacities are 0.002 mol/kg for the strong sites, and 0.04 mol/kg for each of the weak sites. Simulations were performed for a solid to liquid ratio of 0.54 g/L. The solid/liquid ratio determines the total sorption site capacity (CEC and complexation) for the system and what fraction of Ni in the system is associated with the solid. The value for the Ni K_d is calculated by summing the Ni concentrations in all of the solid sites (mol/kg) and dividing by the total Ni concentration in solution. The final K_d is not affected by the solid/liquid ratio.

Table 14 summarizes the calculated Ni sorption values for montmorillonite in different selected solutions at a reference pH of 6.3 using the surface complexation constants provided in Table 12 and Table 13. The contribution of cation exchange to the simulated K_d value is illustrated by % CEC values for Na- and Ca-montmorillonites. At a pH value of 6.3, the cation exchange component can contribute to the overall sorption value, depending upon the concentration of the competing cation in solution. For example, if Ni is sorbing on Na-montmorillonite when the solution has negligible Na, the amount of Ni sorbed by cation exchange can be very high (e.g., in 0.1 mol/L $CaCl_2$ solution, 99.8% of the simulated K_d value of Ni sorption onto Na-montmorillonite was due to cation exchange with Ca^{2+} in solution). The same can be said for sorption on Ca-montmorillonite when there is negligible Ca in solution (e.g., in 0.1 mol/L NaCl solution, the 99.8% of the simulated K_d value of Ni sorption onto Ca-montmorillonite was due to cation exchange with Na^+ in solution). When the concentrations of Na and Ca are higher than around 0.05 mol/L, sorption onto Na-montmorillonite and Ca-montmorillonite due to cation exchange becomes negligible. As expected, at this point sorption on both types of montmorillonite becomes identical.

At a pH of 6.3, sorption due to surface complexation is controlled by the $\equiv S^sONi^+$ surface species. The other surface species become more important at higher pH. If Ni sorption on the weak site is included, then Ni sorption on montmorillonite depends on the concentration of Ni in solution. This is illustrated by the variation in the simulated K_d values with the variation of Ni concentration for the reference Na-Ca-Cl 300 g/L solution used in the laboratory sorption measurements (Vilks et al. 2011, see Table 6). Assuming the total Ni concentration in equilibrium with solids in the sorption tests is represented by a $[Ni]_{total}$ value of 5×10^{-5} mol/L, the simulated sorption value of 35 cm^3/g is in good agreement with the measured Ni sorption values, ranging from 34 to 53 cm^3/g (Vilks et al. 2011). Given that the Ni surface complexation constants were derived from data measured in 0.1 mol/L $NaClO_4$ solutions, the ability of these complexation constants coupled with an aqueous speciation program, such as PHREEQC, to predict experimental results in brine solutions is encouraging. Vilks and Miller (2014) used LFER to estimate surface complexation constants for Cu and Pb, and simulated K_d values that were within a factor 2 of measured values, also indicating that the 2SPNE SC/CE methodology has a good potential for estimating sorption values.

However, one should remember that although surface complexation models can be used to reproduce the results of sorption experiments over a wide range of conditions and to extrapolate the sorption values to different solution conditions, the 2SPNE SC/CE methodology is not a mechanistic method for predicting sorption from a very rigorous understanding of all sorption species. Rather, it is a tool for predicting sorption based on the assumption that sorption occurs by cation exchange and by complexation reactions to surface oxygen sites that are analogous to the formation of hydroxide species in solution. A good fit between model simulations and experimental measurements does not prove the actual existence of the proposed surface reactions. The existence of the proposed surface species needs to be demonstrated by independent experimental methods. Nevertheless, sorption modelling remains a useful tool for furthering the understanding of sorption processes and extrapolating sorption results to new conditions.

Table 14: Simulated Ni K_d Values on Montmorillonite for Selected Solution Compositions

$[Ni]_{total}$ (mol/L)	$[CO_3]_{total}$ (mol/L)	Solution	K_d (cm^3/g)		% CEC Na-mont Contribute to K_d of Na-mont	% CEC Ca-mont Contribute to K_d of Ca-mont
			Na-mont	Ca-mont		
1×10^{-5}	1×10^{-5}	0.1 mol/L NaCl	160	31,000	59.7	99.8
1×10^{-5}	1×10^{-5}	0.1 mol/L $CaCl_2$	31,000	63	99.8	7.5
1×10^{-5}	1×10^{-5}	0.1 mol/L Na-Ca-Cl	61,900	260	99.9	75.4
1×10^{-5}	1.8×10^{-3}	SR-270-PW	74	74	0.4	1.1
1×10^{-7}	5×10^{-5}	Na-Ca-Cl 300 g/L	148	148	0.2	0.3
1×10^{-5}	5×10^{-5}	Na-Ca-Cl 300 g/L	85	85	0.4	0.5
5×10^{-5}	5×10^{-5}	Na-Ca-Cl 300 g/L	35	35	0.9	1.3
1×10^{-4}	5×10^{-5}	Na-Ca-Cl 300 g/L	22	22	1.5	2.1

3.2 **Palladium**

PHREEQC (with SIT database) predicts that in the SR-270-PW brine solution Pd will be present mainly as the anionic $PdCl_4^{-2}$ species, with lesser amounts of $PdCl_3^-$. A Pitzer database would be more appropriate for high ionic strength solutions such as SR-270-PW reference brine. However, Pitzer ion interaction parameters are currently not available for Pd. Therefore, the SIT database was used for speciation calculation for Pd and other elements in this work. In dilute solution the aqueous Pd chemistry will be dominated by $Pd(OH)_2^0$, as well as $PdCl_3^-$ under acidic conditions (pH 4). The hydroxyl species of interest for surface complexation modelling are $Pd(OH)^+$, $Pd(OH)_2^0$, $Pd(OH)_3^-$ and $Pd(OH)_4^{-2}$, with respective hydrolysis constants (log $^{OH}K_x$) values of -1.86, -3.79, -15.93 and -29.36. These log $^{OH}K_x$ values were obtained from the SIT database in PHREEQC (Thermochimie TDB). Assuming that Pd sorption occurs by surface complexation to exposed $\equiv S^sOH$ sites on montmorillonite and illite, surface complexation reactions (Table 15) can be derived based on palladium's known hydrolysis species. The surface complexation constants (log $^sK_{x-1}$) were estimated using the LFER approach and equations 10 and 12. A weak site for montmorillonite was not included because preliminary calculations indicated that it would not have a significant impact.

Although the amount of free Pd^{+2} in solution is predicted to be minimal, the cation exchange reaction with Pd^{+2} was included in the model. The selectivity coefficient for Pd^{+2} exchange for Na^+ on montmorillonite was based on the selectivity coefficient value for Ni^{+2}, reported to be 3.1 (log K_c = 0.49) by Bradbury and Baeyens (2005b). The selectivity coefficient for Pd^{+2} exchange with Na^+ on illite of 11.0 (log K_c = 1.04) was based on Ca^{+2} exchange with Na^+, reported by Bradbury and Baeyens (2009a).

Simulated Pd sorption on montorillonite and illite (and shale) are summarized in Table 1A of the Appendix and illustrated in Figure 17. Sorption on shale was determined by first simulating sorption on illite. The resulting K_d values for illite were reduced by 40% to approximate sorption on shale (i.e. 60% of K_d values on illite), on the assumption that shale contains 60% illite. Since

bentonite contains around 80% montmorillonite, it is reasonable to compare measured K_d values on bentonite with simulated K_d values on montmorillonite. Actual K_d values measured in the reference brine and dilute solutions are also given in Table 1A (see Appendix) as a range of values. The range of measured Pd K_d values were illustrated by plotting the minimum and maximum K_d value of each range.

Table 15: Palladium Surface Complexation Reactions and Surface Complexation Constants for Montmorillonite and Illite

Th Surface Complexation Reaction	Montmorillonite Strong Site log $^{s}K_{x-1}$	Illite Strong Site log $^{s}K_{x-1}$	Pd Hydrolysis log $^{OH}K_{x}$
$\equiv S^{s}OH + Pd^{+2} \Leftrightarrow \equiv S^{s}OPd^{+} + H^{+}$	6.4	6.4	-1.86
$\equiv S^{s}OH + Pd^{+2} + H_2O \Leftrightarrow \equiv S^{s}OPd(OH)^{0} + 2H^{+}$	4.7	4.8	-3.79
$\equiv S^{s}OH + Pd^{+2} + 2H_2O \Leftrightarrow \equiv S^{s}OPd(OH)_2^{-} + 3H^{+}$	-6.2	-5.3	-15.93
$\equiv S^{s}OH + Pd^{+2} + 3H_2O \Leftrightarrow \equiv S^{s}OPd(OH)_3^{-2} + 4H^{+}$	-18.3	-16.5	-29.36

Note: The surface complexation constants for Pd reactions were estimated using LFER developed by Bradbury and Baeyens (2005b, 2009b). Pd hydrolysis constants were taken from the SIT database coming with PHREEQC (Thermochimie TDB).

A comparison of simulated and measured K_d values in Table 1A of the Appendix and Figure 17 shows that the Pd sorption model considered in this report significantly underestimates measured Pd sorption. The model assumed that Pd was sorbed by mechanisms that included the complexation of free Pd^{+2} and Pd hydroxyl species to surface oxygens. In brine the Pd chemistry was dominated by chloride complexes, reducing the amount of hydroxyl species available for sorption. With increasing pH the model predicted that the increased tendency to form hydroxyl species would lead to increased sorption. Nevertheless, the measured Pd sorption K_d values on bentonite and shale was orders of magnitude higher than the simulated K_d values. This suggests that chloride complexes were able to sorb to bentonite and shale surfaces in some way, or else a completely different surface reaction took place to account for Pd sorption. Since the formation of chloride species is not a factor in dilute solution Pd speciation is dominated only by hydroxyl species. As a result the model predicted no pH affect on sorption. However, the sorption model underpredicted Pd sorption in dilute solution by several orders of magnitude. This tends to confirm that the dominant mechanism of Pd sorption was not the surface complexation of hydroxyl species. Other sorption mechanisms (e.g., sorption of Pd chloride complexes) must be considered.

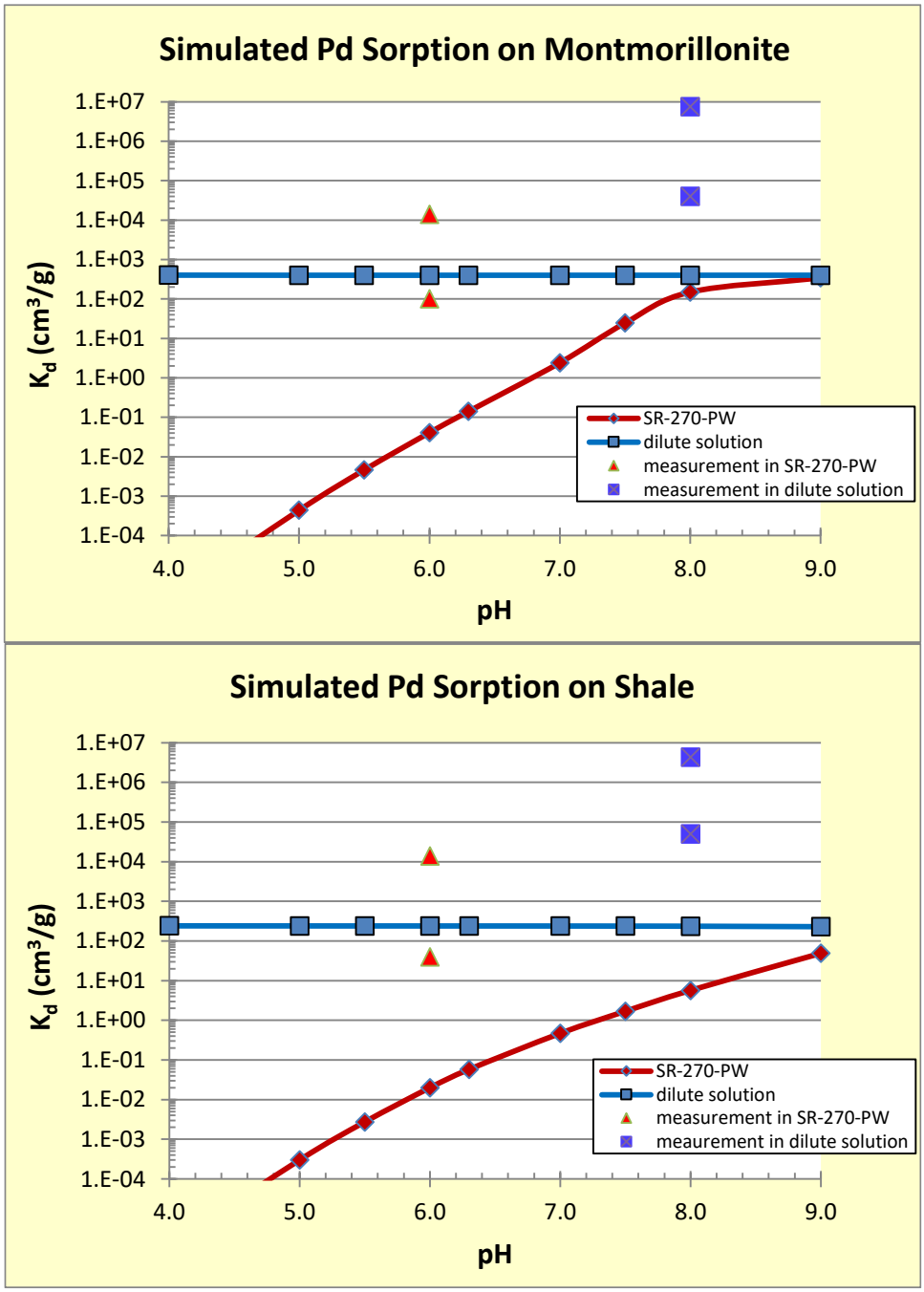


Figure 17: Simulated Palladium Sorption on Montmorillonite and Shale in SR-270-PW Brine and Dilute Solution under Different pH Values (Triangle and Square Points are the Range of Experimental Measurements at pH of 6 and 8)

3.3 **Zirconium**

Given the lack of Zr sorption data, the LFER relations proposed by Bradbury and Baeyens (2005b and 2009b) were used to estimate surface binding constants for Zr sorption on montmorillonite and illite. The hydroxyl species of interest for surface complexation modelling are $Zr(OH)^{+3}$, $Zr(OH)_2^{+2}$, $Zr(OH)_4^0$ and $Zr(OH)_6^{-2}$. The surface species and their associated surface binding constants derived using LFER are given in Table 16. Competition with Ca^{+2} sorption was not included because its chemistry is not similar to that of Zr^{+4}. Since the dominant Zr species in solution is the neutral charged $Zr(OH)_4^0$, cation exchange was not included in the Zr sorption model. The site capacities for both Na-montmorillionite and illite are 0.002 mol/kg for the strong site and 0.04 mol/kg for each of the two weak sites (Bradbury and Baeyens, 2005b, 2009b). The K_d value for Zr is calculated by summing the Zr concentrations in all of the solid sites (mol/kg) and dividing by the total Zr concentration in solution. The purpose of this exercise was to determine whether the sorption surface binding constants estimated by the LFER approach, using the sorption surface constants for other elements determined in diluted $NaClO_4$ solutions, could be used to approximate sorption reactions for Zr in brine solutions. As before, the assumptions are (1) that the thermodynamic code, PHREEQC (with SIT database), can account for Zr interactions with brine salts; (2) that the surface complexation constants determined in diluted $NaClO_4$ solutions are not significantly different from that in brine solutions; and (3) that montmorillonite and illite can be used to approximate the sorption properties of bentonite and shale.

Table 16: Zirconium Surface Complexation Reactions and Surface Complexation Constants for Montmorillonite and Illite and Hydrolysis Constants

Zr Surface Complexation Reaction	Montmorillonite log $^{s}K_{x-1}$	Illite log $^{s}K_{x-1}$	Zr Hydrolysis log $^{OH}K_x$
$\equiv S^sOH + Zr^{+4} \Leftrightarrow \equiv S^sOZr^{+3} + H^+$	8.39 ± 0.31	8.17 ± 0.41	0.32
$\equiv S^sOH + Zr^{+4} + H_2O \Leftrightarrow \equiv S^sOZr(OH)^{+2} + 2H^+$	8.98 ± 0.32	8.71 ± 0.42	0.98
$\equiv S^sOH + Zr^{+4} + 3H_2O \Leftrightarrow \equiv S^sOZr(OH)_3^0 + 4H^+$	6.13 ± 0.34	6.08 ± 0.36	-2.19
$\equiv S^sOH + Zr^{+4} + 5H_2O \Leftrightarrow \equiv S^sOZr(OH)_5^{-2} + 6H^+$	-18 ± 1	-16 ± 1	-29
	Montmorillonite log $^{w1}K_{x-1}$		Zr Hydrolysis log $^{OH}K_x$
$\equiv S^{w1}OH + Zr^{+4} \Leftrightarrow \equiv S^{w1}OZr^{+3} + H^+$	6.51 ± 0.8	-	0.32

Note: The surface complexation constants for Zr reactions were estimated using LFER developed by Bradbury and Baeyens (2005b, 2009b). The uncertainties were estimated from uncertainties associated with the LFER equations. Zr hydrolysis constant were taken from Brown et al. (2005).

Simulations with the reference brine SR-270-PW indicated that $\equiv S^sOZr(OH)_3^0$ was the dominant Zr surface species at neutral pH. This is not surprising since $Zr(OH)_4^0$ is predicted to be the dominant Zr species in the SR-270-PW brine. Simulated Zr K_d values for the reference brine SR-270-PW and the reference dilute solution are presented in Figure 18 and Table 2A (see the Appendix), along with K_d values for bentonite and shale measured in the reference brine and dilute solutions. As was done for Pd, the simulated K_d values for Zr sorption on illite were converted to equivalent values for shale for ease of comparison to measured data.

Simulations of Zr sorption on montmorillonite (Figure 18) indicate that in brine Zr sorption increases with pH up to a pH value of about 3.5, and then remains relatively constant up to a pH of 9. In the dilute solution, simulated Zr sorption on montmorillonite does not vary with pH. Simulated Zr soption on shale in brine indicates an initial sorption increase from pH values of 3 to 3.4, followed by relatively constant K_d values up to pH 8, at which point sorption decreases. Simulated Zr sorption on shale in dilute solution is constant with pH up to a pH value of 8, after which there is a slight decrease in sorption as pH increases to a value of 9. The dominant aqueous species in brine and dilute solution is $Zr(OH)_4^0$, except below pH values of 3.5 in the brine where Zr fluoride complexes become more important than hydroxyl complexes. The presence of fluoride complexes accounts for reduced sorption in brine at low pH.

Measured Zr sorption on bentonite shows a lower K_d value at pH 3, consistent with simulations, and higher K_d values in the pH range of 6 to 7. Measured K_d values on bentonite in brine at pH 6 to 7 are higher than simulated values by a factor of 3 to 8. In dilute solution measured K_d values on bentonite are higher than simulated values by a factor of 18 to 41 and, consistent with simulations, do not indicate variability with pH. Measured Zr sorption on shale in brine shows a lower value at pH 3, and higher values in the pH 6 to 7 range, consistent with simulations. Measured K_d values on shale in brine at pH 6 to 7 are higher than simulated values (i.e. 60% of simulated K_d values for illite) by a factor of 5 to 13. As with bentonite, Zr K_d values on shale measured in dilute solution are higher than simulated values by a factor of 6 to 40.

These results illustrate that simulated Zr sorption K_d values, derived using LFER determined surface complexation constants, provide an approximation within a factor of 13 of Zr sorption values in brine solutions. Although simulated Zr K_d values underpredicted measured K_d values in dilute solution (within a factor of 41), the simulations could be used as conservative estimates of Zr sorption. These observations support the concept that Zr sorption is controlled by the complexation of Zr to surface oxygen sites, as outlined in Table 16.

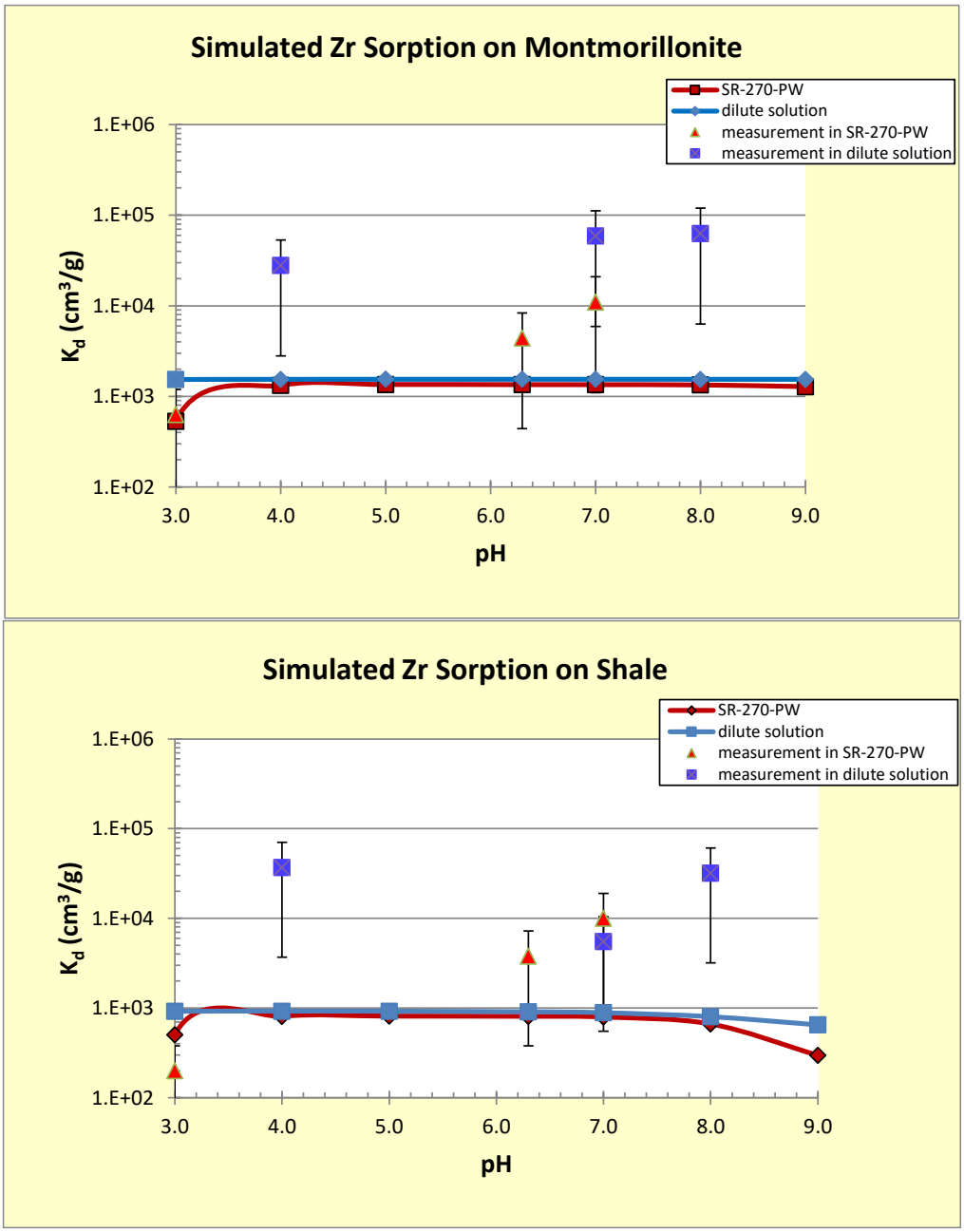


Figure 18: Simulated Zirconium Sorption on Montmorillonite and Shale in SR-270-PW Brine and Dilute Solution under Different pH Values

3.4 **Tin**

Since the solution chemistry of Sn is dominated by hydrolysis species, it seems reasonable that Sn sorption could be controlled by surface complexation reactions that involve hydroxyl species. Proposed Sn surface complexation reactions are presented in Table 17. The surface complexation constants for Sn reactions with montmorillonite were reported by Bradbury and Baeyens (2005b). The surface complexation constants for Sn reactions with illite were estimated with LFER using Sn hydrolysis constants (Table 17) and equation 12, derived by Bradbury and Baeyens (2009b). The main aqueous Sn species in brine and dilute solution under neutral pH are the neutral $Sn(OH)_4^0$ and negatively charged $Sn(OH)_5^-$. Therefore, cation exchange was not included in the sorption simulations.

Table 17: Tin Surface Complexation Reactions and Surface Complexation Constants for Montmorillonite and Illite and Hydrolysis Constants

Sn Surface Complexation Reaction	Montmorillonite log ${}^{s}K_{x-1}$	Illite log ${}^{s}K_{x-1}$	Sn Hydrolysis log ${}^{OH}K_{x}$
$\equiv S^sOH + Sn^{+4} + 2H_2O \Leftrightarrow \equiv S^sOSn(OH)_2^+ + 3H^+$	12	9.2	1.55
$\equiv S^sOH + Sn^{+4} + 3H_2O \Leftrightarrow \equiv S^sOSn(OH)_3^0 + 4H^+$	8	8.2	0.33
$\equiv S^sOH + Sn^{+4} + 4H_2O \Leftrightarrow \equiv S^sOSn(OH)_4^- + 5H^+$	0	1.5	-7.67
$\equiv S^sOH + Sn^{+4} + 5H_2O \Leftrightarrow \equiv S^sOSn(OH)_5^{-2} + 6H^+$	-8.5	-7.1	-18.07

Note: The surface complexation constants for Sn reactions with montmorillonite were reported by Bradbury and Baeyens (2005b). The surface complexation constants for Sn reactions with illite were estimated with LFER using Sn hydrolysis constants (Bradbury and Baeyens 2009b) and equation 12.

The K_d values simulated with the surface complexation reactions are presented in Table 3A (see the appendix) and illustrated in Figure 19. Measured K_d values from batch tests in brine and dilute solutions are also included in Table 3A and Figure 19 for comparison.

Simulated K_d values for montmorillonite and shale in brine solution show a significant rise in sorption from pH 4 to pH 6. As pH increases above a value of 7 there is a gradual decrease in sorption. Simulations for dilute solution do not show lower K_d values in the pH range below 6. Above pH 6 the simulated K_d values in dilute solution are very similar to K_d values in brine. The reason for the reduced sorption in brine at pH values below 6 is not clear, but may result from the formation of chloride complexes.

The measured K_d values on bentonite in brine and dilute solutions are lower than simulated values on montmorillonite. An exception is noted for low pH values where simulated K_d values in brine are lower than measured values. The simulated K_d values for Sn sorption on shale are in closer agreement with values determined from batch sorption tests. The exception is at lower pH values where simulations for brine indicate lower Sn sorption. The measured Sn sorption in brine pH around 3.3 suggests that either Sn chloride complexes sorb in some form, or that some other sorption mechanism(s) is operating in low pH brine solutions.

In summary, the sorption model provides a reasonable approximation for Sn sorption on shale (within a factor of 4) in dilute solution at pH of 4 to 8. Simulations provide an approximation for Sn sorption on bentonite (within a factor of 9) in dilute solution. In brine at pH 6, the sorption model provides an approximation for Sn sorption on shale (within a factor of 3) and bentontie (within a factor of 7). In brine at pH 7, simulations overpredicted sorption on shale and bentonite by a factor of 37 and 220, respectively. The reason for the over-prediction of Sn sorption on bentonite in both brine and dilute solutions is not known. During the sorption tests with bentonite, Sn may not have been able to access all of the sorption sites within the montmorillonite component. Also, no consideration was given to the fact that bentonite is not pure montmorillonite (montmorillonite makes up only 80% of the bentonite). The fitting to the experimental measurements might be improved if the sorption model included sorption of chloride complexes of Sn.

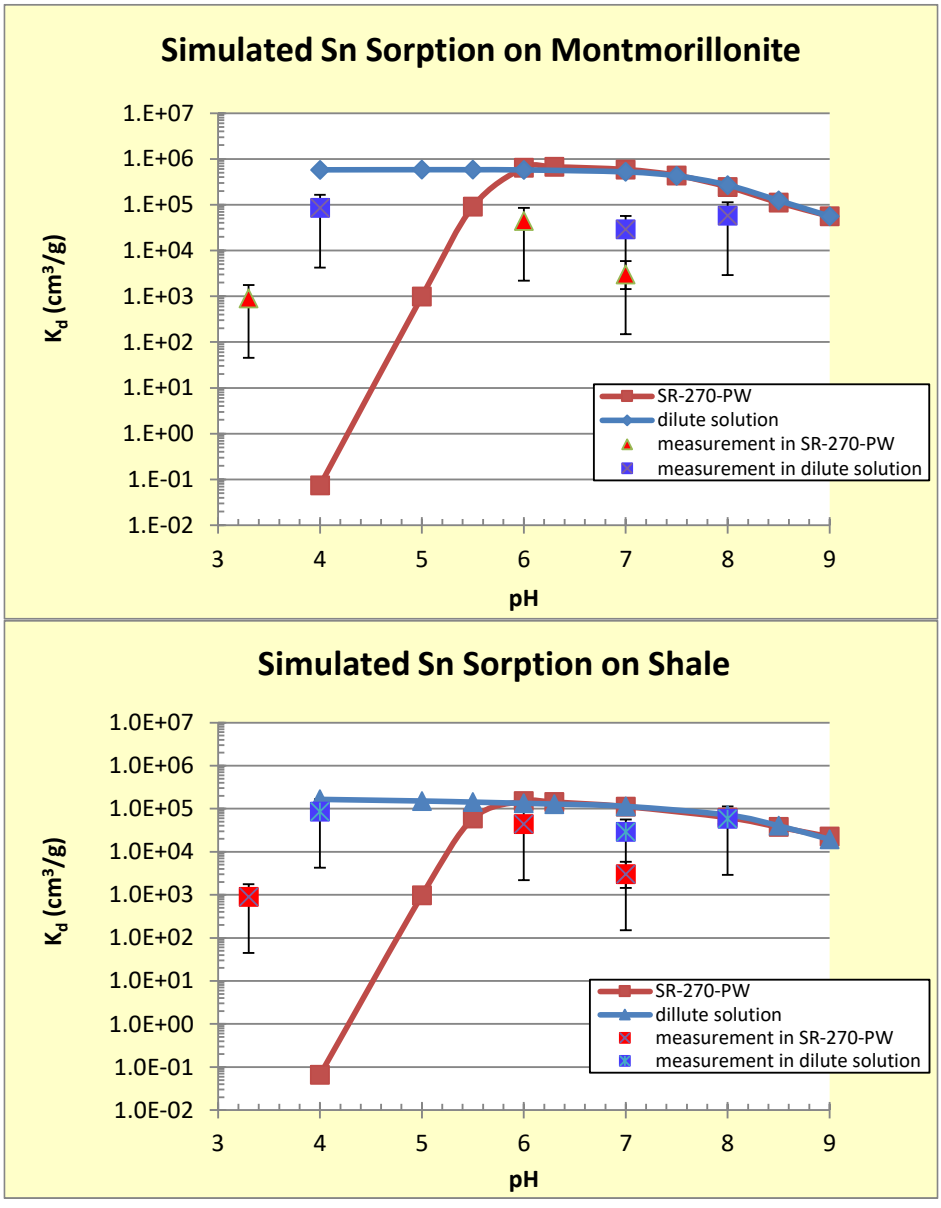


Figure 19: Simulated Tin Sorption on Montmorillonite and Shale in SR-270-PW Brine and Dilute Water Under Different pH Values

3.5 **Thorium**

Bradbury and Baeyens (2005b) reported thorium sorption values for montmorillonite measured in 0.1 and 1.0 mol/L $NaClO_4$ solutions. For pH values of 6 and 7 the sorption coefficients were reported to be 3.6×10^5 and 4.11×10^5 cm^3/g, respectively. The measured data were used to produce a 2-site protolysis non-electrostatic surface complexation model to describe thorium sorption on montmorillonite (Bradbury and Baeyens 2005b). The surface reactions and surface complexation constants for this model are summarized in Table 18. Bradbury and Baeyens (2009b) measured thorium sorption on illite in a 0.1 mol/L $NaClO_4$ solution. The measured sorption data were used to construct a thorium sorption model for illite, with surface complexation sorption constants given in Table 18. The thorium sorption models for montmorillonite and illite were incorporated into PHREEQC (SIT database), assuming that the surface complexation sorption constants in the SR-270-PW brine are the same as those derived from 0.1 and 1.0 mol/L $NaClO_4$ solutions. The simulated values of thorium sorption on illite were used to derive sorption values for shale taking into account that shale contains 60 percent illite.

Table 18: Thorium Surface Complexation Reactions and Surface Complexation Constants for Montmorillonite and Illite

Th Surface Complexation Reaction	[a]Montmorillonite Strong Site log $^sK_{x-1}$	[b]Illite Strong Site log $^sK_{x-1}$
$\equiv S^sOH + Th^{+4} \Leftrightarrow \equiv S^sOTh^{+3} + H^+$	7.2	7.4
$\equiv S^sOH + Th^{+4} + H_2O \Leftrightarrow \equiv S^sOTh(OH)^{+2} + 2H^+$	2.7	2.3
$\equiv S^sOH + Th^{+4} + 2H_2O \Leftrightarrow \equiv S^sOTh(OH)_2^+ + 3H^+$	-2.6	-2.4
$\equiv S^sOH + Th^{+4} + 3H_2O \Leftrightarrow \equiv S^sOTh(OH)_3^0 + 4H^+$	-9.1	-8.8
$\equiv S^sOH + Th^{+4} + 4H_2O \Leftrightarrow \equiv S^sOTh(OH)_4^- + 5H^+$	-16.9	-15.3

[a]Bradbury and Baeyens 2005b
[b]Bradbury and Baeyens 2009b

Cation exchange was not included in the simulation of Th sorption because the amount of Th^{+4} ion in solution is insignificant. The only possible exception was in dilute solution at pH 4, where 3 percent of the total dissolved Th was present as the Th^{+4} ion.

The Th K_d values simulated with the surface complexation reactions for the reference brine and dilute solutions are summarized in Table 4A of the appendix and illustrated in Figure 20. Measured K_d values by batch tests are also included in Table 4A and Figure 20 for comparison.

Simulated K_d values for montmorillonite and shale in the reference brine solution show a significant rise in sorption from pH 4 to pH 6. Above pH values of 6 simulated Th K_d values remain relatively constant with pH. The formation of Th fluoride species at lower pH values in brine explains the reduced simulated K_d values. For example, in the SR-270-PW reference brine at pH of 4, Th fluoride complexes dominate with 99% ThF_2^{+2}, ThF^{+3} and ThF_3^+ species;

while at pH of 6, Th hydrolysis species dominate with 49% $Th(OH)_3^+$ and $Th(OH)_4$, 12% $Th(OH)_3(CO_3)^-$ and 18% thorium fluoride species. Simulations for montmorillonite in dilute solution in the pH range below 6 show slightly higher K_d values than above pH 6, while K_d values on shale in the pH range below 6 are slightly lower than above pH 6. Above pH 6 the simulated K_d values in dilute solution are slightly lower than the simulated K_d values in brine.

In brine the measured K_d values for Th sorption on bentonite and shale indicate reduced sorption around pH 3.3. Although the measured K_d values appear higher than simulated values at low pH, the fact that measured sorption values are lower at pH 3.3 than at pH 6 to 7 does support the supposition that Th sorption is reduced due to the formation of Th fluoride complexes. The measured Th K_d values in dilute solution do not show a clear variation with pH. Since F^- was not present in dilute solution, sorption was not reduced by the formation of Th fluoride complexes. In brine, at pH values of 6 to 7, the measured Th K_d values are lower than simulated values on montmorillonite and shale by a factor of 12 to 26 and 7 to 23, respectively. In dilute solution, considering pH values of 7 to 8, the simulated Th K_d values are similar to measured K_d values for bentonite (within a factor of 2) and shale (within a factor of 7).

The concept for Cs sorption, particularly in brine solution, involves the penetration of clay interlayers, where Cs is able to displace other Group 1 elements because the Cs ion has a significantly smaller hydrated radius. Sorption modelling of Cs was not attempted because the most likely mechanism for its sorption is not consistent with the 2SPNE SC model.

In summary, the 2-site protolysis non-electrostatic surface complexation model simulated K_d values are within a factor of 7 compared to the measured K_d values in dilute solution at pH of 7 to 8, providing a reasonable approximation for Th sorption on bentonite and shale in dilute solution at pH 7 to 8. In brine the simulated K_d values are factors of 7 to 26 greater than the measured values. This finding is consistent with control of Th sorption by complexation to surface oxygen sites, as described in Table 18.

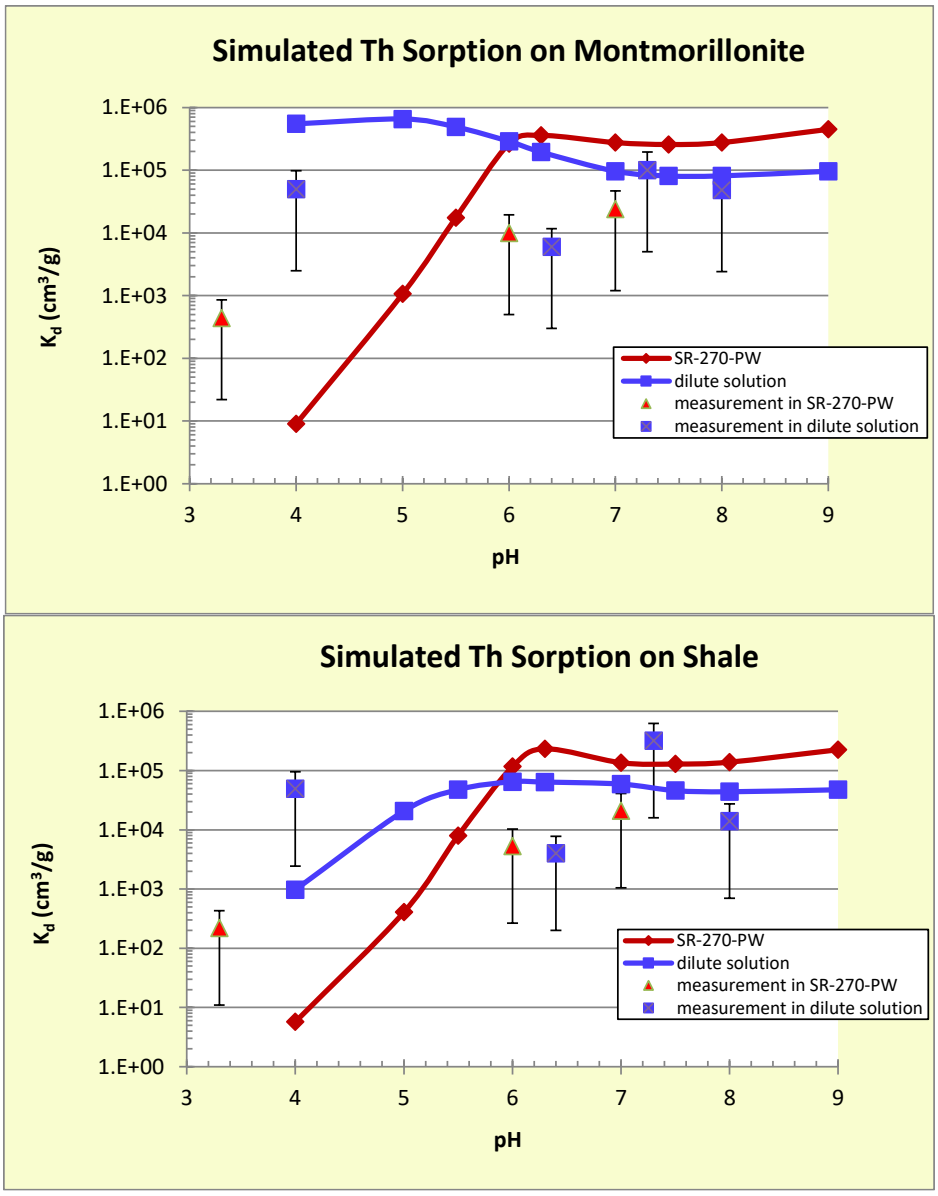


Figure 20: Simulated Thorium Sorption in SR-270-PW Brine and Dilute Water Under Different pH Values

4. DIFFUSION TESTS

Understanding sorption and its role in the transport of radionuclides in Canadian sedimentary rocks under saline conditions requires a combination of batch sorption tests and diffusion tests to demonstrate that sorption coefficients (K_d) measured using batch sorption tests can be applied to explain mass transport results. Diffusion is the primary transport mechanism in the low permeability Ordovician shales and limestones. Therefore, diffusion tests were undertaken for Ordovician shale and limestone rock samples with sorbing tracers to improve the understanding of sorption in mass transport. This was intended to address aspects of specific surface areas, and sorption and desorption kinetics.

The diffusion properties of Ordovician limestone and shale for non-sorbing tracers (iodide and tritium) have previously been determined (Vilks and Miller 2007). The intent of the diffusion tests was to determine the tracer sorption coefficients by comparing the apparent diffusion coefficients of sorbing tracers with those of the non-sorbing tracer. The diffusion of sorbing and non-sorbing tracers was characterized by the diffusion profiles of tracers within the test rock samples, which were determined at the end of the diffusion test by cutting and grinding material from the test rock samples, leaching it to recover tracers and determining tracer concentrations as a function of core length. The experimental configuration was a diffusion cell in which a rock coupon is sandwiched between a tracer reservoir and an elution reservoir (Vilks and Miller 2007). Diffusion tests were performed with two rock samples of shale and two rock samples of limestone using the procedures described by Vilks and Miller (2014). A synthetic brine composition SR-270-PW, equivalent to the reference porewater SR-270-PW composition, was used as the ionic medium for the diffusion tests to facilitate comparison to results (i.e., sorption distribution coefficients) from batch sorption tests conducted using the same reference water. The tracers used in the diffusion tests included those elements that were studied with batch sorption tests as part of this work program (Cs, Pd, Zr, Sn and Th), as well as selected elements which have previously been studied by Vilks and Miller (2014) with batch and diffusion tests (Li, Ni). In brine solutions Li sorption is very low and Li diffusion closely approximates the diffusion of a conservative tracer (Vilks and Miller 2014). The duration of the diffusion tests was 12 months. Diffusion experiments were performed in a glove box, with an O_2 reduced atmosphere. The oxygen concentrations in the glove box were monitored on a regular basis, using Oxoid indicator strips (BR0055 supplied by ThermoFisher).

4.1 DEFINITIONS

Diffusivity is a measure of the ability of a species to move through a medium under the influence of its concentration gradient. Diffusivity is quantified as a diffusion coefficient (D). Diffusivity can be measured under steady state or transient conditions, and each has its advantages and area of applicability.

The processes of diffusion are described by Fick's first and second laws. In generalized situations, such as the conduction of heat in a solid, or the diffusion of species in a single phase medium such as water, Fick's first law states that the mass of a diffusing substance passing through a given cross section per unit of time is proportional to the concentration gradient. In one dimension,

$$J = -D \cdot \frac{\partial C}{\partial x} \quad (13)$$

where

J is the mass flux [mol/m^{2}s],
D is the diffusion coefficient [m^2/s],
C is the species concentration [mol/m^3], and
$\partial C/\partial x$ is the concentration gradient.

Fick's second law relates concentration with both space and time. In one dimension,

$$\frac{\partial C}{\partial t} = D \cdot \frac{\partial^2 C}{\partial x^2} \quad (14)$$

When evaluating diffusion of a fluid in a two-phase system, such as groundwater in a porous rock, it becomes necessary to modify Fick's laws to account for the fact that water only occupies a fraction of the total volume occupied by the rock. The modification is applied by redefining the diffusion coefficient (D) to include factors such as the porosity and the pore geometry, which is defined by a combination of tortuosity and constrictivity.

The diffusion coefficients that are used in Equations 13 and 14 to describe diffusivity in heterogeneous media have been defined to account for various combinations of the effects of porosity, tortuosity and constrictivity. The type of diffusion coefficient used depends on the particular application.

Because species diffuse through water in pore spaces, all diffusion coefficients applied to heterogeneous media can be related to the free-water diffusion coefficients (D_w). Free-water diffusion coefficients have been measured for numerous cations and ions. Values of free-water diffusion coefficients for these cations and anions vary between 5.59×10^{-10} and 9.31×10^{-9} m^2/s (e.g., Harvey 1996). The elements Li, Th, Zr, Sn and Pd studied in this work are not included in Harvey (1996).

For certain applications, diffusion may be considered as a function of species concentration only in porewater. For example, this may be useful if diffusion data is available in the form of a diffusion profile, which shows changes in a species porewater concentration as a function of distance (e.g., Gimmi and Waber 2004). Diffusion in porewater is commonly described with a pore diffusion coefficient (D_p), which accounts for the effects of tortuosity (τ) and constrictivity (δ) within connected pore spaces. This type of diffusion coefficient may be used as one of the input parameters in certain computer models that have porosity and diffusion as separate input parameters. The pore diffusion coefficient (D_p) is defined as follows (Ohlsson and Neretnieks 1995):

$$D_p = \frac{D_w \delta}{\tau^2} \quad (15)$$

Diffusion can also be treated by considering a volume of rock as a whole. In this case, the connected porosity must be included in the calculation of the diffusive flux to account for the small volume of connected pore space compared to the volume of the whole rock. The effective or empirical diffusion coefficient (D_e) is commonly used to describe diffusive fluxes. Some authors (Bradbury et al. 1982) have also referred to this as the intrinsic diffusion coefficient (D_i).

The effective diffusion coefficient is defined as (Choi and Oscarson 1996; Skagius and Neretnieks 1982; Ohlsson and Neretnieks 1995):

$$D_e = \frac{D_w \delta \varepsilon_t}{\tau^2} \quad (16)$$

The through-transport porosity (ε_t) determines the diffusive flux through rock when steady state has been achieved. However, the storage capacity of the rock must also be considered. The storage capacity is quantified by the rock capacity factor (α), which has been defined as (Bradbury and Green 1985):

$$\alpha = \varepsilon_c + \rho \cdot K_d \quad (17)$$

where ρ is the bulk density of the rock, K_d is the sorption coefficient, and the total connected porosity (ε_c) is given by:

$$\varepsilon_c = \varepsilon_t + \varepsilon_d \quad (18)$$

ε_d is the dead end porosity. The rock capacity term can be incorporated into Fick's second law to describe concentration variation with space and time within a rock:

$$\frac{\partial C}{\partial t} = \frac{D_e}{\alpha} \cdot \frac{\partial^2 c}{\partial x^2} \quad (19)$$

The apparent diffusion coefficient (D_a) has been defined as (Bradbury and Green 1985; Choi and Oscarson 1996; Oscarson and Hume 1994; Ohlsson and Neretnieks 1995):

$$D_a = \frac{D_e}{\alpha} = \frac{D_p \varepsilon_t}{(\varepsilon_c + \rho K_d)} \quad (20)$$

In the case of a non-sorbing tracer, such as iodide, the rock capacity term (α) is equal to the total connected porosity (ε_c). If the through-transport porosity (ε_t) is the same as the ε_c, the apparent diffusion coefficient (D_a) for the non-sorbing tracer will be the same as the pore diffusion coefficient (D_p).

The constrictivity (δ) and tortuosity (τ) are difficult, if not impossible, to determine separately by experimental means. Because of the difficulty in separating δ and τ, the term 'tortuosity' is often found in experimental work to have been used to describe the quantity $\tau / \sqrt{\delta}$. Melnyk and Skeet (1987) and Katsube et al. (1986) referred to the quantity $\tau / \sqrt{\delta}$ as an 'effective tortuosity' (τ_D) and defined it as:

$$\tau_D^2 = \frac{\tau^2}{\delta} \quad (21)$$

The effective tortuosity values can be calculated from measured values of effective diffusion coefficients and estimated values of through-transport porosity, using equations 16 and 21, and assuming that ε_t and ε_c are identical. Effective tortuosity values may vary depending upon the tracer because the porosity used for diffusion may vary from one tracer to another. The porosity

value used in equation 16 could be derived from water immersion or from rock capacity factors derived with conservative tracers in diffusion experiments.

In this report the convention for reporting effective tortuosity focuses on the increased path length a solute must diffuse. By this convention, the diffusion coefficient is reduced by effective tortuosity values greater than one.

4.2 **METHODS**

4.2.1 **Experimental**

The shale and limestone test rock samples used in the diffusion tests were taken from the same core locations as were the samples used for batch sorption tests (limestone sample ID: DGR5-733.62, core run #178; shale sample ID: DGR4-460.78, core run #145). The diameter of the core sections was 76 mm. The thickness of the test rock core samples used in the diffusion tests was 10 mm. The properties of Ordovician shale and limestone have been previously studied with diffusion experiments using iodide and tritium (Vilks and Miller 2007). The porosity values of shale and limestone determined by water immersion are 0.0663 ± 0.0048 and 0.0171 ± 0.0027, respectively. The effective tortuosity (τ_D) values for shale and limestone, based on tests with iodide, were 10.7 ± 1.3 and 11 ± 5.6, respectively.

The drill cores were photographed and visually examined for variation in rock type, sedimentary fabric, and any visual evidence of fractures or other defects. Suitable sections of drill core that were chosen for diffusion tests were relatively homogenous, representative of shale or limestone and free of visible defects. Several ~1 cm thick slices were cut from the shale and limestone drill core using a hack saw. The most suitable samples (see Figure 21) were selected for diffusion tests. The remaining drill core material that was close to where *test rock samples* were taken and is representative of the *test rock samples*, was used for batch sorption tests and for assessing background tracer concentrations in the rock.

A schematic of the diffusion cell is illustrated in Figure 22, and actual diffusion cell parts are shown in Figure 23, along with a test rock sample. The diffusion cell contains a 950 cm^3 volume tracer reservoir, contacting one side of the rock sample, and a 155 cm^3 elution reservoir contacting the other side. The core samples were installed in the diffusion cells by cementing them into the sample holders with silicon rubber adhesive sealant (RTV 108, Momentive performance materials). The silicon rubber ensures that tracer cannot diffuse through the contact between the *test rock sample* and the sample holder. The assembled diffusion cells were then transferred to the N_2 filled glove box, along with experimental SR-270-PW reference brine solution, which had been previously purged with N_2 gas for 10 minutes to remove O_2. Initially both reservoirs were filled with SR-270-PW reference brine solution (no tracers) and the sample core was allowed to saturate with brine for a period of 6 days. Figure 24 illustrates an assembled diffusion cell with a test rock sample and solutions. During the conditioning period, the water level on the tracer reservoir side was higher than on the elution reservoir side to promote water flow through the sample (actual flow through the *test rock sample* is expected to be minimal due to its low permeability). At the completion of the conditioning period the conditioning solution was removed from both reservoirs. Both reservoirs were rinsed with fresh SR-270-PW brine solution.

Diffusion tests were initiated by first adding tracer-free SR-270-PW brine solution to the elution reservoir. Then SR-270-PW brine solution with tracers was added to the tracer reservoir, taking

care to make sure that the solutions in both reservoirs are at the same hydraulic level. The injected tracer concentrations, free-water diffusion coefficients and expected sorption properties of the tracer elements based on batch sorption tests are summarized in Table 19. Both reservoirs were kept open to the same atmospheric pressure present in the glove box. The elution reservoir was sampled on a weekly basis to determine if any *tracers* had diffused through the test rock sample. Sampling is done by removing a 5 mL solution sample and immediately replacing it with the same volume of tracer-free SR-270-PW brine solution to ensure that both the tracer and elution reservoirs remained at the same hydraulic level. The sampling rate was kept to a minimum because the diffusion process was expected to be very slow and a faster sampling rate would not allow the tracer concentrations to build up to a measurable concentration within the elution reservoir. A portion (0.2 mL) of the solution sample was diluted by adding 20 mL of 1 mol/L nitric acid and stored for analyses.

The pH of the remaining solution sample was measured to establish the pH at the time of sampling. The pH is determined with a narrow bodied, gel filled combination glass electrode, without stirring. Elution reservoir sampling was continued for the 12 month duration of the diffusion tests.

Table 19: Tracer Properties Used in Diffusion Test

Element	Initial Tracer Concentration (mol/L)	Free-Water Diffusion Coefficient (D_w) (m^2/s)	K_d Values from Batch xperiments (cm^3/g)	
			Shale	Limestone
Li(I)	1.9×10^{-2}	[1] 1.03×10^{-9}	0 - 5	0 - 2
Ni(II)	1.0×10^{-4}	[1] 6.65×10^{-9}	0 - 5	0 - 3
Cs(I)	9.5×10^{-6}	[2] 2.06×10^{-9}	74 - 600	32 - 690
Pd(II)	4.7×10^{-6}	[1] 1.12×10^{-9}	350 – 14,300	49 – 22,000
Zr(IV)	2.1×10^{-6}	[1] 4.90×10^{-10}	320 – 7,800	130 – 4,700
Sn(IV)	3.5×10^{-7}	[3] 6.5×10^{-10}	500 – 44,000	330 – 18,000
Th(IV)	3×10^{-9}	[4] 1.53×10^{-10}	1,600 – 6,800	600 – 2,700

[1]Calculated from ion conductivity using Nernst expression (Robinson and Stokes, 1959)
[2]Uemoto (2000); Harvey (1996)
[3]Yang et al. (2011)
[4]Li and Gregory (1974)

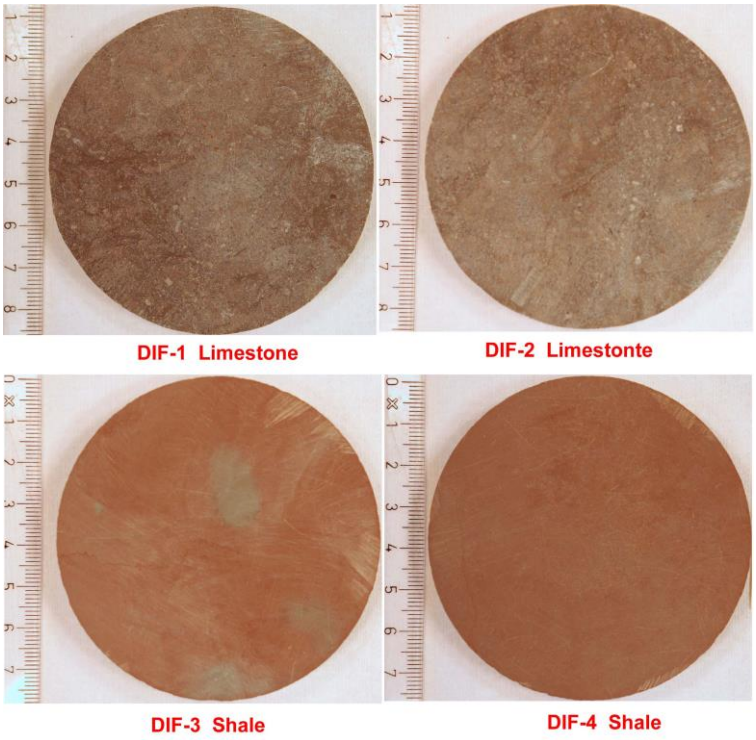


Figure 21: Limestone (DIF1 & DIF2) and Shale (DIF3 & DIF4) Test Rock Samples

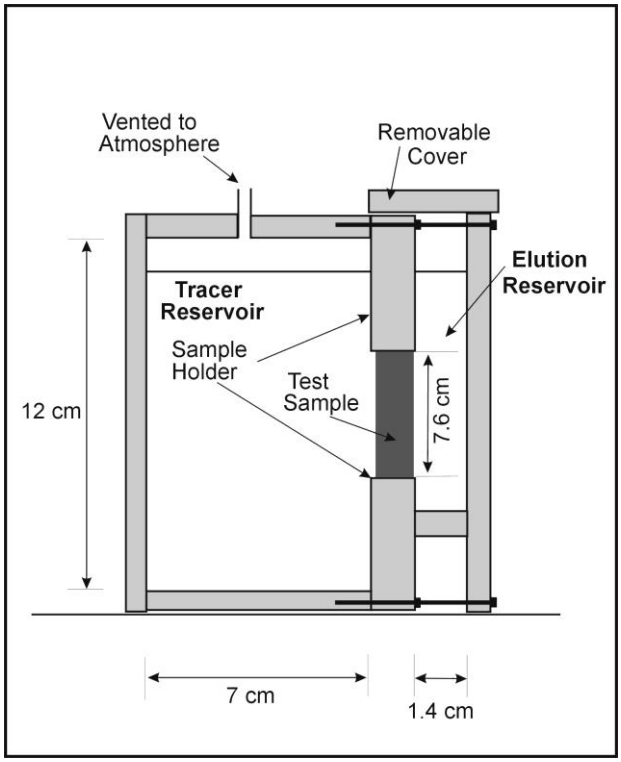


Figure 22: Schematic Diagram of Diffusion Cell

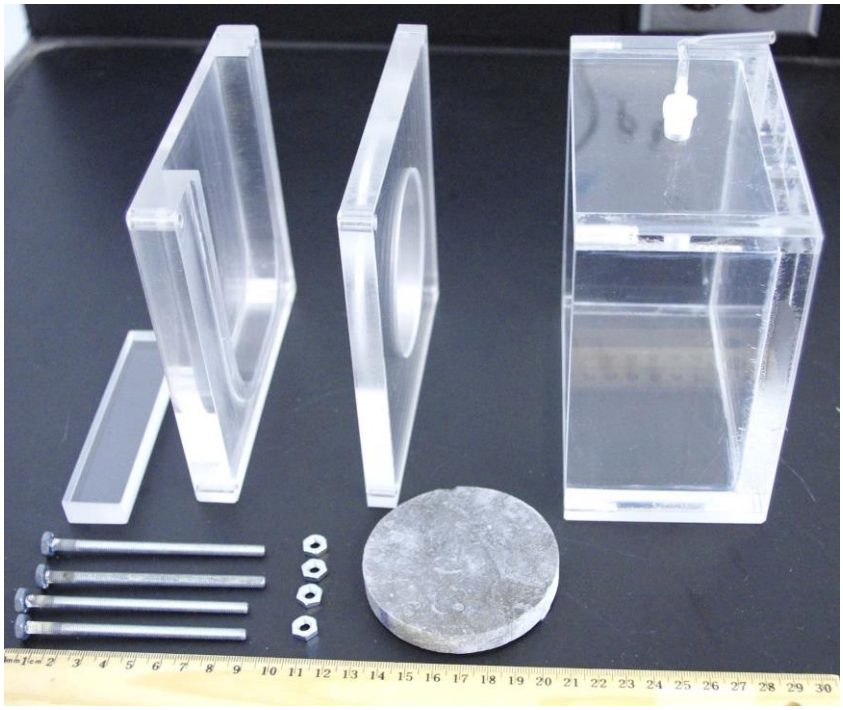


Figure 23: Test Rock Sample and Diffusion Cell Parts

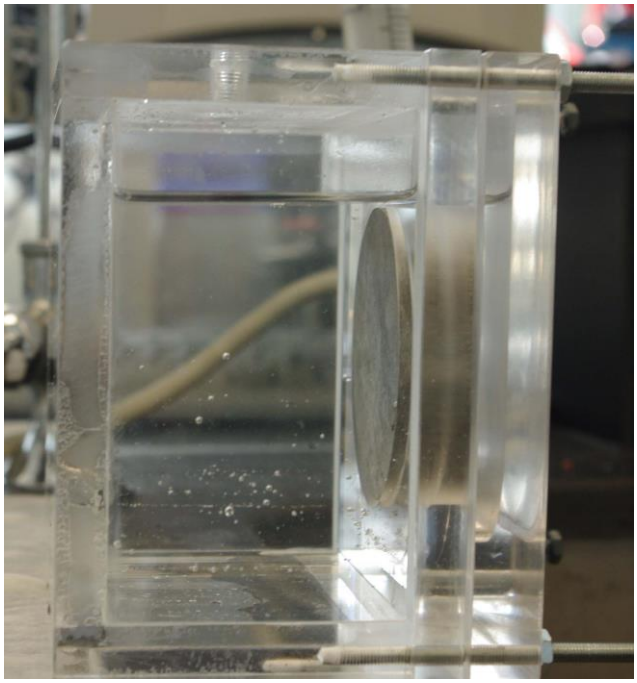


Figure 24: Assembled Diffusion Cell with Test Sample

The four diffusion tests were terminated after 368 days of diffusion. At that time each diffusion test was removed from the glove box and immediately the tracer and elution reservoirs were emptied. The faces of the test samples were towel dried (KIMTUFF KC towel) to remove any remaining ionic medium with tracers. The diffusion cells were disassembled, and the test rock samples were removed from the sample holder by cutting away the silicon rubber adhesive holding the test rock sample in place and pushing the test rock sample out of the holder. Once removed from the cell, the test rock samples were stored in a humid environment to minimize evaporative losses and possible migration of tracers in the core caused by redistribution of pore water due to evaporation.

In order to determine tracer concentration as a function of distance from the tracer reservoir side, two sections of each test rock sample were removed for sampling purposes. The section of test rock sample to be used for post test sampling is chosen to avoid core edges, in case they contain artefacts from the drilling used to extract the rock core from the geologic formation. The remaining portion of the test rock sample is archived. To achieve this, the test rock samples were cut into smaller pieces using a hacksaw (Figure 25). The smaller pieces (Figure 26) were examined and two pieces were selected from each test rock sample to be used for profile sampling.

Starting from the tracer side of the test rock sample, rock material was removed from the test rock sample by sanding with 120 grit wet/dry sandpaper (Figure 27). The sanded rock material was recovered quantitatively. During the sanding/grinding process, the thickness and weight of the remaining test rock sample were periodically determined to monitor the amount of test rock sample removed to become the profile sample. The profile sample should represent a test rock sample thickness of 0.1 to 1.3 mm, with thickness increasing away from the tracer side of the test rock sample. The target number of profile samples was 15. The collected profile samples were weighed and placed in 28 mL Nalgene polycarbonate Oak Ridge centrifuge tubes.

Tracers were leached from the profile samples by adding 2.5 mL of 30% (by volume) HNO_3 acid to each Oak Ridge centrifuge tube (Figure 28). If the amount of sample was greater than about 1 g, care was taken to not to add acid too quickly, otherwise the vigorous reaction with carbonates would cause fizzing that could lead to sample loss from the centrifuge tube. If the acid had not consumed all of the carbonates, and the pH had increased to 4 or higher, another 2.5 mL of 30% acid was added. If required, a third aliquot of 30% acid was added (the intention was for all carbonates to be dissolved so that they do not raise the pH of the leaching solution to basic values). Once fizzing had stopped and acidic conditions were still present, the samples were leached for 2 hours. After that, enough deionized water was added to increase the volume to 20 mL. The samples were centrifuged at 15,000 rpm for 25 minutes. The supernatants were removed, leaving all solids behind. The tracer concentrations of the supernatant samples were analyzed by high resolution ICP-MS.

Background tracer concentrations in shale and limestone rock samples were determined by taking three separate samples from both the shale and limestone drill cores not exposed to tracer and processing them as described above.

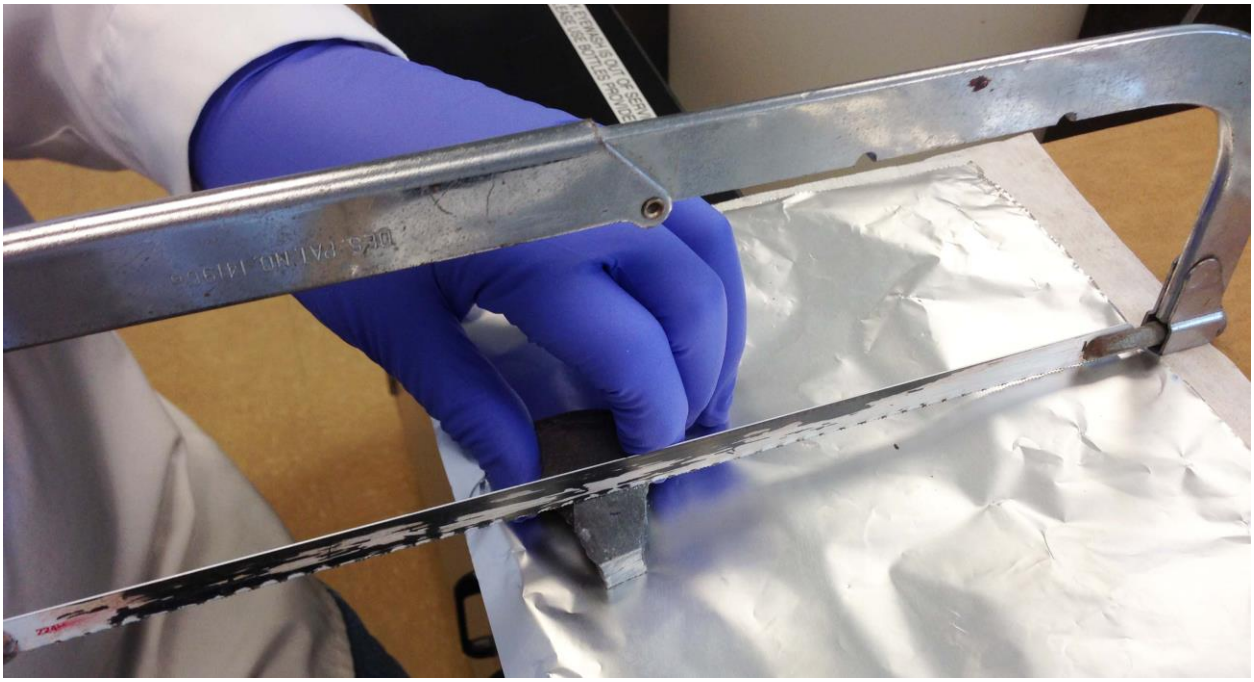


Figure 25: Cutting Test Rock Sample into Smaller Sections for Profile Sampling



Figure 26: Examples of Potential Diffusion Profile Samples

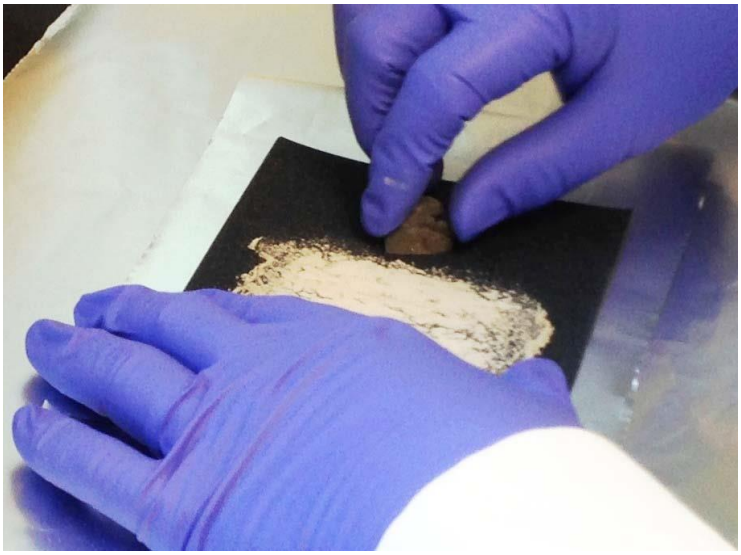


Figure 27: Removing Material from Test Rock Samples to be Used for Determining Tracer Concentrations



Figure 28: Leaching of a Diffusion Profile Sample with Nitric Acid to Extract Tracers

4.2.2 **Calculation of Diffusion Profiles**

Diffusion profiles are tracer concentrations in the *test* rock sample (mol/kg) as a function of distance from the tracer reservoir. The tracer concentration in a profile sample was calculated as:

$$M_{rock} = [M]_{leach} \times V_{leach} / mass_{sample} \text{ (mol/kg)} \quad (22)$$

It was assumed that the leaching procedure with HNO_3 was able to remove all of the tracer that had diffused into the profile sample, including what is in pore spaces and what had sorbed onto mineral surfaces. The leaching process could also extract some of the tracer elements that may have been present in the test rock sample before the diffusion test. Therefore, the background tracer concentrations in the shale and limestone rock samples were removed from the tracer concentrations in the profile samples.

$$M_{corrected} = M_{rock} - M_{background} \quad (23)$$

Where: V_{leach} = volume of sample leachate solution (30% (by volume) HNO_3) used to leach the profile sample (0.020 L)
$[M]_{leach}$ = tracer concentration in sample leachate (mol/L)
$mass_{sample}$ = mass of profile sample that was leached (kg)
M_{rock} = concentration of tracer that was leached from the profile sample (mol/kg)
$M_{background}$ = background tracer concentration in the rock sample before diffusion test (mol/kg)
$M_{corrected}$ = concentration of tracer in the profile sample corrected for background tracer concentration

The diffusion profiles were constructed by plotting $M_{corrected}$ for each profile sample versus the distance of its midpoint from the face of the test rock sample in contact with the tracer reservoir. Sorption coefficient values were determined by comparing measured diffusion profiles with diffusion profiles simulated by modelling as described by Vilks and Miller (2014).

4.3 **RESULTS**

Measured diffusion profiles for shale and limestone rock samples are illustrated in the following seven figures (Figure 29 to Figure 35), showing Li, Ni, Cs, Pd, Zr, Sn and Th concentrations in rock samples (mol/kg) as a function of distance from the tracer reservoir (always on the left side). The plotted distance of each element concentration, for a given profile sample, represents the mid-point distance of the profile sample from the tracer reservoir. Each figure represents a different element, with diffusion profiles for limestone and shale. Limestone is represented by two test rock samples DIF1 and DIF2 (as illustrated in Figure 21), and shale is represented by samples DIF3 and DIF4 (Figure 21). Two diffusion profiles were obtained from each test rock sample, providing a total of four profiles for each rock type. These four profiles provide a measure of rock heterogeneity and experimental variability.

Lithium diffusion profiles are illustrated in Figure 29. Limestone displayed considerable variability in the shape of Li diffusion profiles, with each of the test rock samples having profiles with relatively high and low Li concentrations. This suggests a degree of variability in limestone

for the diffusion of Li. The Li diffusion profiles displayed a gradual decrease in concentration with distance from the tracer reservoir, suggesting a low K_d value. There are no reportable Li concentrations for the first 1 mm in limestone because the profile sample sizes close to the tracer reservoir were too small to produce measurable Li concentrations in the leachates. Lithium concentrations in shale were significantly higher compared to limestone, which is not surprising given the higher clay content in shale. The Li diffusion profiles in shale all displayed a consistent decrease away from the tracer reservoir, consistent with a relatively low Li K_d value. Considering the observed Li concentrations close to the tracer reservoir, combined with the known tracer concentration, one could estimate a Li K_d value for shale that is between 0.025 and 0.034 cm^3/g (details of estimating K_d values by diffusion tests are described in Vilks and Miller (2014).), much lower than the batch test result of Li on shale in SR-270-PW 2 ± 3 cm^3/g.

Nickel diffusion profiles for limestone and shale are shown in Figure 30. In limestone Ni diffusion profiles were similar to each other and showed a rather steep drop in concentration within the first 2 mm from the tracer reservoir. This indicates stronger sorption than Li. Considering the range of Ni concentrations at the interface with the tracer reservoir, the Ni K_d value for limestone would be between 0.58 and 1.9 cm^3/g. This is similar to the batch test results of 1 ± 2 cm^3/g for limestone in SR-270-PW (Vilks and Miller 2014). Nickel concentrations in shale were higher than in limestone. One diffusion profile had higher Ni concentrations than the other 3 profiles. Nickel concentrations decreased rapidly with distance from the tracer reservoir within the first 2 to 4 cm. The Ni diffusion profiles were similar to the diffusion profile reported for shale by Vilks and Miller (2014). The observed Ni concentrations at the interface with the tracer reservoir suggest a Ni K_d value for shale between 2.7 and 5.8 cm^3/g. This is similar to the batch test results of 2 ± 3 cm^3/g for shale in SR-270-PW (Vilks and Miller 2014).

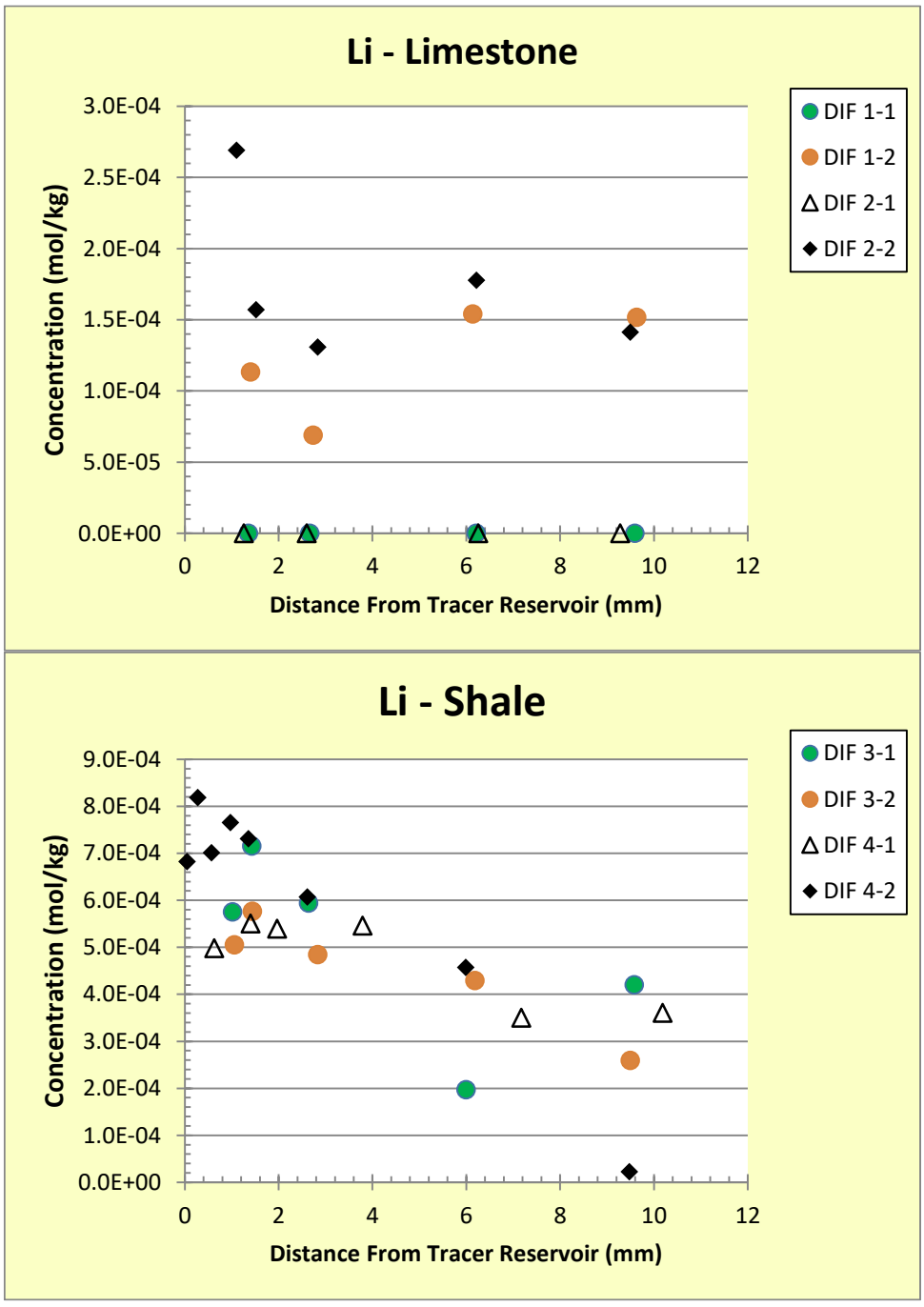


Figure 29: Lithium Diffusion Profiles in Limestone and Shale

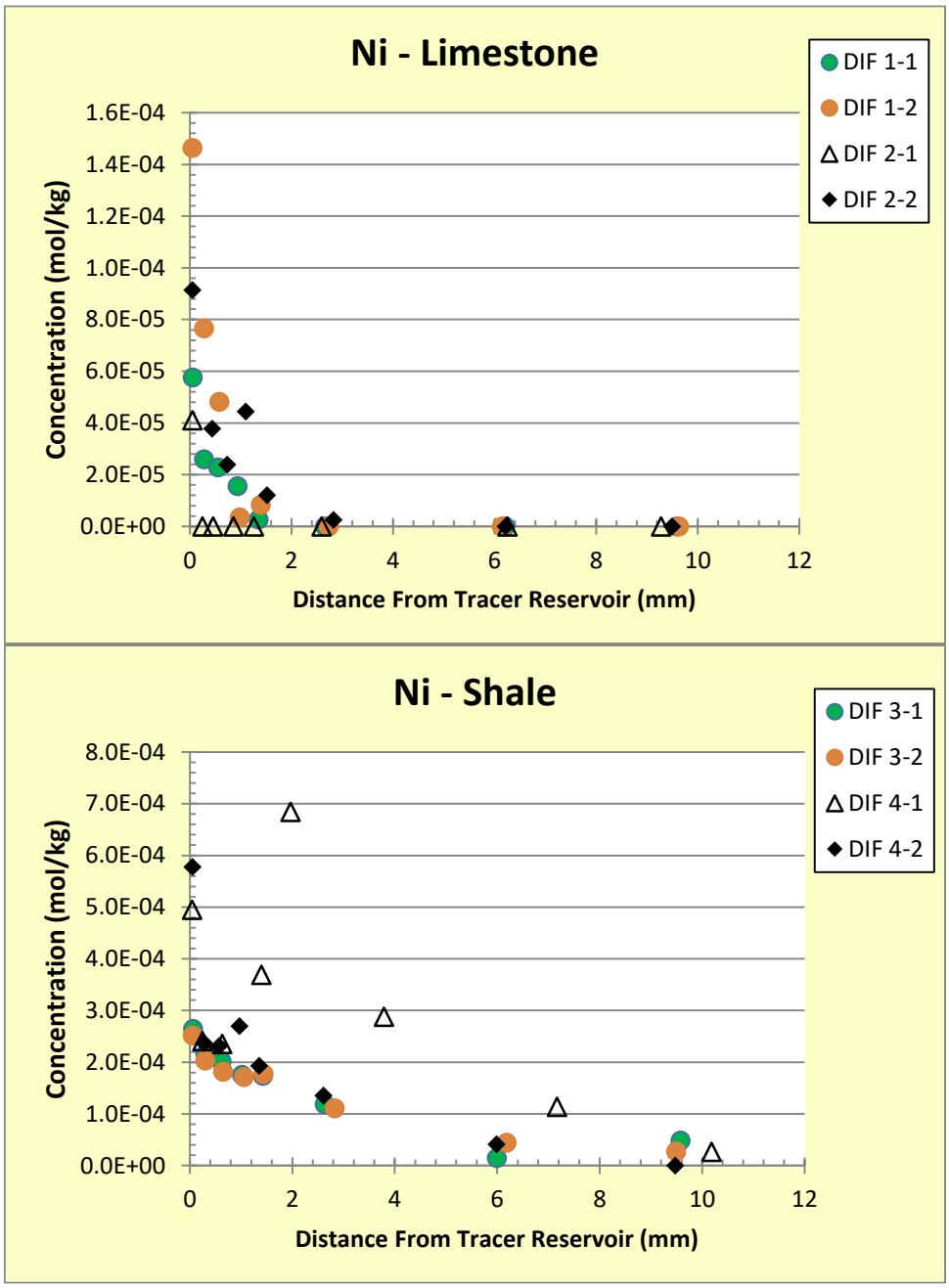


Figure 30: Nickel Diffusion Profiles in Limestone and Shale

Cesium diffusion profiles for limestone and shale are shown in Figure 31. The profiles in both rock types are similar, displaying sharp decreases away from the contact with the tracer reservoir. In limestone the steep slope of the Cs profile stops around 1.5 mm, while in shale the steep profile extends to about 3 to 4 mm. Within each rock type the Cs diffusion profiles are similar, suggesting that with respect to Cs the diffusion properties within each rock type were homogeneous. Considering the measured Cs concentrations at the rock interfaces with the tracer reservoir, the estimated ranges of Cs K_d values in limestone and shale would be 0.11 to 8.6 cm^3/g and 0.30 to 4.8 cm^3/g, respectively. These values are significantly lower than K_d

values determined in batch tests for limestone (32 to 690 cm^3/g) and shale (69 to 630 cm^3/g). This suggests that Cs sorption is significantly affected by accessibility to sorption sites in diffusion transport. In other words, the crushed rocks used in the batch experiments have a higher surface area than intact rock so sorption (i.e., K_d value) should be higher in batch experiments than in diffusion experiments.

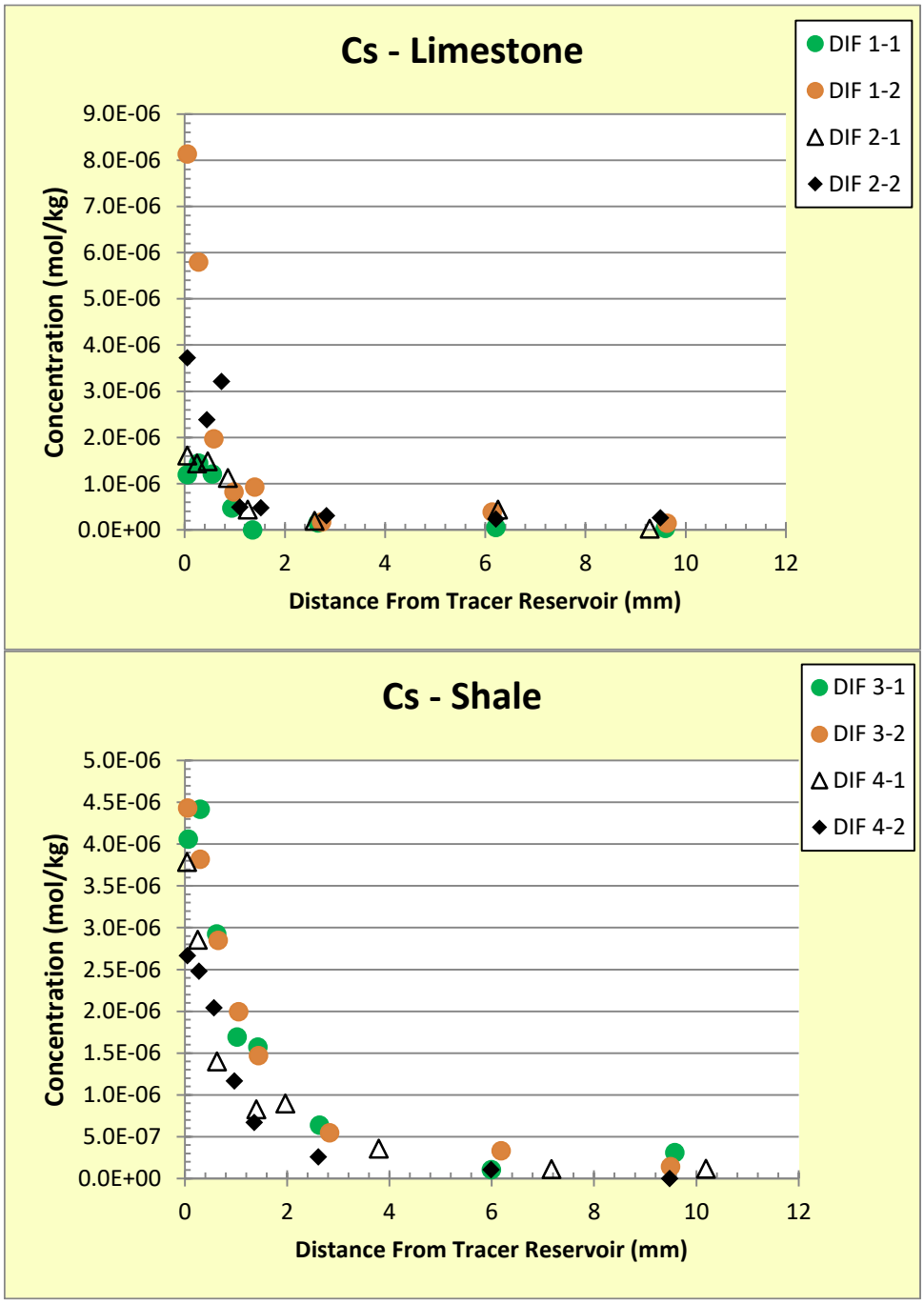


Figure 31: Cesium Diffusion Profiles in Limestone and Shale

The measured Pd diffusion profiles for limestone and shale are shown in Figure 32. Limestone contained significantly lower Pd concentrations compared to shale (by a factor of about 11 to 28). Palladium was detected only in the profile samples that were in direct contact with the tracer reservoir, indicating that there was no significant Pd diffusive transport beyond 0.1 mm.

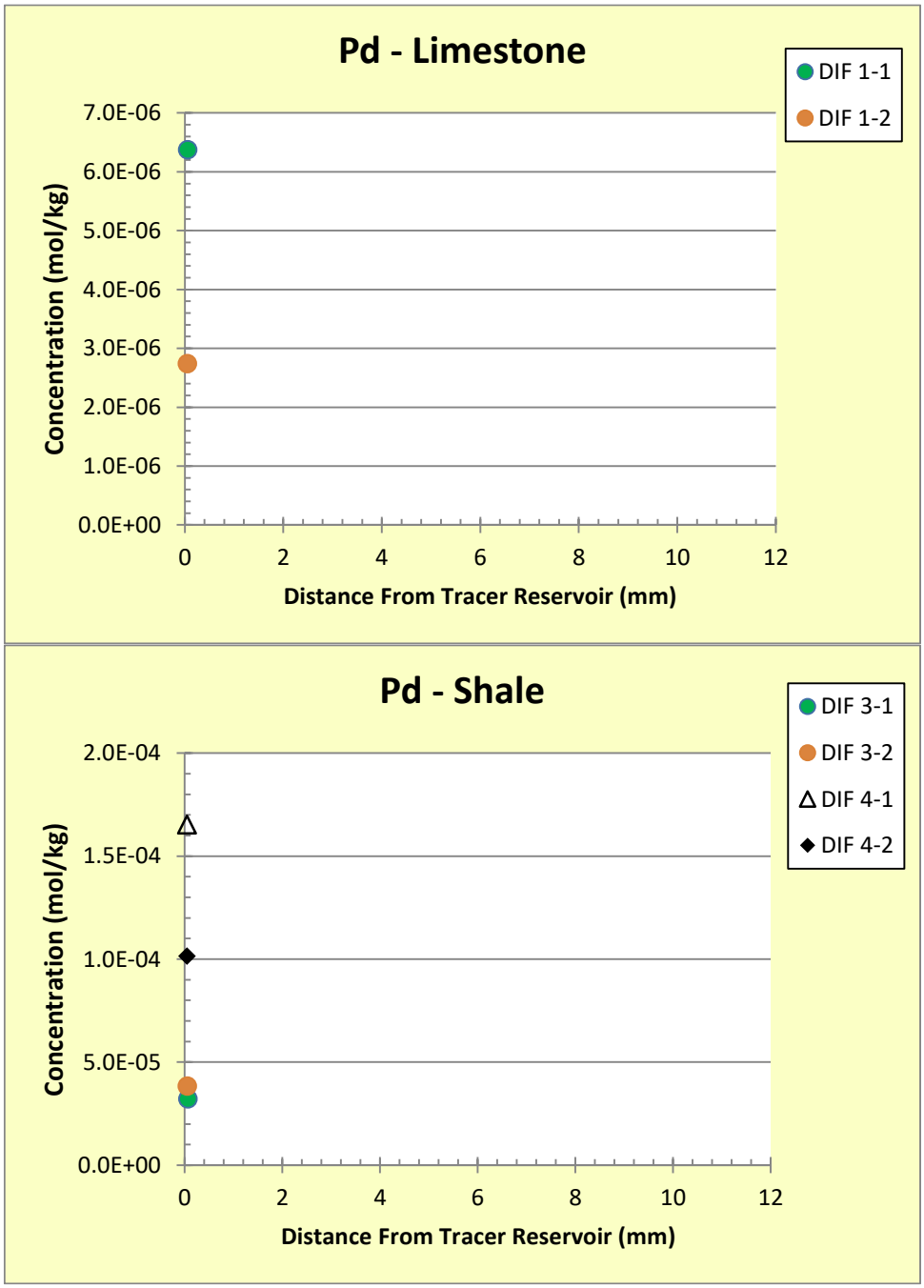


Figure 32: Palladium Diffusion Profiles in Limestone and Shale

Zirconium diffusion profiles for limestone and shale are shown in Figure 33. Measured Zr concentrations in limestone and shale were similar. As with Pd, in most cases Zr diffusion was restricted to a distance not greater than 0.1 mm from the tracer reservoir. There were some exceptions, such as profile DIF4-2, where the steep Zr diffusion profile extended as far as 0.32 mm.

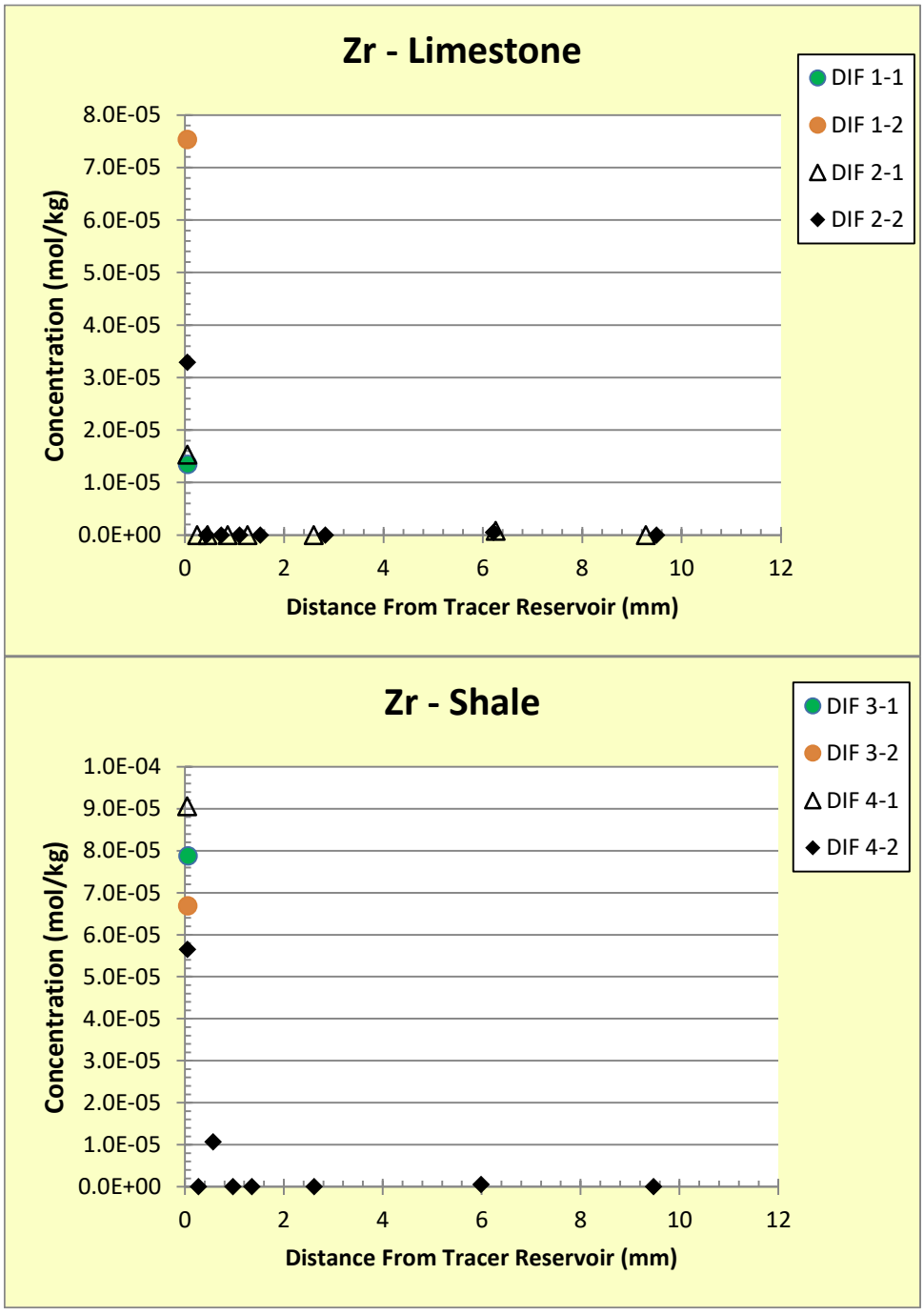


Figure 33: Zirconium Diffusion Profiles in Limestone and Shale

Tin diffusion profiles for limestone and shale are shown in Figure 34. The Sn concentrations in limestone were lower than in shale by a factor 2.4 to 10. The Sn diffusion profile in limestone showed a very steep curve extending as far as 0.33 mm from the tracer reservoir. In shale the Sn diffusion profile was not as steep and extended to as far as 2 to 3 mm from the tracer reservoir. Assuming a penetration distance of 0.33 and 2 mm, the estimated Sn K_d values were 3.2 to 285 cm^3/g for limestone and 30 to 400 cm^3/g for shale. These Sn K_d values are significantly lower than the range of K_d values obtained from batch tests, which produced Sn K_d values of 990 to 18,000 cm^3/g for limestone and 1500 to 44,000 cm^3/g for shale.

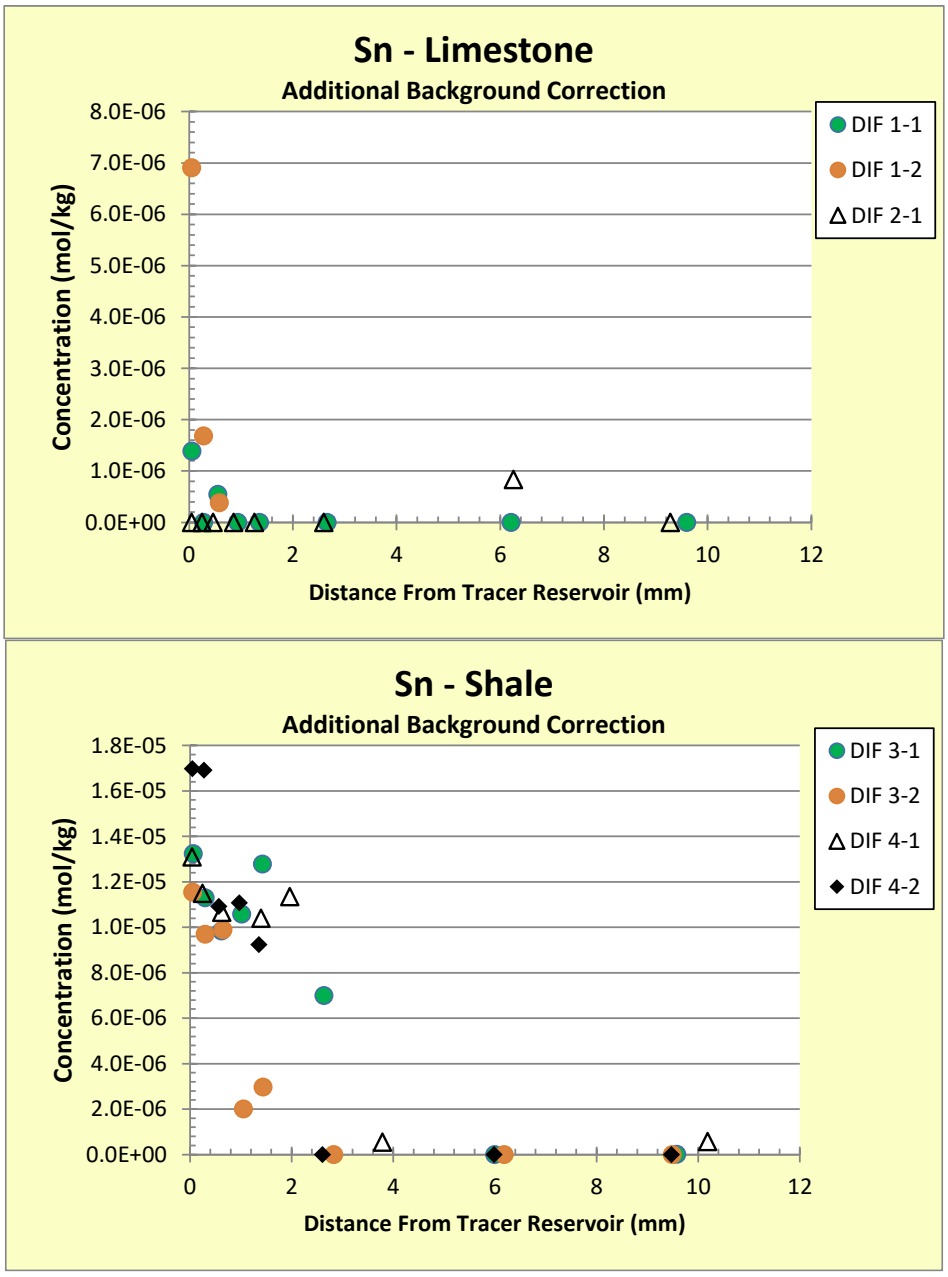


Figure 34: Tin Diffusion Profiles in Limestone and Shale

Thorium concentrations in limestone and shale are shown in Figure 35. Thorium appears to be evenly distributed throughout shale and limestone. With the possible exceptions of profiles DIF1-1 in limestone and DIF3-1 in shale, the pattern of Th concentrations with respect to the tracer reservoir does not indicate the influence of a diffusion process. It seems that the background concentration of natural Th is high and masks the contribution of a diffusive tracer. The use of higher Th tracer concentrations is limited due to solubility concerns. Perhaps the use of a Th radiotracer could provide more meaningfull results since it would be able to distinquish the tracer Th from natural background Th.

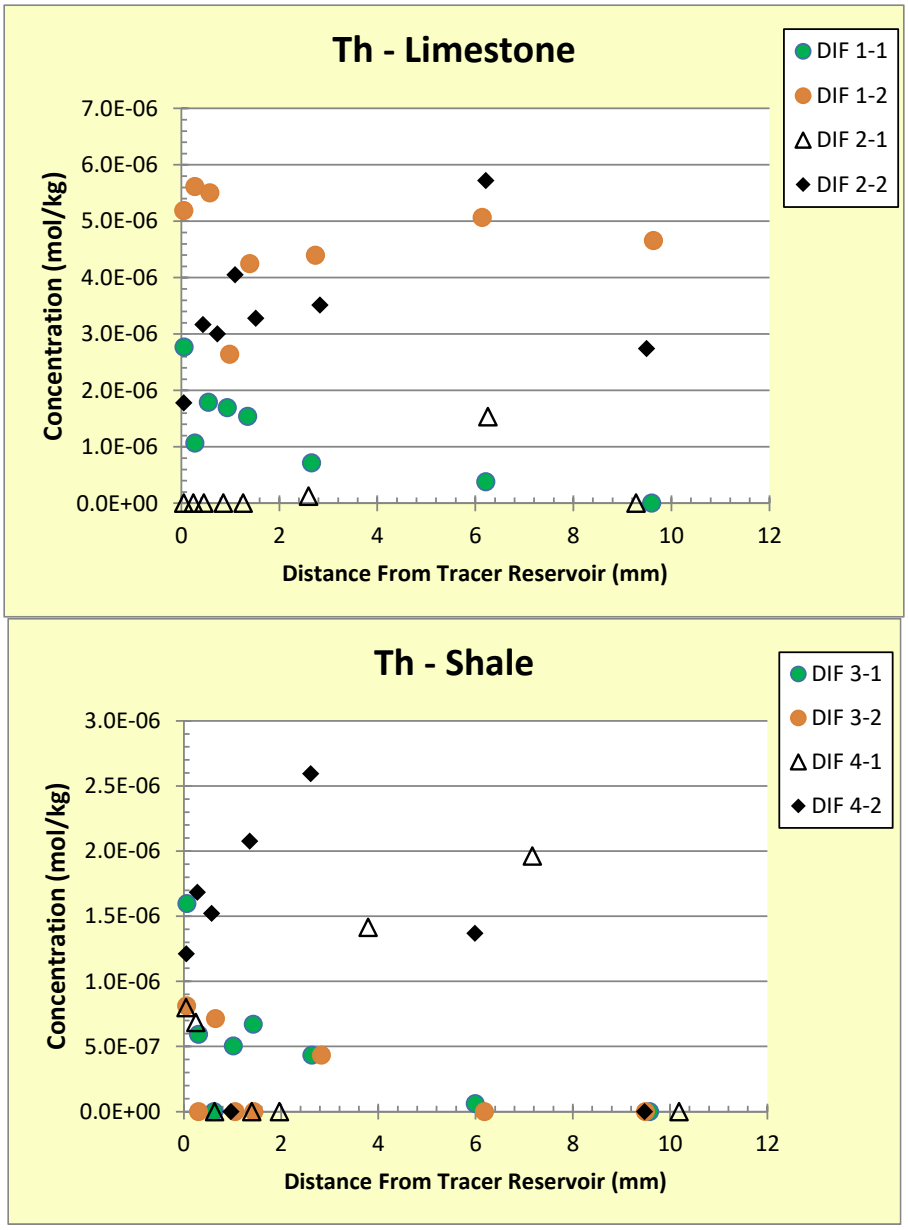


Figure 35: Thorium Diffusion Profiles in Limestone and Shale

4.4 **MODELLING**

4.4.1 **Method**

Sorption coefficient values were determined by comparing measured diffusion profiles with diffusion profiles simulated by modelling as described by Vilks and Miller (2014). Modelling was performed with AMBER, Version 5.5, a code designed and licensed by Quintessa Ltd., Henley-on-Thames, United Kingdom (www.quintessa.org). AMBER was designed to assist in the building of and solving compartment models. In AMBER, the materials of interest, referred to as 'contaminants', were assumed to be uniformly mixed in a series of compartments between which transfers can take place. Each transfer was 'donor controlled', depending directly on the amount of the material present in the compartment from which the material was moving, and could change with time.

Two models were set up, both re-creating the geometry of the diffusion experiment. One model employed the test rock sample shale properties and the other model limestone properties. Values for shale and limestone porosity, tortuosity and density were based on average values reported by Vilks and Miller (2007). In both cases, mass transport was considered to occur in only one direction, from the boundary of tracer reservoir toward the opposite side of the sample. Compartments were set up to represent either a volume of water (tracer reservoir or elution reservoir) or water-saturated test rock sample. The thickness of each compartment within the test rock sample was 0.1 mm. In general, all compartments were assumed to be well mixed (homogeneous). Transport between two test rock sample compartments was assumed to be from the centre of one compartment to the centre of the next compartment. Water compartments had defined volume and concentrations, but a zero thickness to ensure transport was calculated only from the edge of the test rock sample to centre of the first test rock sample compartment. Transport occurred across the entire exposed area of test rock sample.

In the diffusion experiment, the tracer and elution reservoirs were very well mixed and assumed to be homogeneous. Any potential losses due to evaporation, degassing or other passive loss mechanisms were assumed negligible.

The fractional diffusive transfer rates from compartment A to compartment B ($\lambda_{Diff\ A\to B}$) as well as the back transfer from B to A ($\lambda_{Diff\ B\to A}$) were considered. These were determined from the effective diffusion coefficient ($D_{AVG}^{e\ Diff}$), the porosity of compartment A or B (θ_A, θ_B), transport distance between compartment centers (d_{c-c}), the length of compartment A or B (L_A, L_B), and the retardation factors for compartment A or B (R_A^E, R_B^E):

$$\lambda_{Diff\ A\to B} = \frac{D_{AVG}^{e\ Diff}}{\theta_A \cdot d_{c-c} \cdot L_A \cdot R_A^E} \quad [/\text{day}] \qquad (24)$$

$$\lambda_{Diff\ B\to A} = \frac{D_{AVG}^{e\ Diff}}{\theta_B \cdot d_{c-c} \cdot L_B \cdot R_B^E} \quad [/\text{day}] \qquad (25)$$

where

$D_{AVG}^{e\ Diff}$ = effective diffusion coefficient (m^2/day);
L_A = length of compartment A (m);
L_B = length of compartment B (m);
d_{c-c} = transport distance between centres of compartment A and B (m);
R_A^E = retardation factor for element E in compartment A (-);
R_B^E = retardation factor for element E in compartment B (-);
θ_A = porosity of compartment A (-); and
θ_B = porosity of compartment A (-).

The retardation factor was calculated from the porosity, the rock density, and the sorption coefficient, K_d:

$$R_A^E = \left(1 + \frac{\rho K_d}{\theta}\right) \qquad [\text{no units}] \tag{26}$$

K_d = sorption coefficient of tracer in limestone or shale (m^3/kg), and
ρ = density of limestone or shale (kg/m^3).

The initial model parameters used to model diffusive transport are summarized in Table 20. The porosity of the shale and limestone samples were average values of shale and limestone porosity (Vilks and Miller, 2007) determined with the water immersion technique. The porosity term was not manipulated in the transport simulation. The density was based on average values reported by Vilks and Miller (2007). The tortuosity factor in Table 20 is related to the effective tortuosity (τ_D) by:

$$tortuosity\ factor = \frac{1}{\tau_D^2} \tag{27}$$

The tortuosity factor takes into account the effect of pore geometry on diffusive transport, and the tortuosity factor values in Table 20 were calculated from respective τ_D values of 10.7 ± 1.3 and 11 ± 5.6 for shale and limestone, based on iodide diffusion reported by Vilks and Miller (2007).

Table 20: Parameters Used for Diffusive Mass Transport Modelling with AMBER

Parameter	Shale	Limestone
Porosity [-]	0.0663 ± 0.0048	0.0171 ± 0.0027
Density [kg/m^3]	2608	2646
Tortuosity Factor [-]	0.0087 ± 0.0029	0.0083 ± 0.0042
Segment Length [mm]	10.6	10.5
Number of compartments [-]	98	98
Transport Distance [mm] in Each Compartment	0.1	0.1
Radius [mm]	38	38

Water Compartment Properties

Parameter	Tracer reservoir	Elution reservoir
Volume [mL]	950	120
Rate of Water Exchange During Sampling That Reduces Tracer Concentration [mL/sample]	-	5
Transport Distance from Water Compartment to Center of First Shale/Limestone Layer [mm]	0.05	0.05

The tracer properties used in diffusion modelling are summarized in Table 19. The initial tracer concentrations are representative of concentrations used in the diffusion tests. The ranges of K_d values observed in batch sorption tests were used as guides for selecting K_d values for diffusion simulations. The free-water diffusion coefficients were obtained from the literature or estimated from ion equivalent conductivities. Table 21 summarizes the estimation of free-water diffusion coefficients, which were determined as described below.

The Nernst expression relates free-water diffusion coefficients to equivalent conductivities (Robinson and Stokes 1959, p. 317):

$$D_j^0 = \frac{RT\lambda_j}{Z_j F^2} \qquad (28)$$

Where:
D^0_j = free water self diffusion coefficient of ion j (cm^2/s)
R = gas constant (8.314 J mol^{-1} kg^{-1})
T = absolute temperature (i.e. 298 K for 25 °C)
λ_j = equivalent conductivity of ion j (cm^2 S mol^{-1}) (S = Siemens)
Z_j = the absolute value of the charge of ion j
F = Faraday constant (9.648456 x 10^4 C mol^{-1}) (C = Coulomb)

λ_j values can be found in Weast (1972) or Lide (1992). If equivalent conductances are not available, they were estimated from the following equation (Nigrini 1970):

$$\lambda_j = 10.56 + 90.72 \log Z_j + 42.95\, \gamma_j/Z_j \qquad (29)$$

Where:

γ_j = crystal ionic radius of ion j

Table 21: Element Free Water Diffusion Coefficients

Element	Equivalent Conductivity (cm^2 S mol^{-1})	Ionic Radius (Å) (Weast 1978)	Free water Diffusion Coefficient (m^2/s)
Li(I)	[1]38.66	0.68	[2]1.03×10^{-9}
Cs(I)	[1]77.2	1.67	[2]2.06×10^{-9}
Pd(II)	[3]55.0	0.80	[4]1.12×10^{-9}
Zr(IV)	[3]73.7	0.79	[2]4.90×10^{-10}
Sn(IV)	[3]71.3	0.71	[5]6.5×10^{-10}
Th(IV)	[3]76.1	1.02	[6]1.53×10^{-10}
Ni(II)	[1] 50	0.69	[2]6.65×10^{-10}

[1]Lide (1992)
[2]Calculated from equivalent conductivity
[3]Calculated with Nigrini (1970) equation
[4]Uemoto (2000) reported the diffusion of $PdCl_4^{-2}$
[5]Yang et al. (2011)
[6]Li and Gregory (1974)

Tracer diffusion for Li, Ni, Cs, Pd, Zr and Sn was simulated for the limestone and shale test rock samples, using a range of K_d values for each element. Output tracer concentrations within the test rock samples were selected as a function of distance from the tracer reservoir for a diffusion time period of 365 days. The model calculated tracer concentrations were in terms of mol/m^3. For the construction of simulated diffusion profiles these concentrations were converted to mol/kg using limestone and shale densities (Table 20). The simulated diffusion profiles were plotted using the mid-point distance for each compartment. Simulated diffusion profiles were compared to measured tracer concentrations in the test samples with the aim of identifying the K_d values which could best explain the measured diffusion profiles.

As noted in Section 3.3, the concentrations of some tracers in the test rock samples were lower than expected based on K_d values determined by batch tests. It has been noted that in diffusive mass transport not all of the rock mass may be available for sorption (Vilks 2009). Batch sorption tests use rock samples crushed to powder form. Given the large surface to mass ratio of small rock particles, most sorption sites in a crushed rock sample would be available for element sorption from the suspending liquid. When elements diffuse through intact rock they follow the connected pore spaces. Not all of the sorption sites for a given element in the intact rock mass might be in contact with the open porosity. If the sorption of a given element requires a specific mineral or perhaps a specific location in a mineral (such as Cs requiring the interlayer space of clay minerals), then the availability of sorption sites within intact rock may be further restricted.

4.4.2 **Diffusive Transport Modelling Results**

Simulated and measured Li diffusion profiles for limestone and shale are summarized in Figure 36. Measured Li concentrations (mol/kg) appear as single points, and are associated with designated diffusion profiles. DIF1 and DIF2 represent the tests with limestone and DIF3 and DIF4 represent tests with shale. Two profiles were obtained from each test rock sample, for example DIF1-1 and DIF1-2. Simulated curves appear as solid lines, and marked with K_d values (cm^3/g) used in the simulations. Lithium appeared to have diffused throughout the entire thickness of the limestone and shale samples, displaying relatively linear profiles. These diffusion profiles suggest Li diffused with minimal sorption. A comparison with simulated diffusion profiles confirms this, indicating the Li K_d value affecting diffusion in both limestone and shale is 0.01 cm^3/g.

Li K_d values obtained from batch tests for limestone (1 ± 1 cm^3/g, Vilks and Miller 2014) and shale (2 ± 3 cm^3/g, Vilks and Miller 2014) are higher than its diffusion derived values. This could be attributed to the difficulty with precisely determining the low K_d values for weakly sorbing elements such as Li with the batch method protocols used by Vilks and Miller (2014). The low total percentage of sorbed Li resulted in an increased uncertainty in batch determined K_d values. If the batch method protocol was optimized to more precisely determine low K_d values and the batch K_d values were still higher than diffusion derived numbers, then one could conclude that Li access to sorption sites was reduced within intact rock, compared to rock powders used in batch tests.

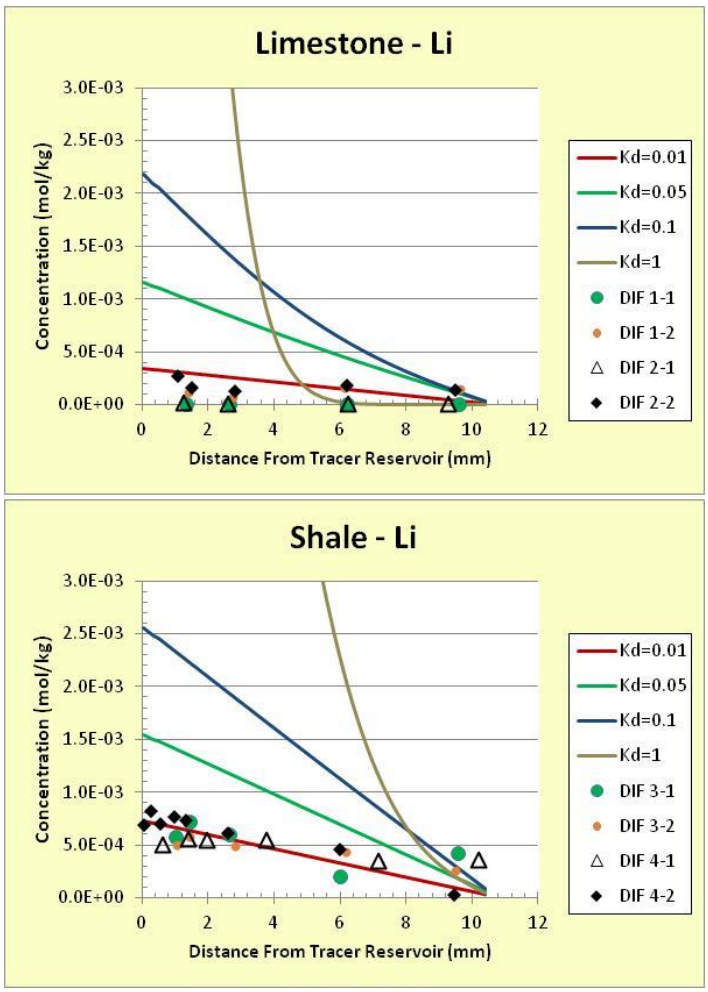


Figure 36: Simulated and Measured Lithium Diffusion Profiles in Limestone and Shale

During the 368 days of diffusion time period, no breakthrough was observed for Ni, Zr, Pd, Sn and Cs. Zr and Pd diffused less than 0.1 mm, which demonstrated that Zr and Pd were strongly sorbed, consistent with the results of the batch tests. Sn diffused ~0.3 mm in limestone and 2 mm in shale, Cs diffused ~1.5 mm in limestone and ~4 mm in shale, Ni diffused ~2 mm in limestone and 9 mm in shale. Due to the short diffusive distance for Zr, Pd and Sn in both limestone and shale rock samples and Ni in limestone, and due to the low Cs concentration in the diffusion profile, it was impossible to derive a reliable K_d value for Zr, Pd, Sn and Cs in shale and limestone and Ni in limestone by fitting the diffusion model AMBER to the diffusion profiles. The diffusion profiles of Th could not be obtained due to the high background concentration of natural Th in limestone and shale. Therefore, diffusion simulations for Ni, Zr, Pd, Sn, Cs and Th in limestone and shale are not presented.

5. SUMMARY AND DISCUSSION

Batch sorption tests and long term diffusion tests were performed to investigate the sorption behavior of Cs(I), Pd(II), Zr(IV), Sn(IV), and Th(IV) onto Canadian sedimentary rocks (shale and limestone) and bentonite. The batch techniques were used to determine sorption coefficient K_d values for Cs, Pd, Zr, Sn and Th in a SR-270-PW reference brine solution (I = 6.0 M) and a reference dilute solution (I = 0.01 M). Diffusion tests were performed for Li, Ni, Cs, Pd, Zr, Sn and Th through shale and limestone rock samples under brine conditions. Although none of the elements used in this study are redox sensitive, the batch and diffusion tests were performed under a controlled, anaerobic atmosphere.

Batch sorption experiments were performed using single element and multiple elements tests lasting up to 6 months. Depending upon the element, the time required to reach steady state, or apparent equilibrium, varied from 1 to 28 days. In all cases the K_d values measured in brine were lower than in dilute solution, with the reduction in K_d values being element dependent. For example, the least effect of salt concentration was observed with Cs, whose K_d values were a factor of 3 to 7 lower in brine. The greatest effect was noted for Pd, with K_d values in brine reduced by a factor of about 100 to 900. Sorption of Zr, Th and Sn in the brine solution was reduced by factors of about 10 to 20, 3 to 30, and 4 to 7, respectively. A contribution to the reduced sorption in brine for Pd could be a pH effect (the pH values of the brine and dilute solutions equilibrated with solid sorbent are around 6 and 8, respectively). pH effects do not account for the difference in average K_d values in brine and dilution solutions for Cs, Zr, Sn and Th. The variation in K_d values with pH did not display any clear trends for most elements. In no instance did elements display a distinct sorption edge. In brine solution, K_d values tended to be higher in the vicinity of pH 6, while in dilute solution K_d values tended to be higher around pH 8, over the pH range of 3 to 8 investigated in this work.

A desorption test was performed after a sorption time of 104 days by diluting the concentration of sorbate in solution. The concentration of remaining sorbate in solution was measured as a function of time for up to 8 days to determine desorption K_d values, which are compared to the sorption coefficient (K_d^o) assumed to represent sorption equilibrium before desorption was initiated. The results indicated that the sorption of Pd, Zr, Sn and Th was reversible for most solids. Cesium sorption was not reversible, possibly due to fixation within clay mineral structures.

The K_d values that were selected to represent sorption in brine and dilute solutions were selected from tests with sorption reaction times of 7 to 187 days at sorption apparent equilibrium. Both the single and multiple elements tests were considered. Tests within the pH range of 5.6 to 6.5 and 7.1 to 8.5 were considered representative of brine and dilute solutions, respectively.

Sorption modelling improves the understanding of sorption processes and has the potential to estimate sorption values that are applicable for in-situ groundwater compositions based on laboratory measured sorption values or sorption properties reported in the literature. This study provided a good opportunity to compare measured K_d with simulated K_d values because parameters required for the 2-site protolysis non-electrostatic surface complexation (2 SPNE SC) model have been developed for montmorillonite and illite, which make up significant fractions of the bentonite and shale, respectively, used in this study. The comparison between

simulated and measured K_d values is provided in Table 22. Simulations of the elements whose aqueous chemistry is determined by hydroxyl species were most comparable to the measured values. Element specific details on important solution species, effects of pH and ionic media, sorption mechanisms, and sorption modelling are summarized in Table 23.

Simulated Zr sorption K_d values, derived using LFER determined surface complexation constants, provide an approximation of Zr sorption values in brine solutions within a factor of 13 and conservative estimates of Zr sorption in dilute solution (within a factor of 41). Zr sorption is controlled by the complexation of Zr to surface oxygen sites. The sorption model provided a reasonable approximation for Sn sorption on shale in dilute solution for pH values 4 to 8 and in brine at pH of 6. Sn sorption on bentonite and shale is controlled to a significant extent by the complexation of Sn to surface oxygen sites. The surface complexation model provided a good approximation for Th sorption on bentonite and shale in dilute solution at pH of 7 to 8 within a factor of 7. In brine the simulated K_d values were greater than measured values by a factor of 12 to 26 and 7 to 23 for bentonite and shale, respectively. Th sorption on benontie and shale is controlled by the complexation of Th to surface oxygen sites. The failure of the surface complexation model to predict Pd sorption indicates that the dominant mechanisms of Pd sorption is not the surface complexation of hydroxyl species, and other mechanisms, such as sorption of Pd chloride complexes, must be considered.

Diffusion tests were performed for one year using multiple elements (Li, Ni, Cs, Pd, Zr, Sn and Th) to study the effect of sorption on diffusion-only transport in shale and limestone in the reference brine solution. Numerical simulations of tracer diffusion through shale and limestone were performed to fit the diffusion concentration profiles to estimate K_d values. Using diffusion tests, it was possible to determine K_d values in shale and limestone for Li. IBatch derived K_d values for shale and limestone were higher compared to its diffusion derived K_d values. Li is weakly sorbing element. K_d values determined by the diffusion method can be more precise than those determined using batch tests.

Due to the lack of measurable Ni, Cs, Pd, Zr and Sn penetration into the test rock samples (e.g., Pd and Zr diffused less than 0.1 mm in limestone and shale rock samples, and Sn diffused 0.3 mm in limestone and 2 mm in shale during the one year experimental period), and due to the high natural background Th concentrations in the limestone and shale rock samples and low Cs concentration in the rock profiles, it was impossible to derive reliable K_d values for Zr, Pd, Sn, Ni, Cs and Th in shale and limestone by fitting the diffusion model to the diffusion profiles. Although we could not obtain the K_d values from the 368 days diffusion tests in this work, the diffusion tests do confirm that Pd, Zr, and Sn were strongly sorbed onto limestone and shale in SR-270-PW reference brine, which agreed well with the experimental results from batch measurements in this work. In order to establish a precise diffusion derived K_d value in limestone and shale for these elements, a longer diffusion time is required.

Table 22: **Sorption Coefficients (cm^3/g) in Brine Solutions Derived from Batch Tests and Sorption Modelling**

Element	Solid	Batch Tests		Sorption Modelling (pH 6)
		Geomean	Range	
Cs	bentonite	4.3×10^2	1.4×10^2 - 1.4×10^3	-
	shale	2.0×10^2	6.9×10^1 - 6.3×10^2	-
	limestone	1.4×10^2	3.2×10^1 - 6.9×10^2	-
Pd	bentonite	1.2×10^3	1.4×10^2 - 1.4×10^4	0.041
	shale	2.2×10^3	4.2×10^1 - 1.4×10^4	0.020
	limestone	1.1×10^3	4.9×10^1 - 2.2×10^4	-
Zr	bentonite	2.1×10^3	4.9×10^2 - 1.5×10^4	1.4×10^3
	shale	1.5×10^3	3.2×10^2 - 7.8×10^3	8.1×10^2
	limestone	8.0×10^2	1.3×10^2 - 4.7×10^3	-
Sn	bentonite	1.9×10^4	4.2×10^3 - 9.5×10^4	6.4×10^5
	shale	1.1×10^4	1.5×10^3 - 4.4×10^4	1.5×10^5
	limestone	4.4×10^3	9.9×10^2 - 1.8×10^4	-
Th	bentonite	8.9×10^3	3.4×10^3 - 1.6×10^4	2.6×10^5
	shale	4.6×10^3	1.7×10^3 - 6.8×10^3	1.2×10^5
	limestone	2.1×10^3	6.0×10^2 - 2.7×10^3	-

- Data not available: sorption modelling was not performed for limestone and for Cs.

As with Vilks and Miller (2014), in this report, elements with K_d values of less than 10 cm^3/g (with retardation factor less than 400) are considered to be weakly sorbing, elements with a K_d value from 10 to 250 cm^3/g (with retardation factor of 400 to 9800) are considered to be moderately sorbing, and elements with K_d values greater than 250 cm^3/g are classified as strongly sorbing. If one uses the geometric means given in Table 22 as a guide for the SR-270-PW reference brine solution, Cs is strongly sorbed to bentonite and moderately sorbed to shale and limestone. The other elements, Pd, Zr, Sn and Th can all be considered as strongly sorbing.

Table 23: Summary of Sorption Properties for Each Element

Cesium	
Aqueous Species	SR-270-PW: CsCl (65%), Cs^+ (35%) Fresh water: Cs^+ (100%)
Concept of Sorption Mechanism	Fixation within interlayers of clay minerals by exchange with group 1 elements with larger hydrated radii (Li^+, Na^+, K^+, Rb^+)
Time to Steady State	SR-270-PW: 1 day for shale and bentonite, 14 days for limestone Dilute solution: 7 days
Effects of pH and Ionic Media on Sorption	Sorption was lower in brine compared to dilute solution by factors of 3 to 7. No clear variation with pH observed experimentally.
Differences Between Solids	Order of increasing sorption in brine: limestone < shale < bentonite Order of increasing sorption in dilute solution: limestone < shale < bentonite
Sorption Simulations	Surface species: None attempted, but focus would be on Cs^+
	Compare simulations with experiments: None attempted
Palladium	
Aqueous Species	SR-270-PW: $PdCl_4^{-2}$ (99%), $PdCl_3^-$ (1%) Dilute solution: $Pd(OH)_2$ (100%)
Concept of Sorption Mechanism	Not entirely clear. Could involve surface complexation of both choride and hydroxyl species.
Time to Steady State	SR-270-PW: 1 day for bentonite, 14 days for shale and limestone Fresh water: 7 days
Effects of pH and Ionic Media on Sorption	Sorption was lower in brine compared to dilute solution by factors of 120 to 900. No clear variation with pH observed experimentally.
Differences Between Solids	Order of increasing sorption in brine: limestone < bentonite < shale Order of increasing sorption in dilute solution: limestone < shale < bentonite
Sorption Simulations	Surface species: $\equiv S^sOPd^+$, $\equiv S^sOPd(OH)^0$, $\equiv S^sOPd(OH)_2^-$, $\equiv S^sOPd(OH)_3^{-2}$
	Compare simulations with experiments: Simulated K_d values were orders of magnitude lower than measured values in brine and dilute solutions. Models must include other sorption mechanisms (e.g. sorption of chloride complexes) in addition to surface complexation of hydroxyl species.
Zirconium	
Aqueous Species	SR-270-PW: $Zr(OH)_4$ (100%) Dilute solution: $Zr(OH)_4$ (100%)
Concept of Sorption Mechanism	Surface complexation of hydroxyl complexes
Time to Steady State	SR-270-PW**:** 1 day for shale, 14 days for limestone and bentonite Dilute solution: 27 days
Effects of pH and Ionic Media on Sorption	Sorption was lower in brine compared to dilute solution by factors of 10 to 20. No clear variation with pH observed experimentally.
Differences Between Solids	Order of increasing sorption in brine: limestone < shale < bentonite Order of increasing sorption in dilute solution: limestone < shale < bentonite
Sorption Simulations	Surface species: $\equiv S^sOZr^{+3}$, $\equiv S^sOZr(OH)^{+2}$, $\equiv S^sOZr(OH)_3^0$, $\equiv S^sOZr(OH)_5^{-2}$, $\equiv S^{w1}OZr^{+3}$
	Compare simulations with experiments: In brine at pH 6-7, simulated K_d values were lower than measured values by factors of 3-8 for bentonite, 5-13 for shale. In dilute solution at pH 7-8, simulated K_d values were lower than measured values by factors of 18-41 for bentonite and 6-40 for shale.

Table 23...continued

Tin	
Aqueous Species	SR-270-PW: $Sn(OH)_4$ (92%), $SnCl_6^{-2}$ (6%), $Sn(OH)_5^-$ (2%) Fresh water: $Sn(OH)_5^-$ (54%) $Sn(OH)_4$ (46%)
Concept of Sorption Mechanism	Surface complexation of hydroxyl complexes
Time to Steady State	SR-270-PW: 28 days Dilute solution: 1 to 7 days
Effects of pH and Ionic Media on Sorption	Sorption was lower in brine compared to dilute solution by factors of 4 to 7. No clear variation with pH observed experimentally.
Differences Between Solids	Order of increasing sorption in brine: limestone < shale < bentonite Order of increasing sorption in dilute solution: limestone < shale < bentonite
Sorption Simulations	Surface species: $\equiv S^sOSn(OH)_2^+$, $\equiv S^sOSn(OH)_3^0$, $\equiv S^sOSn(OH)_4^-$, $\equiv S^sOSn(OH)_5^{-2}$
	Compare simulations with experiments: In brine at pH 6-7, simulated K_d values were greater than measured values by factors of 7-220 for bentonite and 3-37 for shale. In dilute solution at pH 4-8, simulations provided a reasonable approximation to sorption on shale (within a factor of 4) and provided an approximation for bentonite (within a factor of 9).
Thorium	
Aqueous Species	SR-270-PW: ThF_2^{+2} (30%), $Th(OH)_3^+$ (25%), ThF^{+3} (9%), $Th(OH)_4$ (9%), $Th(OH)_3(CO_3)^-$ (8%), $Th(OH)_2(CO_3)$ (7%), $Th(OH)_2^{+2}$ (5%) Dilute solution: $Th(OH)_3(CO_3)^-$ (69%) $Th(OH)_2(CO_3)_2^{-2}$ (20%) $Th(OH)_4$ (10%)
Concept of Sorption Mechanism	Surface complexation of hydroxyl complexes, could also involve surface complexation of florite species
Time to Steady State	SR-270-PW: 8 days dilute solution: 1 day
Effects of pH and Ionic Media on Sorption	Sorption was lower in brine compared to dilute solution by factors of 3 to 30. A slight, but not significant increase with pH in brine for shale from pH 3 to pH 6. No clear trends with pH for bentonite and limestone in brine. No clear variation with pH observed experimentally in dilute solution.
Differences Between Solids	Order of increasing sorption in brine: limestone < shale < bentonite Order of increasing sorption in dilute solution: bentonite < limestone < shale
Sorption Simulations	Surface species: $\equiv S^sOTh^{+3}$, $\equiv S^sOTh(OH)^{+2}$, $\equiv S^sOTh(OH)_2^+$, $\equiv S^sOTh(OH)_3^0$, $\equiv S^sOTh(OH)_4^-$
	Compare simulations with experiments: In brine at pH 6-7, simulated K_d values were greater than measured values by factors of 12-26 for bentonite and 7-23 for shale. In dilute solution at pH 7-8, simulations provided a good approximation of sorption on bentonite (within a factor of 2) and shale (within a factor of 7).

ACKNOWLEDGEMENTS

Jeff Miller performed the diffusion simulations for shale and limestone. Tammy Yang and Frank Garisto of NWMO and Shinya Nagasaki of McMaster University provided fruitful discussion and review.

REFERENCES

Baeyens, B. and M.H. Bradbury. 1997. A mechanistic description of Ni, and Zn sorption on Na-montmorillonite. Part I: Titration and sorption experiments. Journal of Contaminant Hydrology 27, 199-222.

Baumann, E. 1973. Determination of pH in concentrated salt solutions. Analytica Chimica Acta 64, 284-288.

Bertetti, F.P. 2016. Determination of Sorption Properties for Sedimentary Rocks under Saline, Reducing Conditions – Key Radionuclides. Nuclear Waste Management Organization Technical Report NWMO-TR-2016-08, Toronto, Canada.

Bradbury, M.H. and B. Baeyens. 2009a. Sorption modelling on illite Part I: Titration measurements and the sorption of Ni, Co, Eu and Sn. Geochimica et Cosmochimica Acta 73, 990-1003.

Bradbury, M.H. and B. Baeyens. 2009b. Sorption modelling on illite Part II: Actinide sorption and linear free energy relationships. Geochimica et Cosmochimica Acta 73, 1004-1013.

Bradbury, M.H. and B. Baeyens. 2005a. Experimental measurements and modeling of sorption competition on montmorillonite. Geochimica et Cosmochimica Acta 69, 4187-4197.

Bradbury, M.H. and B. Baeyans. 2005b. Modelling the sorption of Mn(II), Co(II), Ni(II), Zn(II), Cd(II), Eu(III), Am(III), Sn(IV), Th(IV), Np(V) and U(VI) on montmorillonite: Linear free energy relationships and estimates of surface binding constants for some selected heavy metals and actinides. Geochimica et Cosmochimica Acta 69, 875-892.

Bradbury, M.H. and B. Baeyens. 1997. A mechanistic description of Ni and Zn sorption on Na-montmorillonite. Part I: Titration and sorption measurements. Journal of Contaminant Hydrology 27,199-222.

Bradbury, M.H. and A. Green. 1985. Measurement of important parameters determining aqueous phase diffusion rates through crystalline rock matrices. Journal of Hydrology 82, 39-55.

Bradbury, M.J., D. Lever and D. Kinsey. 1982. Aqueous phase diffusion in crystalline rock. Materials Research Society Symposium Proceedings 11 (Scientific Basis for Nuclear Waste Management V), 569-578.

Brown, P.L., E. Curti and B. Grambow. 2005. Chemical Thermodynamics of Zirconium. OECE Nuclear Energy Agency Data Bank. Ed. Mompean F.J., Perrone J. and Illemassene M.

Choi, J.W. and D.W. Oscarson. 1996. Diffusive transport through compacted Na- and Ca-bentonite. Journal of Contaminant Hydrology 22, 189-202.

Eberl, D.D. 1980. Alkali cation selectivity and fixation by clay minerals. Clays and Clay Minerals 28, 161-172.

Gimmi, T. and H.N. Waber. 2004. Modelling of profiles of stable water isotopes, chloride and chloride isotopes of pore water in argillaceous rocks in the Benken borehole. Nagra Technical Report, NTB 04-05, Nagra, Wettingen, Switzerland.

Harvey, K.B. 1996. Measurement of diffusive properties of intact rock. Atomic Energy of Canada Limited Report, AECL-11439, COG-95-456.

Hinds, G., P. Cooling, A. Wain, S. Zhou and A. Turnbill. 2009. Technical Note: Measurement of pH in concentrated brines. Corrosion 65, 635-638.

Intera. 2011. OPG's Deep Geologic Repository for Low & Intermediate Level Waste, Descriptive Geosphere Site Model NWMO DGR-TR-2011-24.

Jackson, R. and S. Murphy. 2011. Mineralogical and Lithogeochemical Analyses of DGR-5 and DGR-6 Core, DGR Site Characterization technical report TR-09-06, completed by Geofirma.

Katsube, T.J., T.W. Melnyk and J.P. Hum. 1986. Pore structure from diffusion in granitic rocks. Atomic Energy of Canada Limited Technical Record TR-381.

Lajudie, A., J. Raynal, J-C. Petit and P. Toulhoat. 1995. Clay-based materials for engineered barriers: A review. In Materials Research Society Symposium Proceedings, V 353.

Li, Y.-H. and S. Gregory. 1974. Diffusion of ions in sea water and in deep-sea sediments. Geochimica et Cosmochimica Acta 38, 703-714.

Lide, D.R. (Editor). 1992. CRC Handbook of Chemistry and Physics. CRC Press, New York, N.Y.

Liu, J. and I. Neretnieks. 2006. Physical and chemical stability of the bentonite buffer, SKB Report R-06-103.

Melnyk, T.W. and A.M.M. Skeet. 1987. A mathematical study of the influence of pore geometry on diffusion. Atomic Energy of Canada Limited Report AECL-9075.

Nagasaki, S., T. Saito and T. Yang. 2016. Sorption behavior of Np(V) on illite, shale and MX-80 in high ionic strength solutions, Journal of Radioanalytical and Nuclear Chemistry 308(1): 143-153.

Nagasaki, S., J. Riddoch, T. Saito, J. Goguen, A. Walker and T. Yang. 2017. Sorption behavior of Np(IV) on illite, shale and MX-80 in high ionic strength solutions, Journal of Radioanalytical and Nuclear Chemistry 313 (1), 1-11.

Nagasaki, S. 2018. Sorption Properties of Np on Shale, Illite and Bentonite Under Saline, Oxidizing and Reducing Conditions. Nuclear Waste Management Organization Technical Report NWMO-TR-2018-02, Toronto, Canada.

Nigrini, A. 1970. Diffusion in rock alteration system. I. Prediction of limiting equivalent ionic conductances at elevated temperatures. American Journal of Science 269, 65-91.

NWMO. 2011. OPG's Deep Geologic Repository for Low & Intermediate Level Waste. Nuclear Waste Management Organization, Geosynthesis. NWMO DGR-TR-2011-11 (Available at www.nwmo.ca).

NWMO. 2005. Choosing a way forward. The future management of Canada's used nuclear fuel. Nuclear Waste Management Organization (Available at www.nwmo.ca).

Ohlsson, Y. and I. Neretnieks. 1995. Literature survey of matrix diffusion theory and of experiments and data including natural analogues. SKB Technical Report 95-12.

Oscarson, D.W. and H.B. Hume. 1994. Diffusion of ^{14}C in dense saturated bentonite under steady-state conditions. Transport in Porous Media 14, 73-84.

Parkhurst, D.L. and C.A.J. Appelo. 1999. User's guide to PHREEQC (version 2) - a computer program for speciation, reaction-path, 1D-transport, and inverse geochemical calculations. US Geol. Surv. Water Resour. Inv. Rep. 99-4259, 312p.

Robinson, R.A. and R.H. Stokes. 1959. Electrolyte Solution, 2nd. Ed., Butterworths.

Sawhney, B.L. 1972. Selective Sorption and Fixation of Cations by Clay Minerals: A Review. Clays and Clay Minerals 20, 93-100.

Skagius, K. and I. Neretnieks. 1982. Diffusion in crystalline rocks of some sorbing and non-sorbing species. SKB Report, 82-12, SKB/KBS, Stockholm, Sweden.

Uemoto, M. 2000. Measurements of diffusion coefficients of aqua- and chloro-complexes of palladium(II) and mercury(II) in aqueous solutions. Inorganic Reactions Mechanisms 2, 155-159.

Vilks, P. and N.H. Miller. 2014. Sorption studies with sedimentary rock under saline conditions. Nuclear Waste Management Organization Technical Report NWMO TR-2013-22, Toronto, Canada. (Available at www.nwmo.ca).

Vilks, P. 2011. Sorption of selected radionuclides on sedimentary rocks in saline conditions – literature review. Nuclear Waste Management Organization Technical Report NWMO TR-2011-12, Toronto, Canada. (Available at www.nwmo.ca).

Vilks, P., N.H. Miller and K. Felushko. 2011. Sorption experiments in brine solutions with sedimentary rock and bentonite. NWMO Technical Report NWMO TR-2011-11, Toronto, Canada. (Available at www.nwmo.ca).

Vilks, P. 2009. Sorption in highly saline solutions – State of the science review. Nuclear Waste Management Organization Technical Report NWMO TR-2009-18, Toronto, Canada. (Available at www.nwmo.ca).

Vilks, P. and N.H. Miller. 2007. Evaluation of experimental methods for characterizing diffusion in sedimentary rocks. Nuclear Waste Management Organization Technical Report NWMO TR-2007-11, Toronto, Canada. (Available at www.nwmo.ca).

Wang, X. , X. Tan, C. Chen and L. Chen. 2005. The concentration and pH dependent diffusion of 137Cs in compacted bentonite by using capillary method. Journal of Nuclear Materials 345, 184-191.

Weast, R.C. 1972. CRC Handbook of Chemistry and Physics. 53rd Edition, CRC Press Inc., Cleveland.

Weast, R.C. 1978. CRC Handbook of Chemistry and Physics. 59rd Edition, CRC Press Inc., West Palm Beach, Florida.

Wigston, A. and R. Jackson. 2010. Mineralogy and Geochemistry of DGR-4 Core, DGR site characterization technical report TR-08-23, completed by Intera.

Wu, Y.C., W.F. Koch and R.A. Durst. 1988. Standardization of pH Measurements. NBS Special Publication 260-53, U.S. Department of Commerce / National Bureau of Standards, Gaithersburg, MD, 20899.

Yang, K. K., M.R. Mahmoudian, M. Ebadi, H.L. Koay and W.J. Basirun. 2011. Diffusion coefficient of tin(II) methansulfonate in ionic liquid and methane sulfonic acid (MAS) solvent. Metallurgical and Materials Transactions B 42B, 1274-1278

APPENDIX A: COMPARISON OF SIMULATED AND MEASURED K_D VALUES

LIST OF TABLES

Page

Table 1A: Simulated and Measured Pd K_d Values on Montmorillonite and Illite 88
Table 2A: Simulated and Measured Zr K_d Values on Montmorillonite and Illite 89
Table 3A: Simulated and Measured Sn K_d Values on Montmorillonite and Illite 90
Table 4A: Simulated and Measured Th K_d Values on Montmorillonite and Illite 91

Table 1A: Simulated and Measured Pd K_d Values on Montmorillonite and Illite

	SR-270-PW			Dilute solution		
pH	**Simulated K_d (cm^3/g)**		**Measured K_d (cm^3/g)**	**Simulated K_d (cm^3/g)**		**Measured K_d (cm^3/g)**
	Montmorillonite		Bentonite	Montmorillonite		Bentonite
4	0.000			402		
5	0.000			400		
5.5	0.005			400		
6.0	0.041		$(0.1 \text{ to } 14) \times 10^3$	400		
7	2.41			400		
7.5	24.5			400		
8	139			400		$(0.04 \text{ to } 7.5) \times 10^6$
9	342			400		
	Illite	60% of Illite	Shale	Illite	60% of Illite	Shale
4	0.000	0.000		402	241	
5	0.001	0.000		400	240	
5.5	0.005	0.003		399	240	
6	0.033	0.020	$(0.04 \text{ to } 14) \times 10^3$	399	239	
7	0.782	0.469		398	239	
7.5	2.82	1.69		396	238	
8	9.47	5.68		393	236	$(0.05 \text{ to } 4.3) \times 10^6$
9	81.5	48.9		383	230	

Table 2A: Simulated and Measured Zr K_d Values on Montmorillonite and Illite

	SR-270-PW			Dilute Water		
pH	**Simulated K_d (cm^3/g)**		**Measured K_d (cm^3/g)**	**Simulated K_d (cm^3/g)**		**Measured K_d (cm^3/g)**
	Montmorillonite		Bentonite	Montmorillonite		Bentonite
2	0		-	1,511		-
3	530		$(6.3 \pm 3.7) \times 10^2$	1,537		-
4	1,324		-	1,543		$(2.8 \pm 0.4) \times 10^4$
5	1,354		-	1,546		-
6.3	1,349		$(4.4 \pm 5.4) \times 10^3$	1,546		-
7	1,348		$(1.1 \pm 1.6) \times 10^4$	1,546		$(5.9 \pm 4.6) \times 10^4$
8	1,339		-	1,544		$(6.3 \pm 5.2) \times 10^4$
9	1,283		-	1,544		-
	Illite	60% of Illite	Shale	Illite	60% of Illite	Shale
2	0	0	-	1,491	895	-
3	842	505	$(2.0 \pm 1.7) \times 10^2$	1,534	920	-
4	1,349	809	-	1,541	925	$(3.7 \pm 0) \times 10^4$
5	1,354	812	-	1,538	923	-
6.3	1,349	809	$(3.8 \pm 5.7) \times 10^3$	1,515	909	-
7	1,324	794	$(1.0 \pm 1.4) \times 10^4$	1,479	887	$(5.5 \pm 1.1) \times 10^3$
8.0	1,107	664	-	1,335	801	$(3.2 \pm 3.5) \times 10^4$
9.0	495	297	-	1,083	650	-

Table 3A: Simulated and Measured Sn K_d Values on Montmorillonite and Illite

	SR-270-PW			Dilute solution		
pH	**Simulated K_d (cm^3/g)**		**Measured K_d (cm^3/g)**	**Simulated K_d (cm^3/g)**		**Measured K_d (cm^3/g)**
	Montmorillonite		Bentonite	Montmorillonite		Bentonite
3.3	-		$(9.0 \pm 7.8) \times 10^{2}$	-		-
4	7.41×10^{-2}		-	5.79×10^{5}		$(7.5 \pm 1.5) \times 10^{4}$
5	9.94×10^{2}		-	5.83×10^{5}		-
5.5	9.07×10^{4}		-	5.82×10^{5}		-
6.0	6.40×10^{5}		$(9.5 \pm 0.2) \times 10^{4}$	5.76×10^{5}		-
7	5.88×10^{5}		$(2.7 \pm 2.4) \times 10^{3}$	5.21×10^{5}		$(6.1 \pm 1.1) \times 10^{4}$
7.5	4.37×10^{5}		-	4.25×10^{5}		-
8	2.45×10^{5}		-	2.69×10^{5}		$(7.5 \pm 1.5) \times 10^{4}$
9	5.60×10^{4}		-	5.62×10^{4}		-
	Illite	60% of Illite	Shale	Illite	60% of Illite	Shale
3.3	-	-	$(9.0 \pm 7.8) \times 10^{2}$	-	-	-
4	1.1×10^{-1}	6.6×10^{-2}	-	2.8×10^{5}	1.6×10^{5}	$(8.5 \pm 2.2) \times 10^{4}$
5	1.6×10^{3}	9.7×10^{3}	-	2.5×10^{5}	1.5×10^{5}	-
5.5	9.8×10^{4}	5.9×10^{4}	-	2.4×10^{5}	1.4×10^{5}	-
6	2.5×10^{5}	1.5×10^{5}	$(4.4 \pm 0.7) \times 10^{4}$	2.2×10^{5}	1.3×10^{5}	-
7	1.9×10^{5}	1.1×10^{5}	$(3.0 \pm 3.3) \times 10^{3}$	1.9×10^{5}	1.1×10^{5}	$(2.9 \pm 1.5) \times 10^{4}$
8.0	1.0×10^{5}	6.2×10^{4}	-	1.2×10^{5}	7.1×10^{4}	$(5.8 \pm 1.8) \times 10^{4}$
8.5	6.2×10^{4}	3.7×10^{4}	-	6.7×10^{4}	4.0×10^{4}	-
9	3.7×10^{4}	2.2×10^{4}	-	3.2×10^{4}	1.9×10^{4}	-

Table 4A: Simulated and Measured Th K_d Values on Montmorillonite and Illite

	SR-270-PW			Dilute solution		
pH	**Simulated K_d (cm^3/g)**		**Measured K_d (cm^3/g)**	**Simulated K_d (cm^3/g)**		**Measured K_d (cm^3/g)**
	Montmorillonite		Bentonite	Montmorillonite		Bentonite
3.3	-		$(4.4 \pm 3.8) \times 10^2$	-		-
4	9.0×10^0		-	5.5×10^5		$(5.0 \pm 1.7) \times 10^4$
5	1.1×10^3		-	6.6×10^5		-
5.5	1.7×10^4		-	4.9×10^5		-
6.0	2.6×10^5		$(1.0 \pm 0.5) \times 10^4$	2.9×10^5		-
6.4	-		-	-		$(6.0 \pm 0.6) \times 10^3$
7	2.8×10^5		$(2.4 \pm 1.5) \times 10^4$	9.6×10^4		-
7.3	-		-	-		$(1.0 \pm 0.5) \times 10^5$
7.5	2.6×10^5		-	8.1×10^4		-
8	2.8×10^5		-	8.1×10^4		$(4.8 \pm 3.8) \times 10^4$
9	4.5×10^5		-	9.6×10^4		-
	Illite	60% of Illite	Shale	Illite	60% of Illite	Shale
3.3	-	-	$(2.2 \pm 3.9) \times 10^2$	-	-	-
4	9.5×10^0	5.7×10^0	-	1.6×10^3	9.7×10^2	$(4.9 \pm 0.9) \times 10^4$
5	6.8×10^2	4.1×10^2	-	3.5×10^4	2.1×10^4	-
5.5	1.3×10^4	8.0×10^3	-	8.0×10^4	4.8×10^4	-
6	1.9×10^5	1.2×10^5	$(5.3 \pm 3.0) \times 10^3$	1.1×10^5	6.5×10^4	-
6.4	-	-	-	-	-	$(4.0 \pm 0.8) \times 10^3$
7	2.3×10^5	1.4×10^5	$(2.1 \pm 1.3) \times 10^4$	9.9×10^4	5.9×10^4	-
7.3	-	-	-	-	-	$(3.2 \pm 3.4) \times 10^5$
7.5	2.2×10^5	1.3×10^5	-	7.7×10^4	4.6×10^4	-
8	2.3×10^5	1.4×10^5	-	7.3×10^4	4.4×10^4	$(1.4 \pm 1.1) \times 10^4$
9	3.7×10^5	2.2×10^5	-	7.9×10^4	4.7×10^4	-